APPLICATIONS OF CONTROL THEORY

By

C.K. Taft, J.L. Pokoski,
J.B. Murdoch, D.E. Limbert,
R.W. Alperi

Final Report

NASA Grant NGR 30-002-056

July 1, 1969 to Sept. 30, 1971

March 1972

FINAL REPORT

NASA Grant NGR 30-002-056

July 1, 1969 to Sept. 30, 1971

APPLICATIONS OF CONTROL THEORY

The work completed under this grant could be divided into the following categories:

I. The Decoupling Control of Submersibles

II. Wake Steering Control of Submersibles

III. Electrohydraulic Conversion Method With No Moving Parts

IV. Socio-Economic System Modelling

Several publications, reports and theses resulted from this work; these are listed in the bibliography. Summaries of all of the theses and reports are in the appendices. These summaries serve to provide many of the details of the work accomplished under this program. Briefly, the objectives of these research projects were as follows:

Submersible Decoupling Control: a control strategy which would allow the operator of a submersible independent control of any one of the vehicle's six degrees of freedom, was the desired objective of this research. A submersible is a nonlinear coupled system. The specific strategies devised were evaluated by simulating each strategy using a digital computer and a dynamic model of the Deep Submergence Rescue Vehicle (DSRV) whose dynamics were rather well specified by experimental and analytical work done for the preliminary DSRV designs.(1) There were several approaches to the problem which were evaluated. The object of the second project, Wake Steering Control, was to provide an improved

(1) Refer to references listed at the end of this report.

method of steering submersibles by controlling the direction of the wake of the thrusters so as to provide a momentum force to steer the submersible in a desired direction. This redirection of a thruster propeller wake was to be accomplished by a minimum of moving parts at as low a power level as possible. The third project, The Electro-hydraulic Converter, was concerned with a method of controlling hydraulic power directly from an electrical signal without using moving parts. Such a device could be used for the control of thrusters, control surfaces, tooling, and other hydraulically actuated functions on a submersible. The reliability and dependability of fluidic devices are well known and their application to this particular problem could provide a very reliable solution to a difficult problem. The objective of the Socio-Economic System Modelling program was to use control engineering methods to model the characteristics of transportation systems, in particular, roads in the state of New Hampshire. The methods of curcuit analysis were to be applied to the problem of how the traffic on these roads might be related to the length, and size of individual roads and the topology of the road system in the state.

Submersible Decoupling Control

One of the strategies for submersible decoupling that was investigated involved linearizing the equations of motion for the submersible about sets of operating points. This would yield a linear coupled model for the submersible at each of these operating points. For each of these operating points a decoupling strategy would be devised to provide at each of the selected operating points a linear decoupled controller. For this set of linear decoupled controllers it was hoped to devise a nonlinear controller

which would provide global decoupling for the system. This concept is an extension of the work of Fertik[2]. There are several problems involved with this approach. Even for linear systems, the computation of the decoupling controller parameters is quite tedious. Number two, if the system is complex, the location and number of the operating points is difficult to determine. In particular, the distance in the state space from one operating point to another determines the overall effectiveness of the decoupling controller. As the distance between these points becomes greater and greater, the decoupling controller must of necessity become less effective. Thirdly, the resulting decoupling controller must be somehow tested. It was very difficult to obtain a submersible and construct, with the resources available under this contract, the equipment needed to control such a submersible using any control strategy. Consequently, all of the evaluation of the strategies was conducted using a computer simulation of a particular submersible, namely the DSRV vehicle, for which a dynamic model has been devised by preliminary research done by the Lockheed Corporation.[1]

Mr. Michael Reagan, under the direction of Dr. John Pokoski, was concerned with a method of designing the decoupling control at each of the selected operating points.[3,I] The Wolovich-Falb approach [4] to decoupling was analyzed and applied to simple systems to determine its applicability to the submersible problem. Their method provides a test to determine if the system can be decoupled, and provides a design scheme for decoupling while setting the closed loop poles of the system to desired values. Its application to a large number of operating points would be very difficult. In addition, the method does not lend itself to a digital computer approach. A computational approach developed by Gilbert and

(I, refers to appendix I)

Prvnichny[5] did offer a computerized approach to the problem of designing a decoupling control strategy. This program needed to be modified, to be used on our computional facilities. It was finally made operational and used to design a simplified set of roll-surge and pitch-surge linearized equations for the DSRV. The resulting computer program did provide a way to quickly design a decoupling control strategy once a linearized model at an operating point was obtained.

The problem of determining the degradation of the decoupling strategy as the submersible moves from one operating point in the state space to another, was the concern of Mr. Charles Walker under the direction of Dr. John Pokoski.[6,II] There were no methods existing in the literature which could be applied to the problem of determining how ineffective a decoupling controller might become as the system strayed from the operating point for which the controller was designed. An approach was devised by Mr. Walker to include the lowest order nonlinear terms as variational terms in a linear system of state equations which described the system behavior. He then evaluated how these variations affected the transition matrix for the system. Of particular concern were the terms which had to be zero to cause the system to behave in a decoupled manner. A standard approach was developed for the submersible system and it was shown how the approach could be applied to other types of systems. A simplified set of roll-surge and pitch-surge-heave equations were analyzed using this approach. The method indicated that it was possible to learn from the system equations how much coupling was introduced as the system moved from the initial operating point about which it was decoupled. It also appeared that this approach might provide an experimental method for determining, from measurements of the system velocities, how effective the decoupling was at any point in the state space. Perhaps this effectiveness measure

could be used as a criteria for deciding when to switch from a decoupling control devised at one operating point to another or a strategy for adapting a decoupling controller to maintain its effectiveness over a wide range of operating points.

A digital computer simulation of the DSRV was devised by Mr. Vincent Tawari under the direction of Dr. Hohn Pokoski for the digital computer here at the University of New Hampshire.[7,III] This simulation provided us with a way to evaluate the various decoupling control strategies.

A sensor to provide the magnitude and direction of the relative velocity of the water and the vehicle is needed to provide feedback signals for decoupling the nonlinear hydrodynamic forces and moments. Ralph Cahalane, Robert McIntosh, Robert Ashey and Thomas Tomany worked under the supervision of Mr. Allen Magnuson to develop such a sensor.[8,IV] The frequency of the oscillating force on a cylindrical body moving in a fluid is nearly proportional to its velocity. This force was detected by strain gauges mounted on the rod which supported the cylinder. The gauge location was such as to provide velocity information in a particular direction. Experimental tests on the system showed a fairly good correlation between frequency and velocity. Several of these sensors mounted at selected locations on a submersible would provide velocity information at the vehicle. A potential flow analysis for the flow over the vehicle and information from the sensors not in the separated flow region could be used to find the relative velocity of the vehicle in the fluid. This information could then be used to provide the feedback signals needed for the hydrodynamic coupling terms.

The design and evaluation of the controller using a set of linearized models for the submersible was conducted by Mr. Greg Schoenau under the direction of Dr. Charles K. Taft.[V]

A simple second order, two input-two output nonlinear system was examined to illustrate the method of linearization of a nonlinear system about operating points and the subsequent application of the decoupling synthesis procedure. Two methods of switching between operating points were considered. The effect on decoupling of the number of operating points and the switching methods were investigated through computer simulations of the system.

The method of controller design was generalized into a step-by-step procedure. This method was then applied to the simplified DSRV roll and surge equations. The equations were simulated and the results discussed.

Another method of decoupling the roll-surge equations is possible. In cases where the input operating point for linearized decoupling can be solved exactly, then it is possible to decouple the system globally by direct feedback of the nonlinear state variables.

As shown in Appendix V, decoupling by linearization of the nonlinear equations is a satisfactory method, however, as the number and complexity of system model nonlinearities increases, it requires increasing amounts of computer capacity. The best system response will be obtained when the operating points at which the controller is designed are selected on the basis of the form of the expected time response. A continuous updating strategy which redesigns the controller at each computation instant was found to be the most effective for all the inputs simulated. For simple nonlinear systems it is conceivable that the number of operating points required for decoupling would be so few as to allow the use of an analog decoupling controller which would reduce the control cost significantly.

However, for the DSRV the use of analog controllers would be highly unlikely as evidenced by the large number of operating points required in the simulations. It was also shown that solving for the input variables in terms of the operating points could be used to devise a controller to decouple the system by nonlinear feedback. For systems where the use of a computer in the control loop is necessary, this seems to be the best method to us, if possible.

Another method of decoupling control which was investigated by Karl Tubalkain under the direction of Dr. David E. Limbert can be described as follows:[9,VI]

Wolovich and Falb[4] have determined a set of necessary and sufficient conditions for the decoupling of constant coefficient linear systems. Working along the same lines, E. E. Freund has studied decoupling of linear time varying systems.[10] It would be desirable to have a similar method for nonlinear systems. A specific example was decoupled first, and then a list of sufficient conditions was devised.

The method involves decoupling by subtracting the effects of the nonlinear terms in the system differential equation using measurement of the system state variables.

The limitations of this approach can be specified as follows:

If an m-input, m-output nonlinear system can be specified in state variable form, then sufficient conditions are obtained to determine if the system can be decoupled. Once it is determined that the system can be decoupled, feedback matrices are derived which both decouple the system and force it to behave like a linear system.

The system equations must be of the form

$$\dot{X} = A\ (x)\ x + B\ (x,u)\ u$$

$$Y = C\ (x)\ x$$

Feedback is of the form

$$U = F\ (x,u)\ u + G\ (x,u)\ w$$

The individual terms in the above matrices, A,B,C,F,G, may be functions of the quantities in parentheses.

A synthesis procedure is given in order to specify certain closed loop poles. Two numerical examples demonstrate the computations involved and the applicability of the method.[VI]

Wake Steering Control

A concept was devised which would allow the wake of a propeller to be steered to impart a moment to a submersible vehicle along an axis which was not coincident with the axis of the propeller. Mr. John Wozniak, under the direction of Dr. Taft and Dr. Alperi devised a concept which uses a shroud around the propeller similar to an accelerating nozzle.[11,VII] The shroud is fixed around the propeller and is longer than a conventional Kort nozzle. The purpose of the shroud is to provide a surface to which the wake of the propeller attaches as it moves downstream. The shape of internal surface of the shroud was devised so that in the region just downstream from the propeller the pressure around the inside wall of the shroud was lower than the ambient pressure around the outside of the shroud, (see Figure 1). In this region control ports were introduced between the inside and the outside wall of the shroud which could be opened and closed by exerting a very small force to open or close port

hatches. These ports were located around the shroud at a fixed distance downstream of the propeller. If a port were opened, some of the fluid surrounding the shroud would be induced from the outside of the shroud to the inside of the shroud and cause separation of the propeller wake downstream from that point. This separation causes the wake of the propeller to exit from the shroud at an angle which is no longer coincident with the axis of the propeller. The angle and direction depends upon the internal shape of the shroud near the exit and also on the forward velocity of the shroud and the speed of the propeller. An analytical model of this arrangement was devised which demonstrated that it was possible to provide a radial force on the shroud and propeller combination which was approximately equal to the axial force imparted to the shroud when the control ports were closed. In addition, when any given control port was open, the radial and axial forces were approximately equal to the original forward thrust. In this way, an additional thrust was obtained with any given port open in a direction determined by the location of that port and the speed of the propeller. This force could inpart a steering moment to a vehicle if such a shroud were attached to the vehicle at some appropriate point, as shown in Figure 2.

A scale model was constructed using a propeller of 41 mm in diameter. The shroud was constructed so that it had a multiplicity of pressure taps located to allow the measurement of the pressure distribution inside the shroud downstream and upstream of the propeller. Pressure measurements were taken with the control ports open and closed. From these pressure measurements the pressure profile inside the shroud was determined. A computer program was devised to compute the resulting forces on the

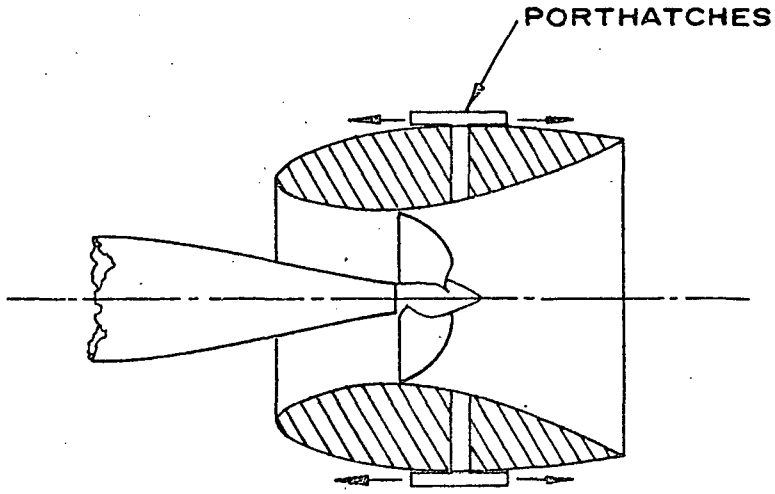

Fig. I. SHROUD

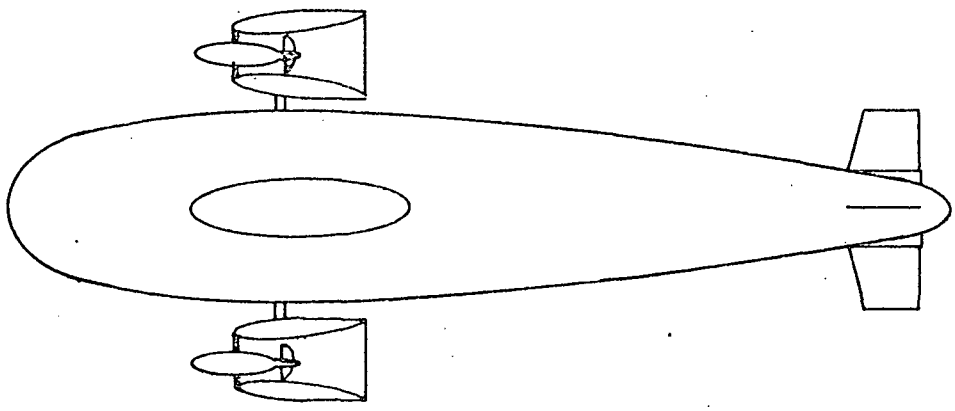

Fig.2. SUBMERSIBLE STEERING CONFIGURATION

shroud and propeller due to this pressure distribution. The result of this computer program indicated that for the scale model used, with all control ports closed, a force of $1.3X10^5$ dynes could be obtained. When any one control port was open, a radial force of approximately $1.2X10^5$ dynes was obtained in addition to an axial force of $1.3X10^5$ dynes. The resulting experimental data agreed reasonably with the analytical model and indicated that the shroud and propeller could provide a steering moment on a submersible which could be directed in any quadrant to accomplish steering.

Considerably more work needs to be done on this project in order to evaluate the effects of system parameters and forward velocity. The experimental data was run with a zero forward velocity. In addition, it can be shown that if the shape of the wall of the shroud is not correctly designed, that positive pressures can result downstream of the propeller which, of course, will not cause separation to occur when these regions are vented to the outside. Consequently, the shape of the shroud appears to be critical. Tests were conducted with a two-bladed propeller which caused the real flow to be three dimensional. A multi-bladed propeller would reduce these effects and probably also increase the effectiveness of the shroud. This should be studied. This work demonstrated the feasibility of the concept and provided enough preliminary information to encourage us to continue with the concept.

Electrohydraulic Converter

Hydraulic power is used for many control purposes in a submersible. The problem of converting electrical signals to hydraulic signals has

usually been approached by converting the electrical signal to a mechanical motion and then using this mechanical motion to control the flow of hydraulic fluid. The resulting hydraulic fluid signals are usually amplified by meams of a moving parts valve to provide control of hydraulic power at considerably higher power levels. This approach has some very serious weakness, especially when it is desired to control something from an electrical signal with very high reliability. The electromechanical conversion process is accomplished at a very low power level. The effects of friction, dirt, and wear of the moving parts all determine the reliability of the device. Consequently, there is strong motivation to produce a method of converting electrical signals to hydraulic signals with no moving parts. Several approaches were investigated by Mr. Ricardo Rivero under the direction of Dr. C. K. Taft and Dr. R. W. Alperi[VIII]. The basic geometry investigated is shown in Figure 3. A supply jet adjacent to a curve wall can be shown to exhibit bistable properties as the supply jet pressure is increased, thereby increasing its Reynolds number. At some critical Reynolds number the jet will attach to the curved wall. As the supply jet pressure is reduced, the jet will separate from the wall at some other critical Reynolds number. Thus, the supply jet angle of deflection θ versus supply pressure relationship exhibits hysteresis and is also discontinuous, as shown in Figure 4. Various methods were investigated for controlling this phenomena by changing the local Reynolds number or degree of turbulence along the lower edge of the jet in order to induce or prevent attachment to the curved wall. Electrostatic methods for inducing this turbulence were examined and it was found that except at very high voltages, it was very difficult to induce any magnitude of turbulence or force on the jet. Also, as shown by Jorgesen,[12] this force varies considerably with the properties of a hydraulic fluid and the amount

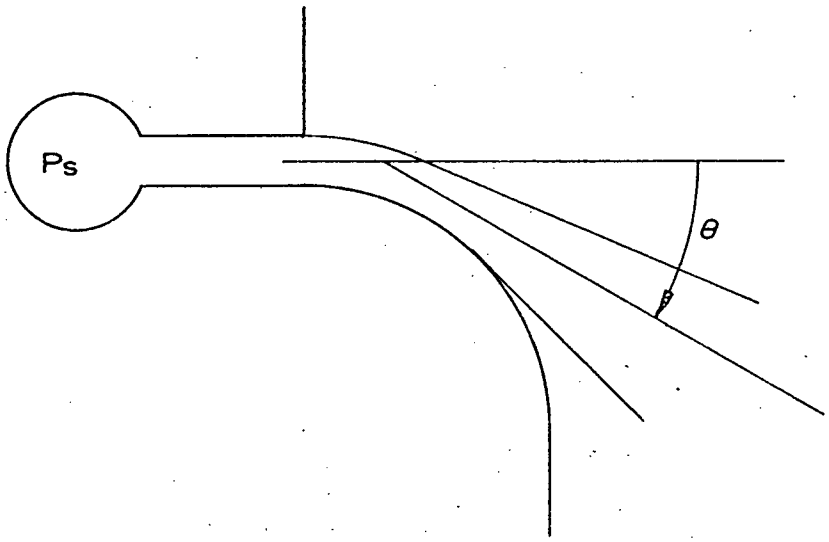

Figure 3. Jet Near Curved Wall

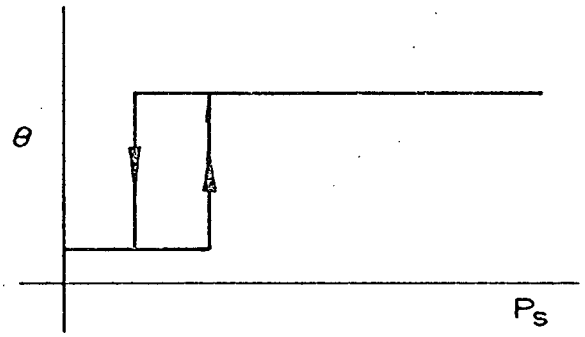

Figure 4. Bistable Properties of Jet Near Curved Wall

of entrained particles which might carry some electrostatic charge. It has been shown by McGlaughlin[13] that heating the curved wall can cause a local change in the Reynolds number along the lower edge of the jet, and may thereby induce or prevent attachment by changing the fluid viscosity. This approach has serious problems because in order to accomplish electro-fluid conversion , it is necessary to use a thin film electric heater fastened to the curved wall. the thin film heater tends to supply heat not only to the fluid, but also to the curved wall itself. This heat must be carried away by the fluid before the local temperature of the heater and the jet can decrease. Consequently, in the operation of such a device, the thermal mass of the curved wall and the heater become a significant part of the dynamics of the system. This approach has been used with air.[13,14] However, dynamic response with air did not appear to promise fast enough response with oil to be a practical solution to the hydraulic control problem. A third approach which seems to offer considerable promise was investigated experimentally under this program. This method uses a pressure disturbance introduced near the exit of the supply jet along the curved wall adjacent to the supply jet. This disturbance can be introduced by an electrically-excited piezoelectrical crystal to produce periodic fluctuations in jet velocity along the bottom of the jet. These fluctuations are basically unstable and cause the jet to become turbulent much closer to the exit of the supply nozzle than it might ordinarily at a particular supply jet Reynolds number. This turbulence will then cause the jet to attach to the curved wall and, if a receiver is located downstream from the supply jet, it is possible to change the amount of fluid collected by the receiver when the

jet sudeenly attaches to the curved wall. This approach was investigated experimentally. It was shown that the amount of fluid connected in the output could be strongly affected by a control signal applied to the piezoelectric crystal. The output could be affected, not only by the amplitude of the signal applied to the piezoelectric crystal, but also by its frequency. As a voltage was applied to the crystal in the region of the natural frequency of the supply jet, the crystal was much more effective in inducing turbulence and thereby causing attachment to the curved wall. In addition, the signal applied to the crystal affected the spreading of the jet and also thereby affected the amount of fluid collected at the output. The design tested experimentally was very inefficient since the crystal used to induce turbulence did not vibrate in a mode which was most efficient in producing disturbances in the jet. However, even at this very low level of efficiency, electrohydraulic conversion was obtained, and the results are quite encouraging. It is believed that the method offers great promise for converting electrical signals into hydraulic information, either digitally or in an analog frequency modulation mode.

Socio-Economics System Modeling

Mathematical models of transportaion systems can be quite useful in planning for highway system expansion. Data on the number of cars traveling the roads in the State of New Hampshire was used to devise a model for the road system in the State. The major arteries were modeled in a way similar to a topological graph used to describe an electrical network. A resistance parameter was devised to characterize these roads which was analogous to resistance in an electrical network. The effects of the cyclic behavior

of car traffic on the roads was studied using Fourier analysis methods and from this the spectral qualities of the road traffic behavior was obtained. From these studies it appears feasible to characterize a road system by a network composed of resistances connecting major cities. From this kind of model one might relate the characteristic resistance of such arteries to their physical properties and also make decisions as to the feasibility of changing the size or location of any of these arteries in order to change the traffic pattern. This study has been done by Major Darrell Lynch[15,IX] and Mr. Anthony Magliveras[16,X] under the direction of Dr. Joseph B. Murdoch and Professor Owen Durgin.

Lastly, some time was devoted to the development of cooperative efforts with other members of the University of New Hampshire faculty outside engineering. A group of faculty in the University met regularly and considerable effort was invested in proposals for cooperative research between the members of the political science, economic resources, education, economics and engineering departments. Considerable amount of trust and cooperation was established in this program and it is felt that this ground work will be the basis for future cooperative efforts.

Summary

The body of this report serves to summarize the results of this research program. The details are continued in the appendices.

The decoupling research resulted in the evaluation of several approaches to the decoupling of nomlinear systems. The subtraction method looks most promising and the analytical approaches developed

should allow it to be easily applied. The linearization method does not look very attractive because of the large number of linearized models needed to satisfactorily decouple even a simplified model of a submersible.

The wake steering method offers great promise for simpler submersible thruster systems. Using this method, fewer thrusters and less steering power would be required for directional control. In addition, steering at low velocities would be particularly simple using this method.

The electrohydraulic converter method appears feasible. More design data is needed to evaluate the power output and dynamic capabilities of the approach. In addition, the phenomenon needs to be incorporated into a geometrical design which best uses its controllable characteristics.

This Socio-Economic system modeling work has demonstrated that many of the methods of large scale electrical system modeling can be used to model social systems. The notion of using a simple set of ideal elements and physically justifiable topological connections to model other types of systems is a very useful strategy for systematizing the modeling of complex systems.

These research funds have allowed us to attack several important problems using the methods of control theory to obtain solutions. In addition, several new hardware concepts have been developed, a theory for the decoupling of nonlinear systems devised and a strategy for modeling has been extended.

1) Lockheed Report No. RV-R-0037A, DSRV Model for Analysis, ML 493-03 Vehicle, May 1968, Contract NObs 63(A) pp. 4.1.1-4.3.1, 5.1.1-5.1.3, 6.0.1-6.3.3.

2) Fertik, H. A., "The Design of Nonlinear Systems from State Dependent Linear Models", Systems Research Center Report SRC 76-C-6S-30, Case Western Reserve University, Cleveland, Ohio, 1965.

3) Reagan, Michael J., "Decoupling of Dynamic Equations", M.S. Project Electrical Engineering Department, University of New Hampshire, June 1970.

4) Falb, P. L. and Wolovich, W. A., "Decoupling in the Design and Synthesis of Multivariable Control Systems", I.E.E.E. Trans. Automatic Control, Vol. AC-12, December 1967, pp. 651-659.

5) Gilbert, E. G., "The Decoupling of Multivariable Systems by State Feedback", SIAM Journal of Control, Vol. 7, No. 1, February 1969.

6) Walker, Charles F., "An Investigation of Methods for Specifying the Sensitivity of Multi-Variable Systems", M. S. Project Report, University of New Hampshire, Electrical Engineering Department, June 1970.

7) Tawari, V. P., "Digital Simulation of the Six Degrees of Freedom of Motion of the DSRV, University of New Hampshire Project, Electrical Engineering Department, June 1970.

8) Magnuson, A. H., and McIntosh, R., " A Velocity Sensor for Deep Submersibles", ISA Paper 737, 1970 International Conference, Philadelphia, Pennsylvania, October 29, 1970.

9) Tubalkain, Karl and Limbert, David E., "Decoupling and Systhesis of Certain Nonlinear Systems", submitted for presentation at ASME 1972 Joint Automation Control Conference.

10) Freund, E. E., "Design of Time-Variable Multivariable Systems by Decoupling and by the Inverse", I.E.E.E. Trans. Automatic Control. Vol. AC-16, April 1971, pp. 183-185.

11) Wozniak, John J., " A Novel Approach to Submersible Vehicle Propulsion, Steering and Control". M.S. Thesis, University of New Hampshire, Mechanical Engineering Department, June 1971.

12) Jorgensen, J. E., An Experimental Study of the Feasibility of Electrostatic Modulation of Fluidic Devices, ScD. Thesis, Massachusetts Institute of Technology, 1968, submitted to ASME Automic Control Division for 1972 JACC.

13) McGlaughlin, D. W., Taft, C. K., "Fluidic Electrofluid Converter", ASME Transactions, June 1967, pp. 334-340.

14) Rehsteiner, Fritz H., "An Electrical To Fluidic Signal Converter using Heated, Curved Walls", 2nd IFAC Fluidic Symposium, Prague, July 21, 1971.

15) Lynch, Darrell D.,"Electrical Network Analysis of Socio-Economic Systems Utilizing Graph Theory", M.S. Thesis, University of New Hampshire, February 1970.

16) Magliveras, Anthony S., "Computerized Network Simulation of the Highway System of the State of New Hampshire", M.S. Thesis, University of New Hampshire, August 1971.

Appendix I

DECOUPLING OF DYNAMIC EQUATIONS

M. S. Project Report

Electrical Engineering Department

University of New Hampshire

by

Michael J. Regan

June 1970

One of the most important considerations in developing a controller for a system is the ability to control one output without effecting the other outputs. The purpose of this project is to use linear decoupling procedures, which modify system behavior so that one input controls one and only one output, on linearized equations which represent the DSRV about selected operating points. The two linear decoupling procedures which are investigated in this report are the procedure by Falb and Wolovich and the procedure by Gilbert. Gilbert's procedure is especially valuable in practical physical problems such as the DSRV control because Pivnichny has written a computer program to calculate all the data required for Gilbert's synthesis procedure. As part of this project, Pivnichny's program was adapted to the UNH computer. Gilbert's procedure with the aid of Pivnichny's program was used to decouple the linearized roll-surge equations about two different surge speeds and to decouple the linearized equations of the DSRV hovering into a constant current with zero yaw and roll angles at two different pitch angles. The decoupling controllers for both the roll-surge and the hovering problems were checked for desired results by calculating the closed loop transfer function about one set of operating points for each problem.

The procedure of Falb and Wolovich was successful in decoupling linear systems. Nonlinear systems can be decoupled about operating points by using linear decoupling theory on the linearized representations of the systems about these operating points. Gilbert's procedure with the aid of Pivnichny's program is highly practical in decoupling the physical systems.

Appendix II

AN INVESTIGATION OF METHODS FOR SPECIFYING THE SENSITIVITY OF MULTI-VARIABLE SYSTEMS

M. S. Project Report

Electrical Engineering Department

University of New Hampshire

by

C. F. Walker

June 1970

The time response of physical systems which can be described by differential equations is dependent on the magnitude and sign of the coefficients of the state variables. The consistency of the time response is dependent on the consistency of the coefficients. For example the transient response of a resistance-capacitance coupled circuit is governed by the time constant RC, so that a change in R or C due to aging, heating or because of replacement will result in a change in the response of the variable i (current). When the system is second order or higher and can be portrayed in matrix form, then the response is a function of the magnitude and sign of the system matrix elements. As in the single variable case the consistency of the time response depends on the consistency of the matrix elements.

For the linear physical systems which are described by differential equations with "constant" coefficients, the "nominal" magnitude of the elements is constant. Constancy of the system is then dependent on, for example, the variation of components from their "nominal" values due to heating, aging or repeatability of manufacture.

For non-linear systems the magnitude of the coefficients of the state variables is a function of the position of the variables in state space. For example $2X^2$ may be thought of as $2X \cdot X$, with $2X$ as the coefficient and X as the variable. Thus the coefficient changes as X changes. In addition, if the "coefficient" of the variable includes another variable, the sign of the "coefficient" may even change at some point in state space.

In both the linear and non-linear cases the way or ways in which the system stability is affected depends on the position of the coefficient (element) in the matrix and the "coupling" between the variables. When one element which affects the coupling changes and all other elements remain constant the response may change in the following ways:

1. The coupling between two variables changes but the eigenvalues of the system remain constant. For example in the system below, the eigenvalues remain constant but the coupling between x_1 and x_2 doubles:

   ORIGINAL SYSTEM

$$\begin{bmatrix} 1 & .1 & 0 \\ 0 & 2 & 0 \\ 0 & 0 & 3 \end{bmatrix} \begin{bmatrix} x_1 \\ x_2 \\ x_3 \end{bmatrix}$$

   CHANGED TO

$$\begin{bmatrix} 1 & .2 & 0 \\ 0 & 2 & 0 \\ 0 & 0 & 3 \end{bmatrix} \begin{bmatrix} x_1 \\ x_2 \\ x_3 \end{bmatrix}$$

   The characteristic equation for both cases:

$$(s-1)\ (s-2)\ (s-3) = 0$$

2. The eigenvalue of a variable may change without a change in coupling:

   ORIGINAL SYSTEM

$$\begin{bmatrix} 1 & .1 & 0 \\ 0 & 2 & 0 \\ 0 & 0 & 3 \end{bmatrix} \begin{bmatrix} x_1 \\ x_2 \\ x_3 \end{bmatrix}$$

   CHANGED TO

$$\begin{bmatrix} 1 & .1 & 0 \\ 0 & 2 & 0 \\ 0 & 0 & 3.5 \end{bmatrix} \begin{bmatrix} x_1 \\ x_2 \\ x_3 \end{bmatrix}$$

Coupling remains as before but the characteristic equation changes:

From: $(s-1)\ (s-2)\ (s-3) = 0$

To : $(s-1)\ (s-2)\ (s-3.5) = 0$

3. The gain of a variable may change:

A change in gain is evidenced by a change in the adjoint matrix since the adjoint matrix appears in the numerator of the transfer functions.

$$G(s) = \text{TRANSFER FUNCTION} = \frac{C\ [\ \text{adj}\ \ (sI-A)]\ B}{\text{Det}\ (sI-A)}$$

Where: B = control matrix; C = output matrix

From example (2) the change in a_{33} from 3 to 3.5 results in a change in adj $(sI-a)_{11}$ and adj $(sI-a)_{22}$ as follows:

ORIGINAL SYSTEM	CHANGED TO
$\text{adj}_{11} = (s-2)\ (s-3)$	$\text{adj}_{11} = (s-2)\ (s-3.5)$
$\text{adj}_{22} = (s-1)\ (s-3)$	$\text{adj}_{22} = (s-1)\ (s-3.5)$

Which may result in a change in G(s) depending on the elements of C and B.

4. A change in one element may result in a combination of the above: the following example illustrates this:

ORIGINAL SYSTEM

$$\begin{bmatrix} 1 & .1 & 0 \\ 0 & 2 & 0 \\ 0 & 0 & 3 \end{bmatrix} \begin{bmatrix} x_1 \\ x_2 \\ x_3 \end{bmatrix}$$

CHANGED TO

$$\begin{bmatrix} 1 & .1 & 0 \\ .1 & 2 & 0 \\ 0 & 0 & 3 \end{bmatrix} \begin{bmatrix} x_1 \\ x_2 \\ x_3 \end{bmatrix}$$

a. The coupling between x_1 and x_2 has been changed to affect x_2 as well as x_1

b. The eigenvalue change so that the characteristic equation changes:

From: $(s-1)\ (s-2)\ (s-3) = 0$

To : $(s-1)\ (s-2)\ (s-3) - .35 = 0$

c. A change of gain is evidenced by a change in adj (sI-a) 33

From: adj $(sI-a)33 = (s-1)\ (s-2)$

To : adj $(sI-a)33 = (s-1)\ (s-2) - .01$

Thus it can be seen that the type of change is dependent, to a degree, on the number of non-zero elements in the original matrix since this will determine if the eigenvalues and the gains will change.

In the case of both linear and non-linear systems, changes in elements can result in instability due to a change in the sign of an eigenvalue. Limit cycles or oscillations may occur in the case of non-linear systems. In addition, for non-linear systems which have been decoupled by the application of a feedback controller whose gains have been based on a linearized representation of the system at some operating point, reappearance of the coupling elements at distance remote from the operating point will cause recoupling with resultant inability to independently control the outputs.

This paper investigates methods of specifying sensitivity of system response to changes in matrix elements. In particular, it reviews the work of Morgan (1) in relating changes in system response and gain to changes in the matrix elements; it reviews the work of Reddy (2) who developed a method for determining the allowable change in matrix elements if the eigenvalues are to be held within a given tolerance.

This paper also develops methods for determining the change in response of a decoupled system due to reappearance of coupling elements in the various matrix.

CONCLUSIONS

The method of specifying the sensitivity of multivariable systems is, to an extent, dependent on the system.

Thus, Morgan's method is an excellent method for predicting the change in the poles and zeroes of a system for small changes to existing parameters. The method would be well suited to predicting the effects of changes in components of a controller designed as a result of DSRV control investigations. As was demonstrated it cannot be used to determine the sensitivity of a non-linear, decoupled system due to excursions from the operating point.

With regard to the system poles, Reddy's method is similar to Morgan's. It is based on the same relationship between the change in the roots, the change in the elements of the system matrix and the system cofactor matrix. Reddy's allows us to determine the allowable component change when it is necessary to limit the shift in the system poles but requires that the system be in companion form. Once again this method is more applicable to investigating controllers than decoupled systems. It also tends to give very conservative results.

Application of the State Transition Matrix (STM) appears to hold the most promise for specifying the sensitvity of decoupled systems since it allows the effect of recoupling to be directly determined. This included gains as well as time response. Although a general STM term

can be developed for sets of first order equations, individual forms have to be developed for systems containing one or more second order equations.

If a system contains all second order equations, the system can be treated as a matrix set of second order equations and sensitivity functions developed using Laplace transform methods. These sensitivity functions are similar in form to those derived using STM methods. They should be particularly useful for investigating systems similar to the V/STOL vehicle.

Appendix III

DIGITAL SIMULATION OF THE SIX DEGREES OF FREEDOM OF MOTION OF THE DSRV AND DECOUPLING OF A SECOND ORDER NONLINEAR SYSTEM

M. S. Project Report

Electrical Engineering Department

University of New Hampshire

by

Vincent P. Tawari

June 1970

In this project, Modern Control Principles are applied to the design of the control system for the Deep Submergence Rescue Vessel. Before designing the controls, it is desirable to obtain a simulation of the motion of the Deep Submergence Rescue Vessel (DSRV). Modern Control Theory is also applied to the examination of a simple system (in the form of a simple circuit) with a single non-linearity. Such things as decoupling, linearization about carefully chosen operating points, and stability in the small and large are considered. The effect on the stability of the system of switching from one control to another between two operating points is also considered.

To carry out these studies, the report is divided into two parts: Part A and Part B. In Part A, simulations of the motion of the DSRV are given. Both analog and digital simulations are considered. The analysis of a simple second order system containing a single nonlinearity is presented in Part B.

The Deep Submergence Rescue Vessel was chosen as the system to work with because of the ample amount of data available for this vessel.

Most of the design of the vessel was done in the MIT Instrumentation Laboratories where a detailed simulation of the vessel's motion has also been carried out. This simulation was done on a fairly complex and sophisticated hybrid computer. Computer programs describing submarine motion in six degrees of freedom (MOTN) have also been written by the Applied Mathematics Laboratory of the Department of the Navy. This later program was written under an IBSYS operating system for use on the IBM 7090 computer.

Although some MIT simulation results are available, it is desirable to have our own simulation here for the following reasons:

1) It would not be easy or practically possible to use the MIT computer facilities.
2) We could adapt neither the MIT nor Applied Mathematics Laboratory programs to fit into our computer system at UNH.
3) It is very desirable to have our own simulation handy for decoupling purposes.

This simulation would be simpler than simulations made at MIT because the simulation here would be carried out on a simple IBM 360/40 system and would entail simple Fortran IV programing language and methods. The MIT simulation is more difficult because a fairly sophisticated hybrid-computer is used, and the programs are made complex enough as to allow on-the-site model simulation of the DSRV and pilot training to be carried out on the computer. The scope of our project is purposely limited by the group because it is not the intention of the group to design and/or build the control for the DSRV. The purpose of the project is to simulate the motion of the DSRV as simply as

possible and yet have the simulation contain all the information necessary for completely describing the motion of the DSRV.

It is, therefore, the object of this report to present the "Simulation of the Six Degrees of Freedom of Motion of the DSRV".

At the early stages of the simulation, an analog simulation and a "Continuous System Modeling Program" (CSMP) simulation are carried out with simplified versions of the equations of motion.

The main simulation, however, uses a mathematical model that contains all equations in all degrees of freedom. All control surfaces are also included. The equations are rearranged to obtain one equation for the acceleration in each degree of freedom. Pitch, roll, and yaw angles are also generated. The rearranged differential equations are solved at regular time steps by the Fourth Order Runge Kutta Method. The coding of the simulation is done in Fortran IV language under an operating system (OS) for use on the IBM/360 Model 40 computer.

The equations of motion are obtained from the MIT and Lockheed reports.

For the simple nonlinear second order electrical system, simulation is carried out digitally using the IBM/360 Model 40 computer. The circuit is first analyzed using P. C. A. P. (Princeton Circuit Analysis Program), then continuously decoupled digitally by introducing the single nonlinearity as a piece-wise continuous function. For stability considerations, two operating points on the nonlinearity are chosen and FORTRAN IV program again used to determine the system performance by switching from one operating point to another. The system is finally examined for stability.

Appendix IV

A VELOCITY SENSOR FOR DEEP SUBMERSIBLES

A Senior Project

Mechanical and Electrical Engineering Departments
University of New Hampshire
by

Allen H. Magnuson

Robert McIntosh

June, 1970

ABSTRACT

This paper describes the development of a velocity sensor for use in the automatic hovering control of a deep submersible. The sensor system provides measurements of the three components of relative fluid velocity encountered by the submersible. The sensor probes use the Karman vortex shedding principle where the frequency of the oscillatory lift on the probes is proportional to the local fluid velocity. The method of obtaining the components of relative fluid velocity from the probe measurements is described using a potential-flow model.

INTRODUCTION

Development of a sensor for relative fluid velocity of a deep submersible is described. The motivation for the development of the sensor was provided by a need to sense all the state variables, including the relative fluid velocity components, for a proposed submersible hovering controller that utilizes state variable feedback. The system differential equations used for the submarine control strategy were obtained from experimental model studies where submersible hydrodynamic forces and moments are functions of far field relative fluid velocity.

The development of a sensing system for submersible relative fluid velocity can be broken down into three major phases:

1) Velocity Probe Development - Measurement of local velocity near the submersible's surface.
2) Far-Field Velocity to Local Velocity Relationship - A functional relationship must be established between the far-field relative fluid velocity components (U, V, W) and the local (probe) velocities. In addition, a suitable configuration or array of sensors must be developed using the functional relationship between velocities.
3) Circuitry Design for Automatic Computation of Velocities - The functional relationship obtained in step (2) must be used to compute the desired output (U, V, W) from the sensor signals using appropriate electronic circuitry.

The paper covers the first two phases only. The third phase would involve the design of a computer circuitry to mechanize the equations developed in phase two using the sensor signals as inputs.

The velocity probe developed and tested was a circular cylinder with a thin section near the base on which strain gages were mounted (Figure IV-2.) The probe uses the linear relationship between the frequency of oscillatory lift and the fluid velocity. The oscillatory lift results from the random periodicity of the Karman vortex shedding in the wake of the cylinder (Figure IV-1). The linear relationship between lift frequency and fluid speed is due to the constancy of the Strouhal number in the Reynolds number range of interest. (1,2)[1]

A relationship between the far-field velocity (i.e., the velocity that would exist in the absence of the submersible) and the local

---

[1] Bracketed numbers refer to similarly numbered references at the end of this paper.

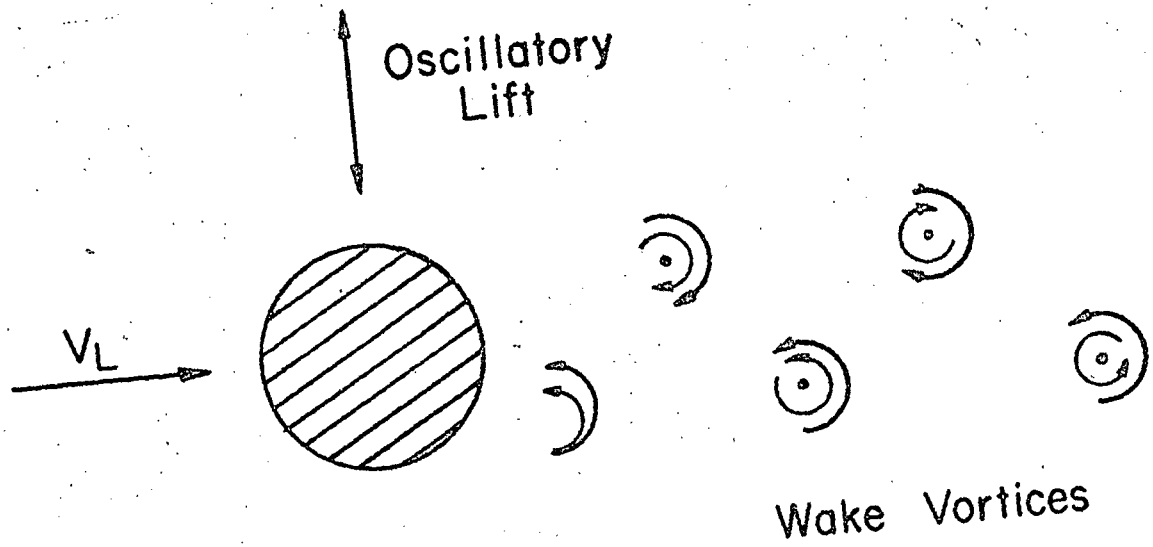

Figure IV-1. Flow Past a Circular Cylinder, Showing the Vortex Shedding

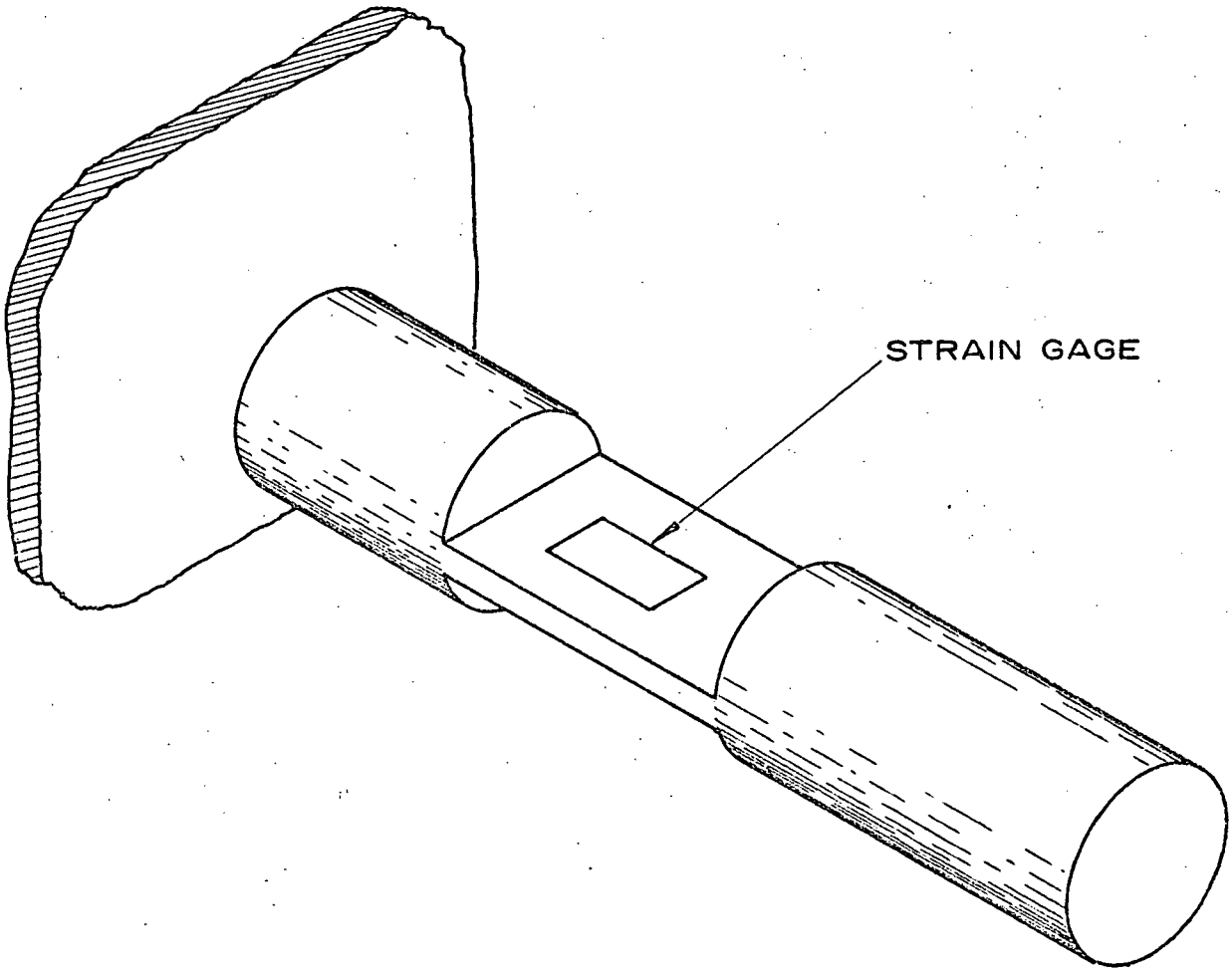

Figure IV-2. Sketch of Velocity Probe Used for Flume Tests

velocities was developed using a potential - flow model of the fluid flow. An ellipsoid of revolution was used to approximate the shape of the submersible (see Appendix V-A). This model of the flow is useful only for a relatively "clean" external submersible shape, i.e. no appendages or other protuberances in the vicinity of the sensor array. In addition, it is valid only for unseparated flow near the bow, or forward part of the submersible in ahead motion with angles of attack less than about 25 degrees.(3) The potential flow model is presented here in spite of its restrictions to illustrate the effect of the submersible in distorting the far-field flow. For an actual design application of this sensor system, a local-to-far-field velocity relation would have to be obtained experimentally using wind-tunnel or towing basin tests. However, the model in Appendix A represents a good first approximation to the flow of a submersible with a nearly ellipsoidal shape forward for low angles of attack.

VELOCITY SENSOR DESIGN CRITERIA

1) The sensor must function at all operating depths and speeds. (Corresponding to hydrostatic pressures up to about 2,500 psi, and through a water speed range of 0.5 to 10 fps).

2) It must be capable of surviving in the marine environment. In particular, it must be insensitive to salt-water corrosion, free from fouling due to silting and marine growth, and it must be rugged enough to withstand light "brushes" against marine life, submerged objects and the surface support vessel.

3) If a protruding probe is used, it must either be designed to minimize the danger of its becoming entangled in underwater cables etc., or it must be designed to break off cleanly when snagged to avoid entrapping the submersible.

VELOCITY SENSOR DESIGN

Initially, several velocity sensing concepts were considered. These included impellers, hot-wire anemometers, pitot tubes and various types of pressure transducers. The first three concepts appeared undesirable due to their vulnerability to damage in the marine environment and to the possibility of fouling etc. The use of pressure transducers looked attractive because they may be flush mounted, making them relatively invulnerable to damage. This approach was used on wind tunnel tests of dirigible models with some success.(3, 4) However, due to the low velocity range required for the present application (.5 to 10 fps), the pressure differentials are very small. In addition, the transducers are sensitive to structural vibration and waterborne noise. It was concluded that the combination of low velocities and vibration would result in an unacceptably low signal-to-noise ratio, which eliminated pressure transducers as a design possibility.

Eventually, a sensor design concept evolved that was based on the oscillatory lift produced by a cylinder placed across a fluid stream. The oscillatory lift is produced by the Karman vortex shedding phenomenon (Figure IV-1). The frequency of the vortex shedding can be expressed as a nondimensional frequency S, called a Strouhal number, as follows:

$$S = \frac{nd}{V_L}$$

where n = frequency of vortex shedding in hz

d = diameter of cylinder in meters

V_L = fluid velocity in meters/sec

In general, the Strouhal number is a function of the Reynolds number (R) for a given flow geometry:

$$R = \frac{V_L d}{\nu}$$

where ν = kinematic viscosity (m^2/sec)

For the speed ranges of interest in this project, the Strouhal number is essentially constant and independent of Reynolds number at a value of 0.21.(1, 2) Consequently, the shedding frequency is proportional to the velocity V_L as follows:

$$n = S \frac{V_L}{d} = 0.21 \ (V_L/d)$$

One advantage of this approach is that the quantity measured is a frequency, which avoids the necessity of a precise calibration of the probe. The thickness of the flexure section upon which the strain gages are mounted (Fig. IV-2) was determined roughly from sensitivity considerations. A design trade-off was determined where the probe sensitivity was limited by the lowest acceptable natural frequency in bending of the probe. The lowest acceptable bending frequency was determined to be several times the highest expected frequency of vortex shedding. This limitation was necessary to avoid having the vortex shedding drive the probe in resonance.

Another advantage of the proposed velocity sensing concept is the simplicity of the probe design. The probe can be made cheaply, making it expendable in case of serious damage. The probe does not require a calibration; consequently, light impacts on the probe will not affect its accuracy. A production design of the probe would incorporate modular construction to facilitate replacement or repair. In addition, the probe may be made more rugged by using a concentric design, where the outer surface of the probe consists of a cylindrical shell connected to

an inner cantilever by flexures with strain gages.

It should be noted that the vortex shedding frequency is not discrete for the Reynolds numbers of interest, but is actually distributed over a narrow band width. That is, the lift due to vortex shedding is not a pure sinusoid but, instead, is a sinusoidal curve with a slowly varying random amplitude and frequency, upon which is superimposed a low level noise signal. The output signal from the probe would then be expected to appear as an amplitude modulated sine wave with superimposed broadband noise. Upon testing, this proved to be the case, as can be seen from Figure 4.

VELOCITY PROBE TESTING

A probe design (Figure IV-2) was tested in a flume at the University's Fluid Mechanics Laboratory (Figure IV-3) at water speeds up to .655 m/s. The probe was fabricated solely for testing purposes. This probe had two horizontal flats near the base on which were mounted strain gages to sense vertical lift. (A probe used for a submersible would require two sets of gages mounted on flexures oriented 90^{o} apart.)

The strain gage output was amplified, sent through a low-pass filter, and monitored on an oscilloscope. A photograph of the strain gage output is shown in Figure IV-4). It can be seen that the signal is roughly the expected modulated sine wave plus broadband noise. Average frequencies for several water speeds were computed by averaging the peak-to-peak times from photographs similar to Figure IV-4). The results are plotted in Figure IV-5). It can be seen that the average frequencies increase in a fairly linear fasion as the speed increases. The difference between the expected S = 0.21 line and the test points can be attributed to:

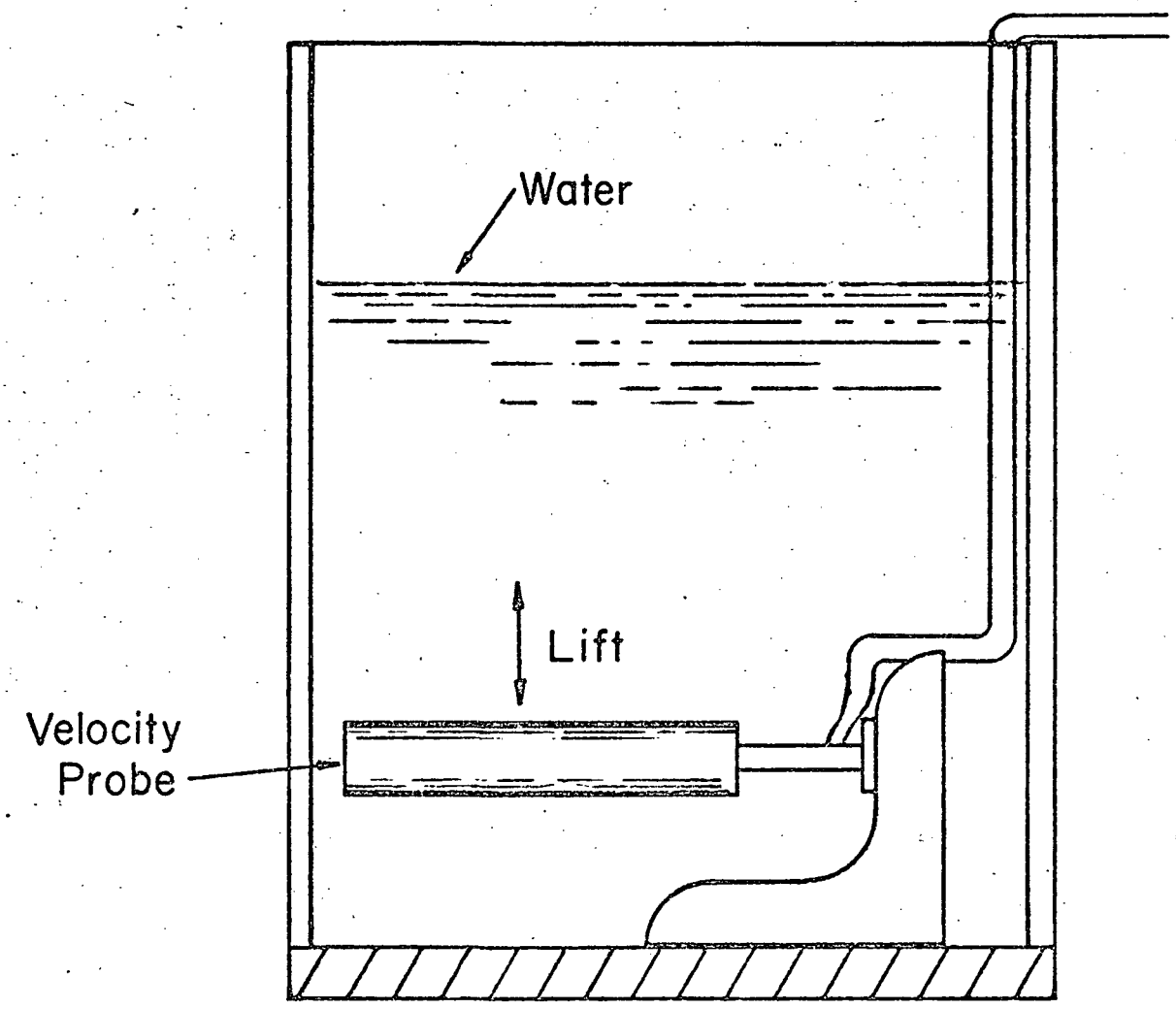

Figure IV-3. Sketch of Probe Arrangement in Flume

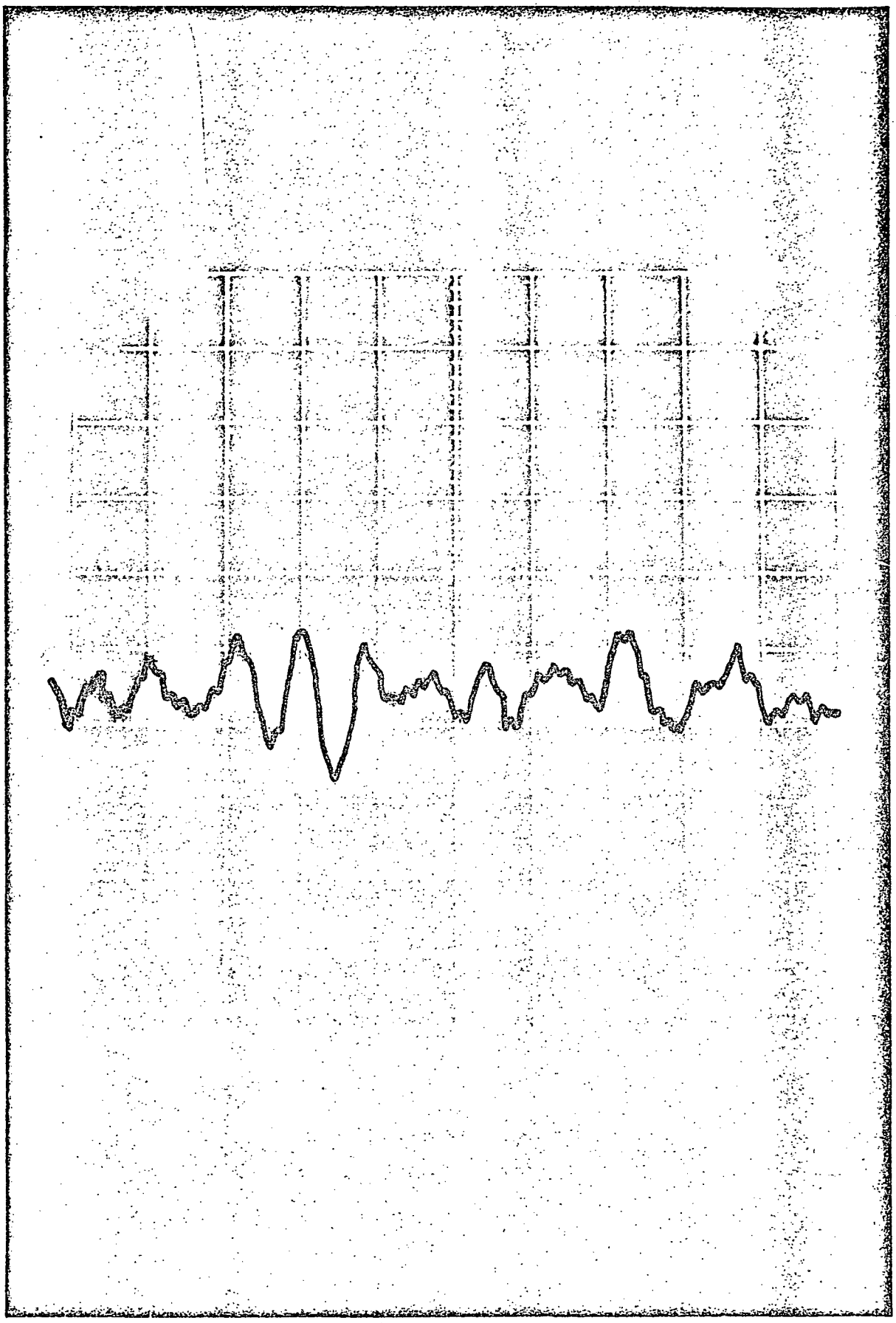

Figure IV-4. Sensor Output for U = .655 m/s

Results of Sensor Tests in Flume

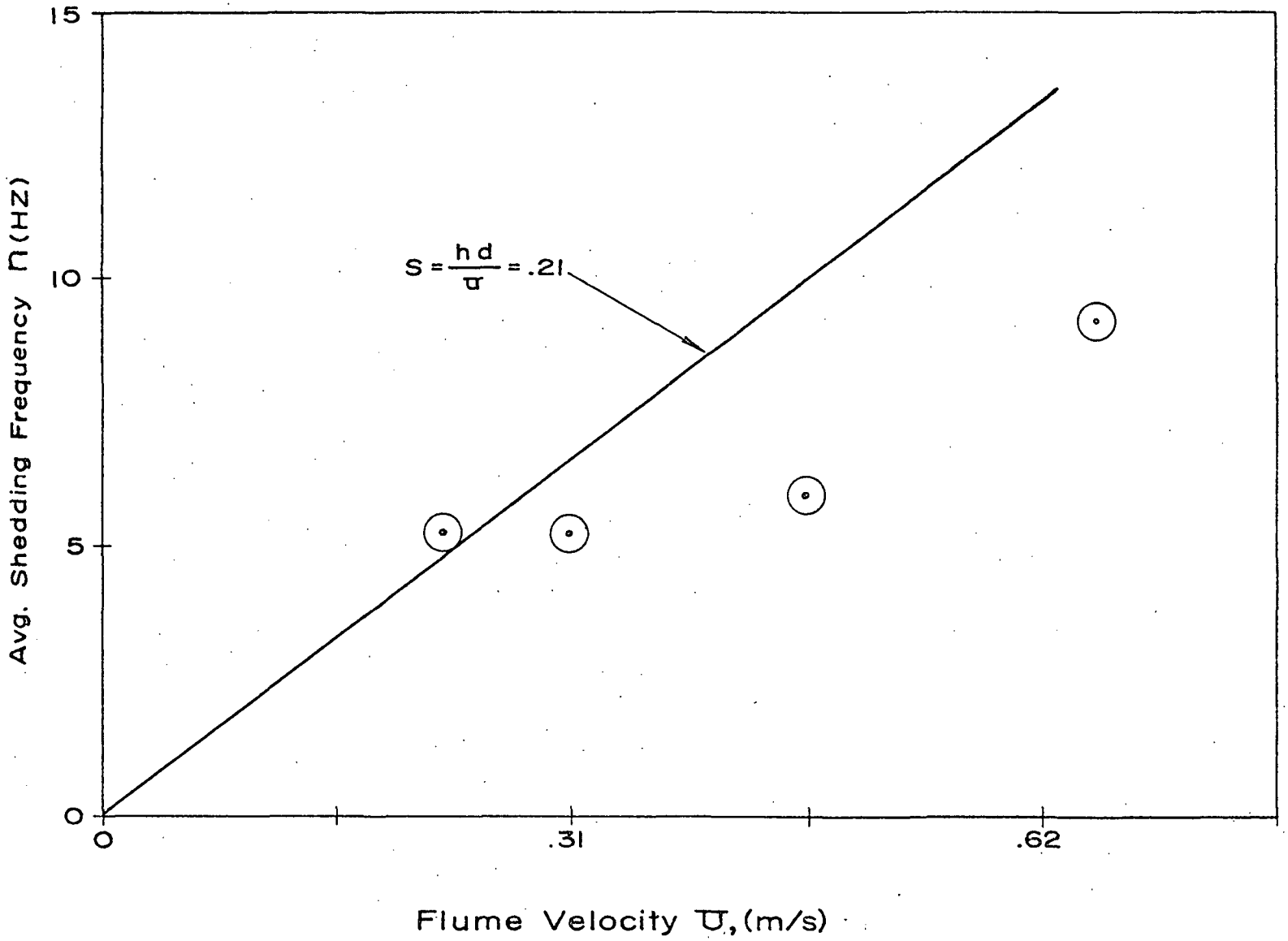

Figure IV-5

1) Inaccuracies in the measurement of the flume speed;

2) The nonuniform velocity profile in the flume; and

3) Free-surface effects.

Unfortunately, the flume speed was limited to a maximum of about .655m/s, so the probe could not be tested throughout the desired speed range. However, the test results show that the concept of using the vortex shedding principle for a velocity sensor is feasible for this application. It was felt that a spectral analysis of the signal would provide better results, but time did not permit further testing or analysis.

OBTAINING FAR-FIELD VELOCITY FROM LOCAL VELOCITY MEASUREMENTS

Assuming that we have available several local velocity measurements (V_L) from an array of sensors, the next problem is to convert these to far-field velocity components (U, V, W). A relation between the two sets of measurements is given for ellipsoidal geometry and potential flow in Appendix A, along with a discussion of the limitations of the results. Appendix B gives the relation between the U, V, W velocity components and the resultant velocity V_∞ and two "angles of attack", α and β. For a given array, the results of Appendix A may be utilized as follows.

For the i^{th} velocity measurement (V_{Li}), we have the corresponding probe location in ellipsoidal coordinates (ζ_i, μ_i, ω_i). We may solve the V_{Li} expressions

$$V_{Li} = V_{Li}(\zeta_i, \mu_i, \omega_i, U, V, W)$$

simultaneously to yield U, V and W, or alternatively to yield V_∞, α, and β. Apparently a minimum of three V_L measurements are required; however, redundancy can and should be designed into the final array.

AUTOMATIC COMPUTATION OF FAR-FIELD VELOCITY COMPONENTS

This stage was beyond the scope of the present project; however, a few points should be mentioned. First, the array of sensors may be arranged so that a simple (possibly linear) relation exists between velocities, at least for a limited range of angles of attack. This may eliminate the need for a sophisticated computer to calculate the far-field velocities.

Another point to mention is that for large angles of attack, flow separation will occur. Flow separation is characterized by high pressures, or lack of pressure recovery, and low velocities in the region of separation downstream. This sensing scheme should be able to predict roughly the angle of attack even for separated flow, since the pressure or velocity in a separated region is roughly constant, and the velocities in the non-separated region (upstream) are roughly those predicted by oetential theory.

ACKNOWLEDGEMENTS

The authors wish to acknowledge the guidance and assistance given by the design group faculty adviser, Dr. Charles K. Taft, of the Mechanical Engineering Department. They also wish to acknowledge the contributions of two other members of the design team, Messrs. R. Ashey and R. Cahalane. In addition, they wish to thank Professor Charles Dawson of the Civil Engineering Department for his assistance and cooperation in the use of the flume during the testing phase.

Key Words

Velocity Sensor

Submersible

Submarine

Vortex Shedding

CONCLUSIONS

The feasibility of using the Karman vortex shedding phenomenon for sensing of submersible relative fluid velocity has been demonstrated by tests. The method of converting the local velocity measurements to far-field velocity components is outlined using potential-flow and a simplified geometry.

REFERENCES

1) Roshko, Anatol, "The Development of Turbulent Wakes from Vortex Streets," NACA REPORT 1191, 1954.

2) Roshko, Anatol, "Experiments on the Flow Past a Circular Cylinder at Very High Reynolds Number," JOURNAL OF FLUID MECHANICS, Volume 10, 1961.

3) Allen, H. J., "Pressure Distribution and Some Effects of Viscosity on Slender Inclined Bodies of Revolution," NACA TECHNICAL NOTE 2044, March, 1950.

4) Upson, R. A. and Klikoff, W. A., "Application of Practical Hydrodynamics to Airship Design," NACA REPORT No. 405, 1932.

5) Durand, F. D. (Ed), "Aerodynamic Theory, Volumes I and II," Dover Publications, Inc., 1963, pp. 277-289.

Appendix IV-A POTENTIAL-FLOW CALCULATION OF THE VELOCITIES AROUND AN ELLIPSOID OF REVOLUTION

We want to find a functional relation between the velocities measured near the surface of the submersible (V_{Li}) and the x, y, and z components of the far-field velocity (U, V, W) relative to the submersible. Here we approximate the shape of a submersible by an ellipsoid of revolution with the same length-diameter ratio and the same overall dimensions. The solution is valid only for potential flow; consequently, the results of the calculation are accurate only for non-separated flow away from any appendage or protuberance on the submersible. In particular, for a typical submersible, the results are valid only in the forward sections of the vessel for ahead motion with angles of attack up to 20 to 25 degrees.*

This approach closely follows Reference 5. We start with a normalized ovary semi-elliptic coordinate system defined as follows (see Figure IV-6):

$$x = \mu\zeta \tag{1}$$

$$r = (1 - \mu^2)^{\frac{1}{2}} (\zeta^2 - 1)^{\frac{1}{2}} \tag{2}$$

$$y = r \cos \omega \tag{3}$$

$$z = r \sin \omega \tag{4}$$

The coordinate system is normalized by setting the distance between the foci to 2. Surfaces of ζ = constant are ellipsoids of revolution. The ratio a/b denotes the ratio of the semi-major axis to the semi-minor axis of the ellipse. If we denote ζ_0 as the surface corresponding to the desired a/b ratio, ζ_0 is given by

---

* This has been experimentally confirmed by tests on dirigible models in wind tunnels (3)

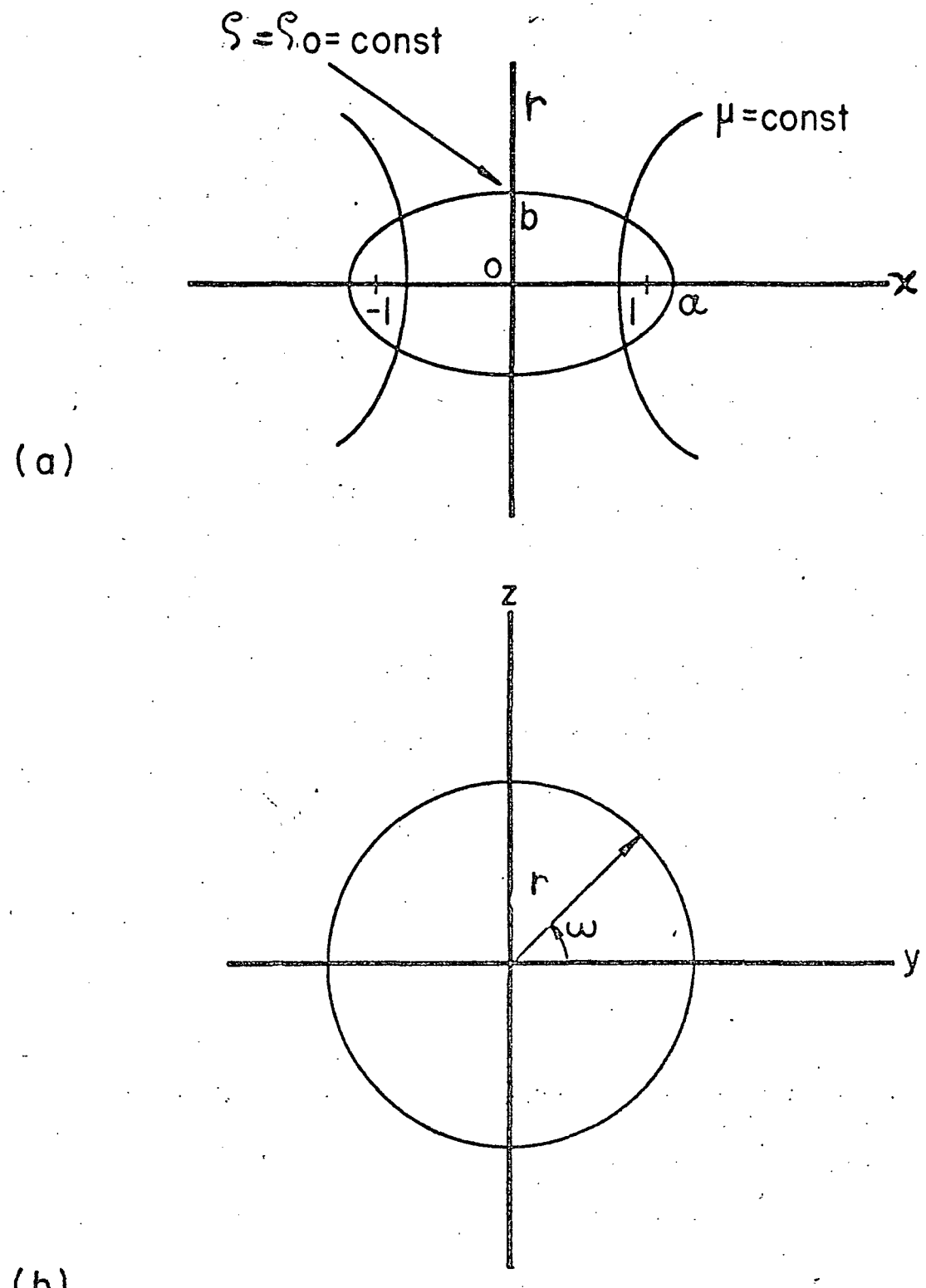

Figure IV-6. Ellipsoidal Coordinate System, (a) r-x Plane, (b) z-y Plane

$$\zeta_0 = a = \frac{a/b}{[(\frac{a}{b})^2 - 1]^{\frac{1}{2}}} \tag{5}$$

The velocity potential given in Reference 5 can be expressed in the following form:

$$\phi = \frac{U}{A_1}\mu[\tfrac{1}{2}\zeta\log(\frac{\zeta+1}{\zeta-1}) - 1] - \frac{V}{A_2} r [\tfrac{1}{2}\log(\frac{\zeta+1}{\zeta-1}) - (\frac{\zeta}{\zeta^2-1})]$$
$$\cos\omega + -\frac{W}{A_2} r [\tfrac{1}{2}\log(\frac{\zeta+1}{\zeta-1}) - (\frac{\zeta}{\zeta^2-1})]\sin\omega \tag{6}$$

where

$$A_1 = \frac{\zeta_0}{\zeta_0^2 - 1} - \tfrac{1}{2}\log(\frac{\zeta_0+1}{\zeta_0-1}) \tag{7}$$

$$A_2 = \tfrac{1}{2}\log(\frac{\zeta_0+1}{\zeta_0-1}) - \frac{\zeta_0 - 2}{\zeta_0(\zeta^2-1)} \tag{8}$$

and U, V, W are the x, y, z components of the far-field velocity, respectively. The quantities ζ, μ, and ω represent the ellipsoidal coordinates of a point in the fluid flow. The points we are interested in are the mid-points of the cylindrical velocity sensors arranged normal to the surface of the submersible in an array. We may assume that the length of the sensor is small compared to the overall dimensions of the submersible. In addition, the sensors only sense local velocity in a plane normal to their axis. They do not sense direction, i.e., they are omnidirection with respect to velocities in a plane normal to their axis. Consequently, we are interested in two components of the local velocity: V_μ and V_ω, the component normal to μ = constant surfaces (longitudinal tangential) and the component normal to ω = constant surfaces (lateral tangential). (The component V_ζ is the velocity normal to the surface, which cannot be sensed by the probes used here.) The

assumption that the length of the probe is small compared to the dimensions of the submersible is necessary to ensure that the plane defined by the tangent at the submersible surface at the sensor location is approximately parallel to the plane constructed normal to the sensor axis mid-point.

The desired velocity components are obtained from the velocity potential (6) using the following expressions

$$V_\mu = - \frac{\partial \phi}{\partial \zeta_\mu} \tag{9}$$

$$V_\omega = - \frac{\partial \phi}{\partial \zeta_\omega} \tag{10}$$

where

$$d\zeta_\mu = d\mu \left(\frac{\zeta^2 - \mu^2}{1 - \mu^2}\right)^{\frac{1}{2}} \tag{11}$$

and

$$d\zeta_\omega = d\omega(1 - \mu^2)^{\frac{1}{2}}(\zeta^2 - 1)^{\frac{1}{2}} = r d\omega \tag{12}$$

From (9) - (11)

$$V_\mu = - \frac{\partial \phi}{\partial \omega} \cdot \frac{d\mu}{d\zeta_\mu} = - \frac{\partial \phi}{\partial \mu} \left(\frac{\zeta^2 - \mu^2}{1 - \mu^2}\right)^{-\frac{1}{2}} \tag{13}$$

$$V_\omega = -\frac{\partial \phi}{\partial \omega} \left[(1 - \mu^2)\ (\zeta^2 - 1)\right]^{-\frac{1}{2}} = - \frac{\partial \phi}{\partial \omega} \frac{1}{r} \tag{14}$$

From (6), and differentiating

$$\frac{\partial \phi}{\partial \mu} = \frac{V}{A_1} \left[\tfrac{1}{2}\zeta \log \left(\frac{\zeta + 1}{\zeta - 1}\right) - 1\right] + (V \cos\omega + W \sin \omega)$$

$$\times \frac{\mu(\zeta^2 - 1)}{A_2 r} \left[\tfrac{1}{2} \log \left(\frac{\zeta + 1}{\zeta - 1}\right) - \left(- \frac{\zeta}{\zeta^2 - 1}\right)\right] \tag{15}$$

$$\frac{\partial \phi}{\partial \omega} = (V \sin \omega - W \cos \omega) \frac{r}{A_2} \left[\tfrac{1}{2} \log \left(\frac{\zeta + 1}{\zeta - 1}\right) - \left(\frac{\zeta}{\zeta^2 - 1}\right)\right] \tag{16}$$

combining (13) - (16), we obtain the simplified expressions

$$V_\mu = -\left(\frac{1-\mu^2}{\zeta^2-\mu^2}\right)^{\frac{1}{2}} \frac{U}{A_1}\left[\tfrac{1}{2}\zeta \log\left(\frac{\zeta+1}{\zeta-1}\right) - 1\right] + -(V\cos\omega + W\sin\omega)$$

$$\frac{\mu}{A_2}\left(\frac{\zeta^2-1}{\zeta^2-\mu^2}\right)^{\frac{1}{2}}\left[\tfrac{1}{2}\log\left(\frac{\zeta+1}{\zeta-1}\right) - \left(\frac{\zeta}{\zeta^2-1}\right)\right] \qquad (17)$$

$$V_\omega = \frac{-(V\sin\omega - W\cos\omega)}{A_2}\left[\tfrac{1}{2}\log\left(\frac{\zeta+1}{\zeta-1}\right) - \left(\frac{\zeta}{\zeta^2-1}\right)\right] \qquad (18)$$

Equations (17) and (18) are the desired expressions for the velocity components sensed by the probes. Using the ζ, μ, ω coordinates of each sensor for particular values of U, V, and W, we obtain the components V_μ and V_ω. The probe actually senses the resultant local velocity denoted V_L, defined as follows:

$$V_L = (V_\mu^2 + V_\omega^2)^{\frac{1}{2}} \qquad (19)$$

Appendix IV-6 NOTE ON KINEMATICS

We have derived the expression for the local sensed velocities (V_L) as functions of the far-field x, y, z components U, V, W. We may also express the far-field velocity with respect to the resultant velocity V_∞, and two "angles of attack", α and β. The new quantities may be defined as follows:

$$V_\infty = (U^2 + V^2 + W^2)^{\frac{1}{2}} \tag{20}$$

$$\alpha = \tan^{-1} \left(\frac{W}{U}\right) \tag{21}$$

$$\beta = \tan^{-1} \left(\frac{V}{U}\right) \tag{22}$$

The original components can be expressed in terms of V_∞, α, β, using (20) - (22).

$$U = [V_\infty^2 \, (1 + \tan^2\beta + \tan^2\alpha)^{-1}]^{\frac{1}{2}} \tag{23}$$

$$V = U \tan \beta \tag{24}$$

$$W = U \tan \alpha \tag{25}$$

APPENDIX V - Development of Decoupling Controller Using Linearized System Models About a Finite Number of Operating Points.

The Decoupling of Linear Systems

A considerable amount of literature has been published on the decoupling of linear-time-invariant multivariable systems [8,9,10,11,12] whereas very little has been published concerning the decoupling of nonlinear multivariable systems.[13] Linearization of nonlinear differential equations should allow the methods of decoupling developed for linear systems to be applied to the nonlinear cases.

Consider a system of linear-time-invariant differential equations as being represented by the following matrix equations

$$\dot{\bar{X}} = A\bar{X} + B\bar{U}$$

$$Y = C\bar{X}$$

Where
- $\bar{X} \equiv$ nx1 vector representing the system state variables
- $\bar{U} \equiv$ mx1 vector representing the system input variables
- $\bar{Y} \equiv$ mx1 vector representing the system output variables
- $A \equiv$ nxn coefficient matrix
- $B \equiv$ nxm coefficient matrix
- $C \equiv$ mxn coefficient matrix

The Wolovich-Falb decoupling procedure uses state variable feedback of the form:

$$\bar{U} = F\bar{X} + G\,\bar{W}$$

Where
- $\bar{W} \equiv$ mx1 matrix representing the inputs to the decoupled system
- $F \equiv$ mxn coefficient matrix
- $G \equiv$ mxm coefficient matrix

A block diagram of the resulting decoupled system is shown in Figure 1

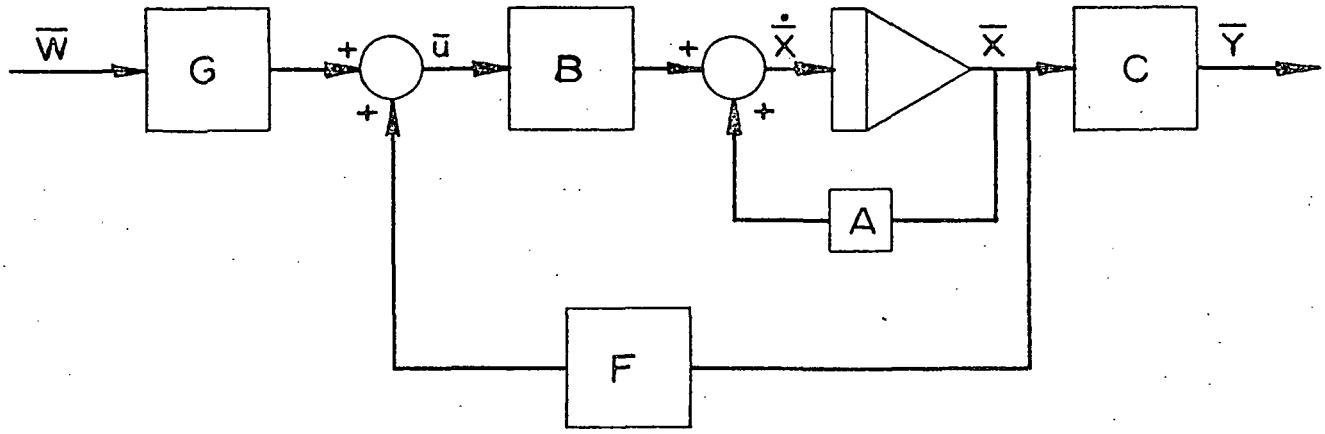

Figure V,1: DECOUPLED SYSTEM

Test for Decoupling:

Let $d_1, d_2 \ldots\ldots$ be given by

d_i = min {j such that $C_i A^j B \neq 0$, j = 0, 1, . . ., n-1}

= n-1 if $C_i A^j B = 0$ for all j

where C_i = i^{th} row of the matrix C

For a matrix B* as follows:

$$B^* = \begin{bmatrix} C_1 A^{d_1} B \\ C_2 A^{d_2} B \\ \vdots \\ C_m A^{d_m} B \end{bmatrix}$$

In order for the pair (F,G) to decouple the system

$$\det B^{*} \neq 0$$

Formation of F and G matrices:

$$G = B^{*-1}$$

$$F = G \left[\sum_{K=0}^{\delta} M_k C A^k - A^{*} \right]$$

where

$$\delta = \max d_i$$

$$M_k = \begin{bmatrix} m_k^1 & \cdots & 0 \\ \vdots & \ddots & \vdots \\ 0 & \cdots & m_k^m \end{bmatrix}$$

where the entries are the coefficients of the closed loop transfer function and can be chosen by the designer and

$$A^{*} = \begin{bmatrix} C_1 A^{d_1+1} \\ C_2 A^{d_2+1} \\ \vdots \\ C_m A^{d_m+1} \end{bmatrix}_{mxn}$$

Use of the above procedure results in a decoupled system of which

$$m + \sum_{i=1}^{m} d_i$$

of the closed loop poles can be specified.

Application to Nonlinear Systems:

As an example of the linearization decoupling procedure, consider a second order, two input-two output system with a single state nonlinearity. The example will serve to illustrate the linearization and decoupling procedure and assist in the formation of a generalized procedure. The system under consideration is given as:

$$\dot{X}_1 = -2X_1 - X_2^2 + 2X_2 + u_1 = f_1(X_1, X_2, u_1) \tag{1}$$

$$\dot{X}_2 = -X_1 - 3X_2 + u_2 = f_2(X_1, X_2, u_2) \tag{2}$$

Linearizing equations (1) and (2) using the first two terms in a taylor series expansion about an operating point yields:

$$\Delta\dot{X}_1 = \frac{\partial f_1}{\partial X_1}\bigg|_{o.p.} (\Delta X_1) + \frac{\partial f_1}{\partial X_2}\bigg|_{o.p.} (\Delta X_2) + \frac{\partial f_1}{\partial u_1}\bigg|_{o.p.} (\Delta u_1)$$

where $\Delta\dot{X}_1 = \dot{X}_1 - f_1(X_{10}, X_{20}, u_{10})$, $X_1 = X_{10} + \Delta X_1$, $X_2 = X_{20} + \Delta X_2$,

$u_1 = u_{20} + \Delta u_2$

Similarly for equation (2):

$$\Delta\dot{X}_2 = \frac{\partial f_2}{\partial X_1}\bigg|_{o.p.} \Delta X_1 + \frac{\partial f_2}{\partial X_2}\bigg|_{o.p.} \Delta X_2 + \frac{\partial f_2}{\partial u_2} \Delta u_2$$

Evaluating the partial derivatives and writing the equations in matrix form:

$$\begin{bmatrix} \Delta\dot{X}_1 \\ \Delta\dot{X}_2 \end{bmatrix} = \begin{bmatrix} -2 & K \\ -1 & -3 \end{bmatrix} \begin{bmatrix} \Delta X_1 \\ \Delta X_2 \end{bmatrix} + \begin{bmatrix} 1 & 0 \\ 0 & 1 \end{bmatrix} \begin{bmatrix} \Delta u_1 \\ \Delta u_2 \end{bmatrix} \tag{3}$$

$$\begin{bmatrix} \Delta Y_1 \\ \Delta Y_2 \end{bmatrix} = \begin{bmatrix} 1 & 0 \\ 0 & 1 \end{bmatrix} \begin{bmatrix} \Delta X_1 \\ \Delta X_2 \end{bmatrix}$$

where $K = -2X_{20} + 2$

Decoupling

Applying the synthesis procedure

$$C_1B = [1\ 0] \therefore d_1 = 0$$

$$C_2B = [0\ 1] \therefore d_2 = 0$$

$$B^* = B^{*-1} = G = \begin{bmatrix} 1 & 0 \\ 0 & 1 \end{bmatrix}$$

$$A^* = CA = A$$

$$F = \begin{bmatrix} 1 & 0 \\ 0 & 1 \end{bmatrix} \begin{bmatrix} m_0^1 & 0 \\ 0 & m_0^2 \end{bmatrix} - \begin{bmatrix} -2 & K \\ -1 & -3 \end{bmatrix} = \begin{bmatrix} (m_0^1 + 2) & -K \\ 1 & (m_0^2 + 3) \end{bmatrix} \tag{4}$$

$$\bar{q} = F\bar{X} + G\bar{w}$$

$$\begin{bmatrix} \Delta u_1 \\ \Delta u_2 \end{bmatrix} = \begin{bmatrix} (m_0^1 + 2) & -K \\ 1 & (m_0^2 + 3) \end{bmatrix} \begin{bmatrix} \Delta X_1 \\ \Delta X_2 \end{bmatrix} + \begin{bmatrix} 1 & 0 \\ 0 & 1 \end{bmatrix} \begin{bmatrix} \Delta w_1 \\ \Delta w_2 \end{bmatrix} \tag{5}$$

thus $\Delta u_1 = (m_0^1 + 2)\Delta X_1 - K\Delta X_2 + \Delta w_1$

$$\Delta u_2 = \Delta X_1 + (m_0^2 + 3)\Delta X_2 + \Delta w_2$$

substitute for Δu_1, Δu_2, ΔX_1, ΔX_2, Δw_1, Δw_2 and K their equivalents

$$u_1 = m_0^1X_{10} + 2X_1 - 2X_{10} - 2X_2 + 2X_{20} + 2X_2X_{20} - 2X_{20}^2 + w_1 - w_{10} + u_{10} - M_0^1X_{10}$$

$$u_2 = X_1 - X_{10} + m_0^2X_2 - m_0^2X_{20} + 3X_2 - 3X_{20} + w_2 - w_{20} + u_{20} \tag{6}$$

then substituting u_1 and u_2 back into equations (1) and (2) yields the decoupled system.

$$\dot{X}_1 = -X_2^2 + m_0^1X_1 - m_0^1X_{10} - 2X_{10} + 2X_{20} + 2X_{20}X_2 - 2X_{20}^2 + w_1 - w_{10} + u_{10} \tag{7}$$

$$\dot{X}_2 = -X_{10} + m_0^2X_2 - m_0^2X_{20} - 3X_{20} + w_2 - w_{20} + u_{20} \tag{8}$$

which can also be written as:

$$\dot{X}_1 = f_1\big|_{o.p.} + m_0^1X_1 - m_0^1X_{10} + w_1 - w_{10} - 2X_2^2 + 2X_{20}X_2 \tag{9}$$

$$\dot{X}_2 = f_2\big|_{o.p.} + m_0^2 X_2 - m_0^2 X_{20} + w_2 - w_{20} \tag{10}$$

where $f_1\big|_{o.p.} = \dot{X}_{10}$

$f_2\big|_{o.p.} = \dot{X}_{20}$

For very small changes in system state variables resulting from small changes in input, a satisfactory assumption at the operating point is to let:

$\dot{X}_{10} = \dot{X}_{20} = 0$

u_{10} and u_{20} are determined by solving the equations:

$f_1\big|_{o.p.} = 0$

$f_2\big|_{o.p.} = 0$

which satisfies the assumption of zero velocity at the operating point.

For large changes in input, for example steps, the proceeding method may prove unsatisfactory because of large velocities. In this case, a form of dynamic switching is necessary in which $\dot{X}_{10}$ and $\dot{X}_{20}$ are not zero but are set equal to the differential equations of the desired decoupled system response.

For the example under consideration this will be:

$$\begin{aligned} \dot{X}_{10} &= m_0^1 X_{10} + w_{10} \\ \dot{X}_{20} &= m_0^2 X_{20} + w_{20} \end{aligned} \tag{11}$$

and the equations for solving for u_{10} and u_{20} are:

$$\begin{aligned} f_1\big|_{o.p.} &= m_0^1 X_{10} + w_{10} \\ f_2\big|_{o.p.} &= m_0^2 X_{20} + w_{20} \end{aligned} \tag{12}$$

Solving for u_{10} and u_{20}

$$u_{10} = 2X_{10} + X_{20}^2 - 2X_{20} + m_0^1 X_{10} + w_{10} \tag{13}$$

$$u_{20} = X_{10} + 3X_{20} + m_0^2 X_{20} + w_{20} \tag{14}$$

Substitution of equations (13) and (14) into equations (7) and (8) result in the desired decoupled dynamic system given by equations (15) and (16).

$$\dot{X}_1 = m_0^1 X_1 + w_1 - X_2^2 + 2X_{20}X_2 - X_{20}^2 \tag{15}$$

$$\dot{X}_2 = m_0^2 X_2 + w_2 \tag{16}$$

Equation (15) will be perfectly decoupled only when $X_{20} = X_2$, while equation (16) is decoupled for all $\bar{X}$. This is to be expected since the original system equation for $\dot{X}_2$(2) is linear. Now that a satisfactory method has been developed for calculating the values of all the variables at an operating point, it remains to determine the number of operating points required for a specific maneuver and develop a criterion for switching between operating points so as to minimize cross-coupling.

Simulations of Two Switching Methods:

I. Sampled Data Switching

This method involves sampling of the state variables at specified instants of time. The state variables at each sample instant corresponds to an operating point. At each operating point, t = nT, a new decoupling controller would be designed to be used until t = (n+1)T. The sampling rate would be determined by the degree of decoupling desired. As T becomes smaller, the number of operating points increases and more effective decoupling results.

ex. Set: $X_{20} = X_2(nT)$

$X_{10} = X_1(nT)$

X_{20}, X_{10} would then be used to design the controller to be used until $t = (n+1)T$.

n = integer

T = sampling time.

II. Discontinuous Switching:

This method uses the magnitudes of the state variables to determine when to switch from one set of operating points to another. One approach is to divide the state variables into intervals of equal magnitude, Δ. These values of the state variable are then the operating points about which the system equations are linearized and decoupling controllers developed. Switching from one set of operating points to the next is performed whenever one of the state variables crosses the mid-point of the interval between two operating points. In this and subsequent simulations the decision to switch from one set of operating points to another set was based on the behavior of only one of the state variables; the state variable corresponding to the output being manipulated. It would be possible to extend this decision to include all the state variable values.

ex. X_2 is the desired output or output being controlled

$$\Delta = \frac{X_2(t_f)}{n_p}$$

where t_f = final time or steady state

n_p = number of sets of operating points

$X_2(t_f)$ = the desired output of X_2 as t goes to infinity

The following graph shows the values for one of the state variables X_{20} used in the linearized model plotted versus time for each method for a given output of a state variable

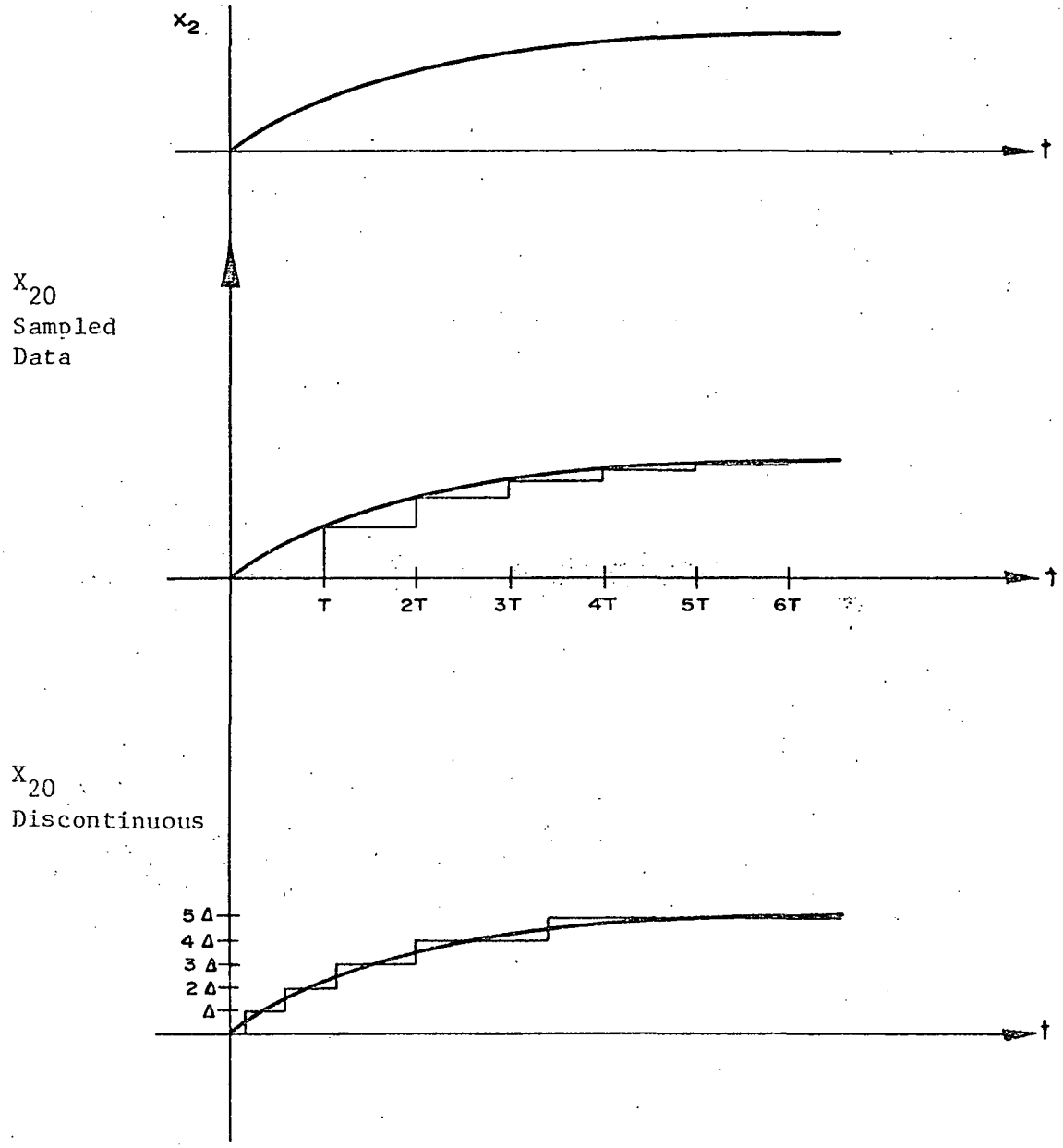

A system simulation was conducted to determine the relative effectiveness of the decoupling methods. For the system described by equations (1) and (2) an input w_2 was applied to effect a change in X_2. Figure 2 gives a comparison of the effectiveness of the methods in eliminating the undesired output X_1.

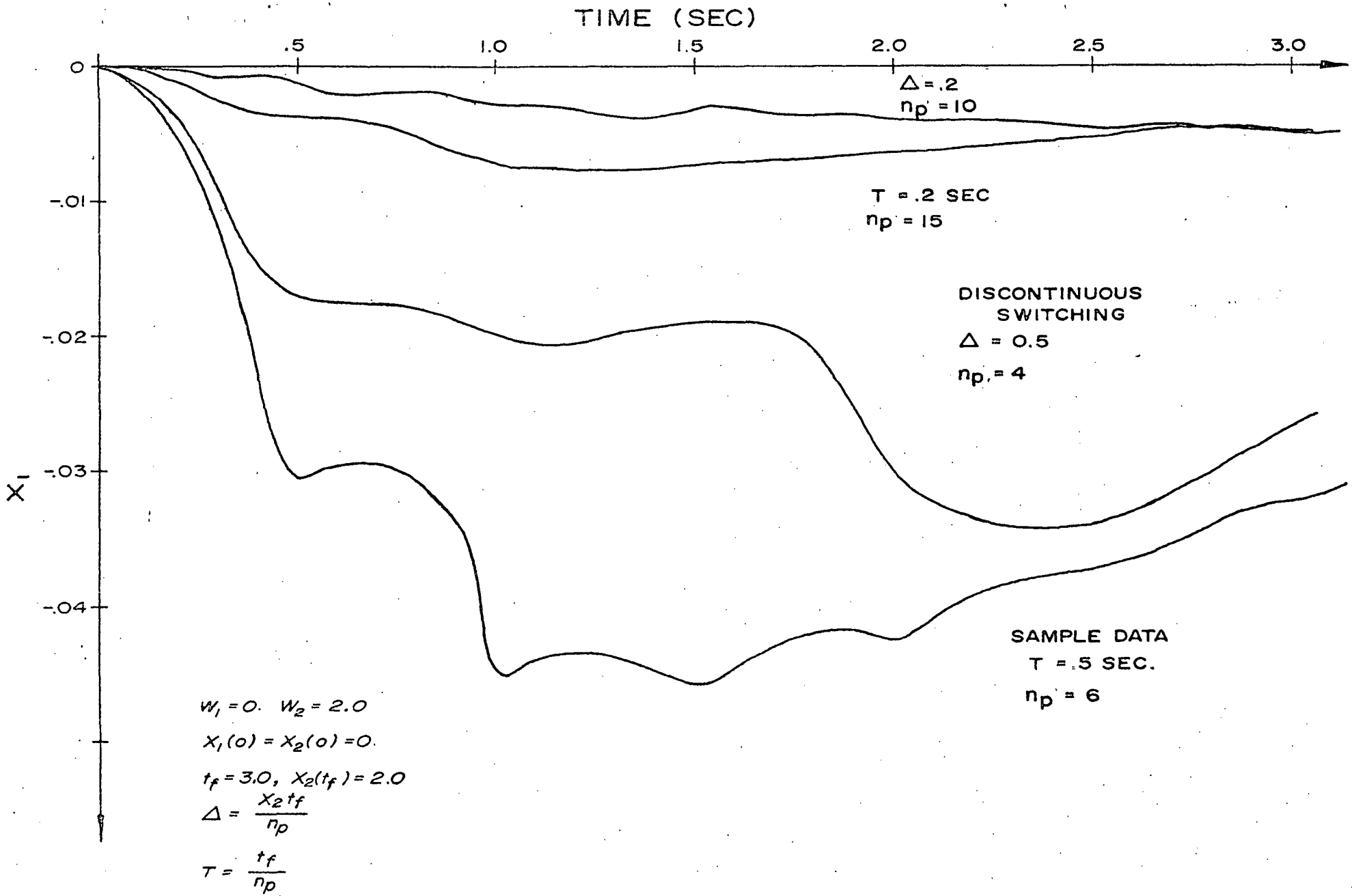

Fig. V 2. COMPARISON OF DECOUPLING METHODS

Referring to Figure 2 it is apparent that with both methods as the number of operating points used increases, the error, or undesired output, X_2, decreases. Of the two methods described, discontinuous switching exhibits the least error even though it has fewer operating points (4 versus 6 for $\Delta = T = .5$). The method of discontinuous switching is more effective because operating point switching is done between operating points minimizing the error away from the operating points due to linearization. Discontinuous switching has the disadvantage of being more difficult to mechanize, particularly for complex higher order systems where the higher derivatives of the outputs would be needed to specify the switching point. A knowledge of the steady state value of the state variables is also necessary to ensure that the last operating point corresponds to the desired plant output.

4.1 Generalized Procedure for Decoupling

The following summarizes step by step the procedure for linearization and decoupling:

1) Linearization of the nonlinear equations which represent the system model at unspecified operating points: $\bar{X}_0$, $\bar{u}_0$.

2) Formation of the perturbation equations and converting to a matrix representation

3) Application of the Wolovich-Falb synthesis procedure for decoupling to the linearized model.

4) Solving for the input variable operating points from the following equations:

$$f_i\big|_{o.p.} = 0$$

or

$$f_i\big|_{o.p.} = \text{desired system response}$$

5) Specification of the number of operating points required and the method of updating the decoupling controller.

5. Application to the DSRV Equations

Ignoring thruster dynamics and suppressing motion in the pitch, heave, yaw and sway degrees of freedom, the roll-surge equations are given by:

$$f_1 = \dot{P} = -.444\phi - .0443pu - .781|P|P + .0125n^2 - 1.54\times10^{-4}un - .958\times10^{-4}u^2 + 1.05\times10^{-4}w \quad (17)$$

$$\dot{\phi} = P \quad (18)$$

$$f_2 = \dot{u} = -4.55\times10^{-3}u^2 + 1.68n^2 - .0129un \quad (19)$$

where: P = roll rate (rad/sec)

ϕ = roll angle (rad)

u = forward velocity (ft/sec)

n = propellor speed (rev/sec)

w = weight of mercury in ballast tanks contributing to voll torque (lbs)

After linearization and substitution the perturbation equations are

$$\dot{\Delta p} = K_1\Delta p - .444\Delta\phi + K_2\Delta u + \Delta w' + K_3\Delta n \quad (20)$$

$$\dot{\Delta\phi} = \Delta p \quad (21)$$

$$\dot{\Delta u} = K_5\Delta u + K_4\Delta n \quad (22)$$

$$\text{where } K_1 = \left.\frac{\partial f_1}{\partial p}\right|_{o.p.} = -.0443u_0 - 1.562|P_0|$$

$$K_2 = \left.\frac{\partial f_1}{\partial u}\right|_{o.p.} = -.0443P_0 - 1.54\times10^{-4}n_0 - 1.916\times10^{-4}u_0$$

$$K_3 = \left.\frac{\partial f_1}{\partial n}\right|_{o.p.} = .025n_0 - 1.54\times10^{-4}u_0$$

$$K_4 = \left.\frac{\partial f_2}{\partial n}\right|_{o.p.} = .336n_0 - .0129u_0$$

$$K_5 = \left.\frac{\partial f_2}{\partial u}\right|_{o.p.} = -9.1\times10^{-3}u_0 - .0129n_0$$

$$\Delta w' = 1.05\times10^{-4}\Delta w$$

Writing this in matrix form yields:

$$\begin{bmatrix}\dot{\Delta P}\\ \dot{\Delta\phi}\\ \dot{\Delta u}\end{bmatrix} = \begin{bmatrix}K_1 & -.444 & K_2\\ 1 & 0 & 0\\ 0 & 0 & K_5\end{bmatrix}\begin{bmatrix}\Delta P\\ \Delta\phi\\ \Delta u\end{bmatrix} + \begin{bmatrix}1 & K_3\\ 0 & 0\\ 0 & K_4\end{bmatrix}\begin{bmatrix}\Delta w'\\ \Delta n\end{bmatrix}$$

$$\begin{bmatrix}\Delta Y_1\\ \Delta Y_2\end{bmatrix} = \begin{bmatrix}0 & 1 & 0\\ 0 & 0 & 1\end{bmatrix}\begin{bmatrix}\Delta P\\ \Delta\phi\\ \Delta u\end{bmatrix}$$

Applying the Wolovich-Falb Synthesis Procedure

$$C_1B = 0$$

$$C_1AB = [1 \quad K_3] \therefore d_1 = 1$$

$$C_2B = [0 \quad K_4] \therefore d_2 = 0$$

$$B^* = \begin{bmatrix}1 & K_3\\ 0 & K_4\end{bmatrix} \quad \therefore \quad |B^*| = K_4$$

Note that if $K_4 = 0$ the system will not decouple

i.e. if $u_0 = 26.25n_0$

Solving for the matrix F:

$$F = B^{*-1}\left[\sum_{k=0}^{\delta} m_k CA^k - A^*\right]$$

$$m_0 CA^0 = \begin{bmatrix} m_0^1 & 0 \\ 0 & m_0^2 \end{bmatrix}\begin{bmatrix} 0 & 1 & 0 \\ 0 & 0 & 1 \end{bmatrix} = \begin{bmatrix} 0 & m_0^1 & 0 \\ 0 & 0 & m_0^2 \end{bmatrix}$$

$$m_1 CA = \begin{bmatrix} m_1^1 & 0 \\ 0 & 0 \end{bmatrix}\begin{bmatrix} 0 & 1 & 0 \\ 0 & 0 & 1 \end{bmatrix}\begin{bmatrix} K_1 & -.444 & K_2 \\ 1 & 0 & 0 \\ 0 & 0 & K_5 \end{bmatrix}$$

$$= \begin{bmatrix} m_1^1 & 0 & 0 \\ 0 & 0 & 0 \end{bmatrix}$$

$$A^* = \begin{bmatrix} K_1 & -.444 & K_2 \\ 0 & 0 & K_5 \end{bmatrix}$$

$$G = B^{*-1} = \begin{bmatrix} 1 & \frac{K_3}{K_4} \\ 0 & 1/K_4 \end{bmatrix}$$

$$F = \begin{bmatrix} 1 & -\frac{K_3}{K_4} \\ 0 & 1/K_4 \end{bmatrix}\begin{bmatrix} m_1^1 & m_0^1 & 0 \\ 0 & 0 & m_0^2 \end{bmatrix} - \begin{bmatrix} K_1 & -.444 & K_2 \\ 0 & 0 & K_5 \end{bmatrix}$$

$$\begin{bmatrix} (m_1^1 - K_1) & (m_0^1 + .444) & (-K_2 - K_3/K_4[m_0^2 + K_5]) \\ 0 & 0 & (m_0^2 - K_5)/K_4 \end{bmatrix}$$

Solving for $\Delta w'$ and Δn from the equation $\bar{u} = F\bar{X} + G\bar{w}$

$$\Delta w' = (m_1 - K_1)\,\Delta P + (m_0^1 + .444)\Delta\phi - \left[K_2 + \frac{K_3}{K_4}(m_0^2 - K_5)\right]\Delta u + \Delta w_1 - \frac{C_3}{C_4}\Delta w_2$$

$$\Delta n = \frac{1}{C_4}(m_0^2 - C_5)\,\Delta u + \frac{1}{C_4}\Delta w_2$$

To obtain the operating point values (w_0', n_0)

$$f_1\big|_{o.p.} = m_1'P_0 + m_0^1\phi_0 + w_{10} \tag{23}$$

From which

$$w_0' = .444\phi_0 + .0443P_0u_0 + .781P_0|P_0| - .0125n_0^2 + 1.54\times10^{-4}u_0n_0$$

$$+ .958\times10^{-4}u_0^2 + m_1'P_0 + m_0'\phi_0 + w_{10} \tag{24}$$

and

$$f_2\big|_{o.p.} = m_0^2u_0 + w_{20} \tag{25}$$

$$n_0 = \frac{.0129u_0 \pm \sqrt{(.0129u_0)^2 + .672(4.55\times10^{-3}u_0^2 + m_0^2u_0 + w_{20})}}{.336}$$

For a stable decoupled system $m_0^2 < 0$, m_0^2 must be sufficiently small so the quantity under the square root sign is always positive.

The decoupled roll-surge equations were simulated using the two previous methods of switching and operating point selection. Figure 3 shows the roll response for a number of simulations where the DSRV is given a surge command of 3 ft/sec, the system being initially at rest. Comparison of the coupled response with the decoupled response shows that both time and state variable updating require a large number of linearized operating points to significantly reduce the amount of coupling below the magnitude of the coupled response.

It is important to note that if an exact solution exists for the linearized system input variable operating points, u_0 and n_0, then decoupling and pole placement should also be possible by solving the system equations for u and n and using nonlinear state variable feedback. The solution for u and n is the same as for u_0 and n_0. This method is covered in the next section.

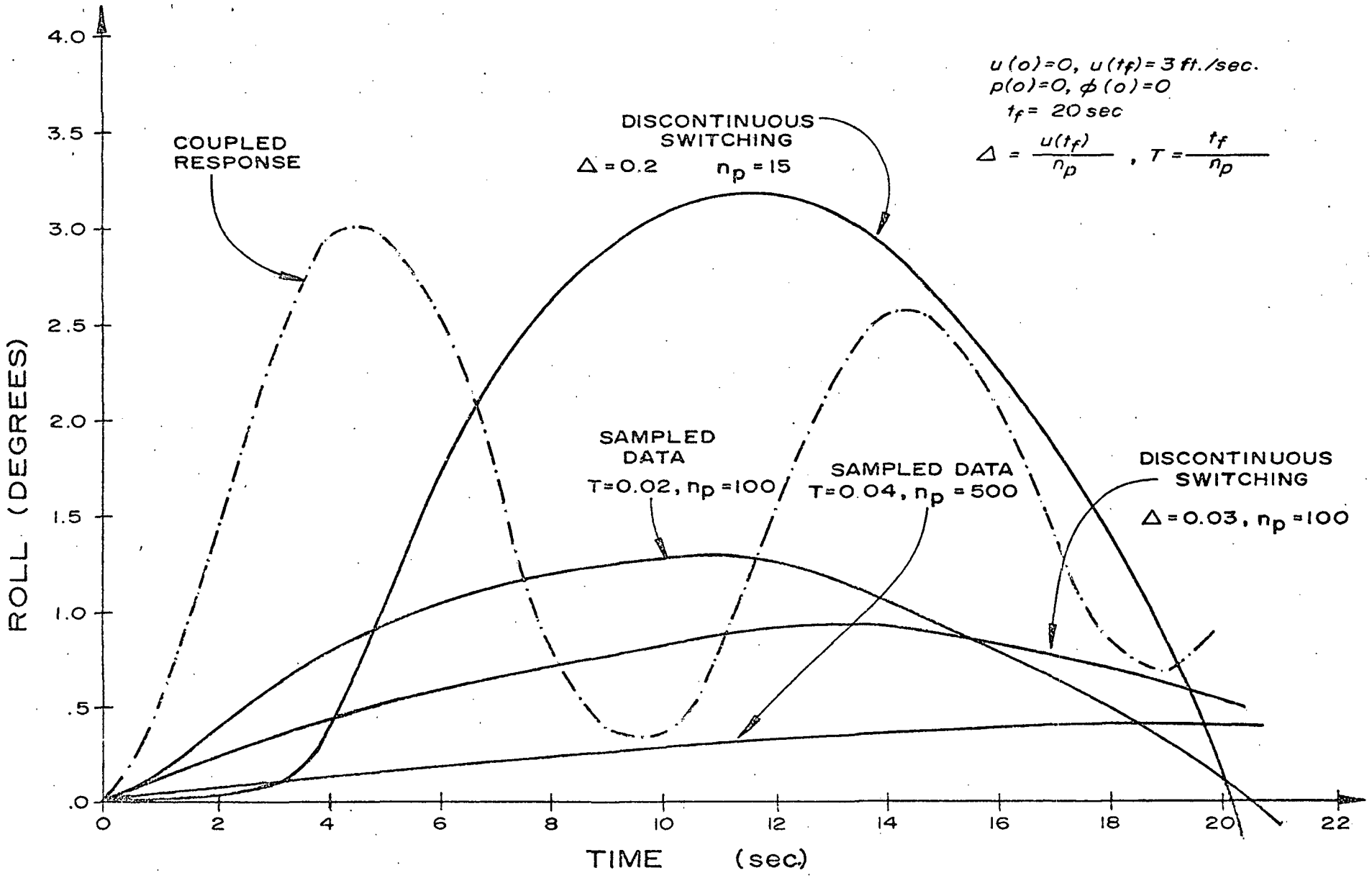

Fig. V 3 EFFECT ON ROLL OF LINEARIZED DECOUPLING

Decoupling By Subtraction of Terms

As long as the nonlinear equations are factorable with real roots the following design method can be used to both linearize and decouple nonlinear systems.

Given the DSRV equations the desired decoupled system response could be specified by the equations:

$$\dot{P} = m_1^1 P + m_0^1 \phi + w_1 \tag{26}$$

$$\dot{u} = m_0^2 u + w_2 \tag{27}$$

Equating the right side of equations (26) and (17), and solving for the input yields:

$$w^1 = m_1^1 P + (m_0^1 + .444)\phi + .0443pu + .781P|P| - .0125n^2 + 1.54\times10^{-4}un + .958\times10^{-4}u^2 + w_1 \tag{28}$$

Equating the right side of equations (27) and (19) yields:

$$.455\times10^{-3}u^2 + .168n^2 - .0129un = m_0^2 u + w_2 \quad \text{or}$$

$$.168n^2 - .012un - 4.55\times10^{-3}u^2 - m_0^2 u - w_2 = 0 \tag{29}$$

Solving this for n yields:

$$n = \frac{.0129u \pm \sqrt{(.0129u)^2 + .672(4.55\times10^{-3}u^2 + m_0^2 u + w_2)}}{.336}$$

A solution will exist so long as the result is real.

For $w_2 < 0$ and $t = 0^+$, the expression under the square root sign will be negative; however, the equation used describes forward motion only and $w_2 > 0$ for this case.

The term $m_0^2 u$ is the only negative term and as long as m_0^2 is chosen sufficiently small the solution will still be real.

This was simulated using one of the roots for n and $m_0^2 = -.2$. The system decoupled perfectly for several magnitudes of input w_2. Both sets of equations behaved in a linear manner as well.

APPENDIX VI

DECOUPLING BY SUBTRACTION

The subtraction method can be best illustrated by an example. Consider the following non-linear coupled equations.

$$\dot{x}_1 = x_1^2 + x_1x_2 + 1.5u_1 + u_2^2$$

$$\dot{x}_2 = 2x_1x_2 + u_1 + 2u_2$$

It is desired to make the system behave as follows:

$$\dot{x}_1 = x_{1c} - x_1$$

$$\dot{x}_2 = x_{2c} - x_2$$

Equate the equations for $\dot{x}_1$ and $\dot{x}_2$:

$$x_{1c} - x_1 = x_1^2 + x_1x_2 + 1.5u_1 + u_2^2$$

$$x_{2c} - x_2 = 2x_1x_2 + u_1 + 2u_2$$

Solve for the old inputs:

$$u_1 = \frac{1}{1.5}\left[x_{1c} - x_1 - x_1^2 - x_1x_2 - u_2^2\right]$$

$$u_2 = \frac{1}{2}\left[x_{2c} - x_2 - 2x_1x_2 - u_1\right]$$

These inputs will decouple the original system. Suppose that u_1 and u_2 are not the real inputs to the system, but have transfer characteristics $u_1(s)$, $u_2(s)$ associated with them such that the real inputs are u_{1c} and u_{2c}

$$u_1 = u_1(s)u_{1c} \quad , \quad u_2 = u_2(s)u_{2c}$$

The system can still be decoupled with proper compensation. Consider the previous example with $u_1(s)$ and $u_2(s)$ defined as follows:

$$u_1(s) = \frac{1}{1+s} \quad , \quad u_2(s) = \frac{1}{(1+.7s)(1+.2s)}$$

Solving for u_{1c} and u_{2c} we obtain:

$$u_{1c} = \frac{(1+s)}{1.5}\left[x_{1c} - x_1 - x_1^2 - x_1x_2 - u_2^2\right]$$

$$u_{2c} = \frac{(1+7s)(1+.2s)}{2}\left[x_{2c} - x_2 - 2x_1x_2 - u_1\right]$$

To determine u_{1c} and u_{2c} the indicated differentiations must be performed. Derivatives of x_{1c} and x_{2c} are undesirable. The easiest solution would be to compensate x_{1c} and x_{2c} i.e.

replace x_{1c} by $u_1(s)x_{1c}$

replace x_{2c} by $u_2(s)x_{2c}$

The equations with the new x_{1c} and x_{2c} are:

$$u_{1c} = \frac{x_{1c}}{1.5} + \frac{1+s}{1.5}\left(-x_1 - x_1^2 - x_1x_2 - u_2^2\right)$$

$$u_{2c} = \frac{x_{2c}}{2} + \frac{(1+.7s)(1+.2s)}{2}\left(-x_2 - 2x_1x_2 - u_1\right)$$

Look at $u_1(s)$ and $u_2(s)$ again

$$(1 + s)u_1 + u_{1c}$$

$$\text{or } su_1 = u_{1c} - u_1$$

$$(1+.7s)(1+.2s)u_2 = u_{2c}$$

$$\text{or } s^2u_2 = \frac{1}{.14}\left(u_{2c} - u_2 - .9su_2\right)$$

$$\text{or } su_2 = \frac{1}{.14}\left(\frac{u_{2c} - u_2}{s} - .9u_2\right)$$

Now perform the indicated differentiation in the first equation.

$$u_{1c} = \frac{x_{1c}}{1.5} + \frac{1}{1.5}\left(-x_1 - x_1^2 - x_1x_2 - u_2^2\right) + \frac{s}{1.5}\left(-x_1 - x_1^2 - x_1x_2 - u_2^2\right)$$

however,

$$\frac{s}{1.5}\left(-x_1 - x_1^2 - x_1x_2 - u_2^2\right) = \frac{-1}{1.5}\left[\dot{x}_1 + 2x_1\dot{x}_1 + (\dot{x}_1x_2 + \dot{x}_2x_1) + 2u_2\dot{u}_2\right]$$

$\dot{x}_1$, $\dot{x}_2$, and $\dot{u}_2$ are available in terms of the other state variables. The actual substitution will not be performed, but should be obvious. Two differentiations must be performed to determine u_{2c}. The only term which will cause a difficulty will be u_1: i.e.

$$u_{2c} = \frac{1}{2}(1 + .9s + .14s^2)(- x_2 - 2x_1x_2 - u_1)$$

u_1 must be compensated to avoid differentiating an input variable. Therefore, change $u_1(s)$:

that is replace $u_1(s)$ by $\frac{1}{(1+s)(1+.2s)}$

This will involve both expressions, the one for u_{1c} and u_{2c}, but the reasoning involved should be apparent. The final result will not be given, but the method of achieving that result should be clear. The example was given to motivate the following sufficient conditions for subtraction of terms.

I. Specify a set of decoupled equations.

II. Equate the two sets of equations.

III. If it is possible to solve for the old inputs in terms of the other variables, the system can be decoupled.

If the inputs to the coupled equations have transfer functions associated with them, as long as the equations are differentiable, the system can be decoupled with proper compensation. This compensation is necessary to avoid derivatives of command values.

Subtraction Decoupling Theory Applied to the DSRV

Consider the forward motion of a submersible. The acceleration of the vehicle requires a change in the propeller speed, which also produces a torque causing an undesired rolling movement. To counteract this torque, mercury may be pumped between tanks to balance the torque of the propeller. The motion of the submersible is decoupled when the roll angle and forward speed can be independently controlled.

The simplified equations of motion of the DSRV for roll and surge alone are, from the Lockheed Report (Ref. 1):
Only terms including roll and surge have been kept.

SURGE: $u \geq 0,\ n \geq 0$

$$4507\dot{u} = 755n^2 - 58un - 20.5u^2$$

PUMP DYNAMICS: $$W = \int_0^t \dot{W} dt \quad , \quad \dot{W} = \frac{\dot{W}_c}{1+.083s}$$

ROLL: $$42330\dot{p} = -18740\phi - 1870pu - 33000p|p| + 4.42W + 530n^2 - 6.5un - 4.05u^2 + 131\dot{n}$$

PROPELLER DYNAMICS: $$n = \frac{(1+.49s)N_c}{(1+.7s)(1+.245s)}$$

Definition of terms:

u = Surge Velocity

$\dot{u}$ = Surge Acceleration

ϕ = Roll Angle

p = Roll Rate

$\dot{p}$ = Angular Acceleration

W = Difference in Weight of Mercury Trim Tanks

$\dot{W}$ = Pumping Rate

$\dot{W}_c$ = Command Pumping Rate

n = Propeller Speed

$\dot{n}$ = Rate of Change of Propeller Speed

N_c = Command Propeller Speed

The equations of motion were simulated by Tawari (Ref. 7) using a fortran program. For this simplified model the control could be more easily simulated using a CSMP program. Both programs gave the same results for the uncontrolled case. These results indicated the DSRV behaved as an underdamped system with a roll period of 9.5 seconds, and maximum roll angle of 3.1^{o} for a propeller step input of 1 rev/sec.

Suppose it is desired to maintain a zero roll angle for various propeller speeds. Look at the roll equation and assume that the roll angle is zero. The following equation results:

$$4.42W + 530n^2 - 6.5un - 4.05u^2 + 131\dot{n} = 0 \qquad (1)$$

Solve for W:

$$W = \frac{1}{4.42}\left(-530n^2 + 6.5un + 4.05u^2 - 131\dot{n}\right) \qquad (2)$$

Assuming a pump transfer function of the form: $W = \frac{W_c}{1+.083s}$, and setting W_c equal to the W in equation 2, results in a tenfold reduction of coupling. However, as will be shown later, the maximum pumping rate of 54.3#/sec. will probably be exceeded.

Return to the propeller transfer function

$$(.1715s^2 + .945s + 1)n = (1 + .49s)N_c$$

$$\dot{n} = sn = -\frac{(1+.945s)}{s}n + \left(\frac{1+.49s}{s}\right)N_c$$

Substitute for W and $\dot{n}$ in equation (1)

$$4.42\,\frac{\dot{W}_c}{s(1+.083s)} + 530n^2 - 6.5un - 4.05u^2 + 131\left(-\left[\frac{1+.945s}{s}\right]n + \frac{1+.49s}{s}\,N_c\right) = 0$$

Solve for N_c and perform any necessary differentiations.

$$N_c = \frac{1}{131}\left[-\frac{4.42\dot{W}_c}{(1+.083s)(1+.49s)}\right] + \frac{1+.945s}{1+.49s}\,n$$

$$-\frac{1}{1+.49s}\left[2{\cdot}530n\dot{n} - 6.5(u\dot{n}+\dot{u}n) - 2{\cdot}4.05u\dot{u}\right]$$

Notice that N_c is a sum of parameters which can be measured or generated Because N_c is now a function of the pumping rate, the maximum pumping rate will not be exceeded. In this case a certain pumping rate determined the propeller speed which moved to DSRV. The following diagrams indicate what is happening

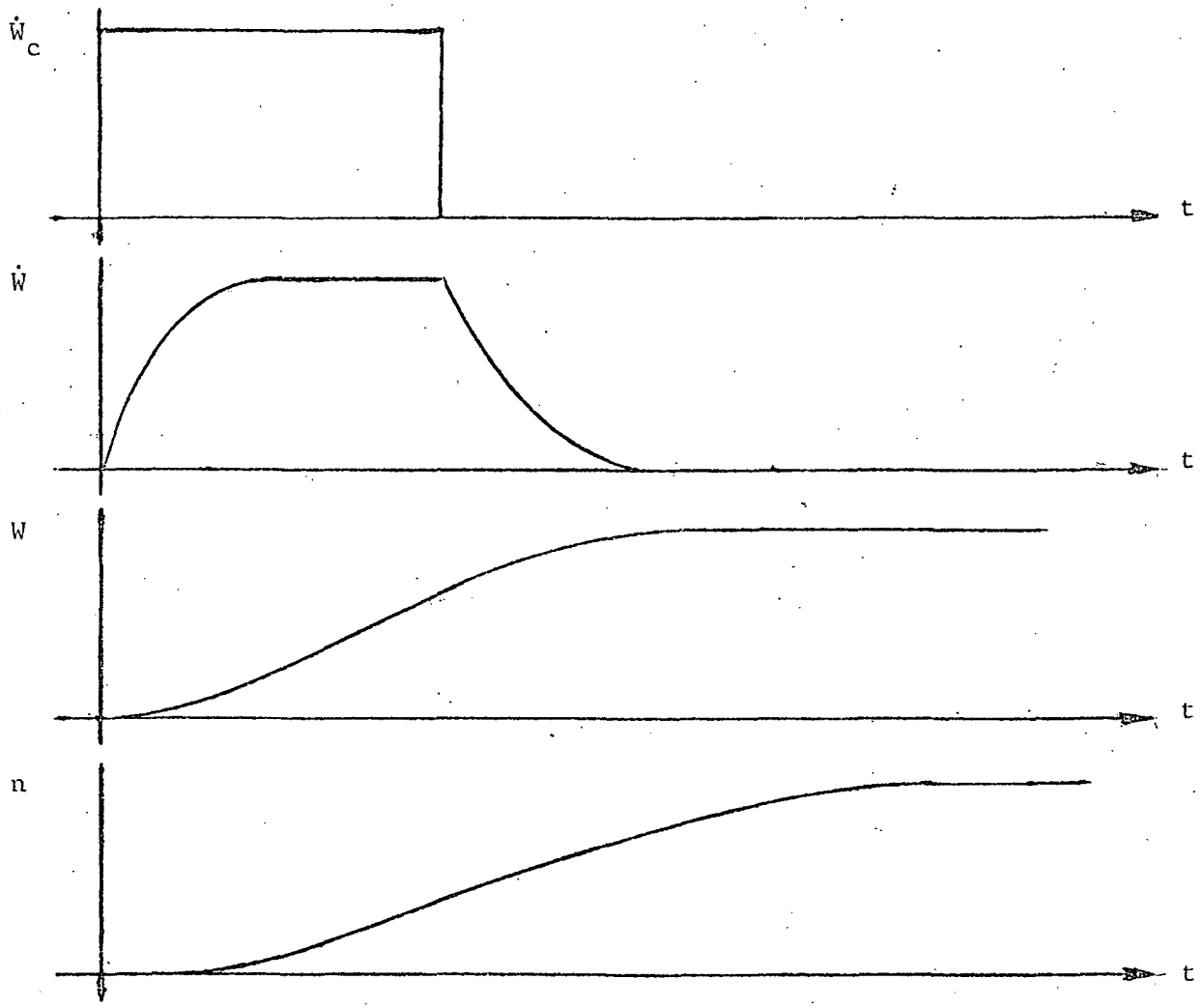

The computer simulation proved that the roll angle remained zero. See figure "DSRV: ROLL-SURGE DECOUPLING" on the following page.

The system cannot be considered truly decoupled until the roll angle and the forward speed can be independently controlled. Suppose it is desired to have roll behave as an ordinary second order system:

equate the two expressions for $\dot{p}$

$$K(p_c-p) = \frac{1}{42330}\,(-18740\phi-1870pu-33000p|p|+4.42W+530n^2-6.5un-4.05u^2+131\dot{n})$$

Lump all of the non-linearities together as a disturbance:

$$K(p_c-p) = \frac{1}{42330}\,(4.42W + \text{Dist.})$$

solve for W:

$$W = \frac{42330\cdot K}{4.42}\,(p_c-p) - \text{Dist}$$

As K is increased, the relative magnitude of the disturbance becomes small. If $P_c = 0$, the equation becomes approximately, for large K:

$$W = -(\frac{42330}{4.42})p$$

$$\text{or } \dot{W} = -\frac{42330}{4.42}\,\dot{p}$$

A simulation was performed assuming $\dot{W}_c = \dot{W}$, and the results showed a decrease in coupling, but also large values for $\dot{W}$, making implementation difficult. A practical decoupling scheme might involve a combination of different appraches.

DSRV: ROLL-SURGE DECOUPLING

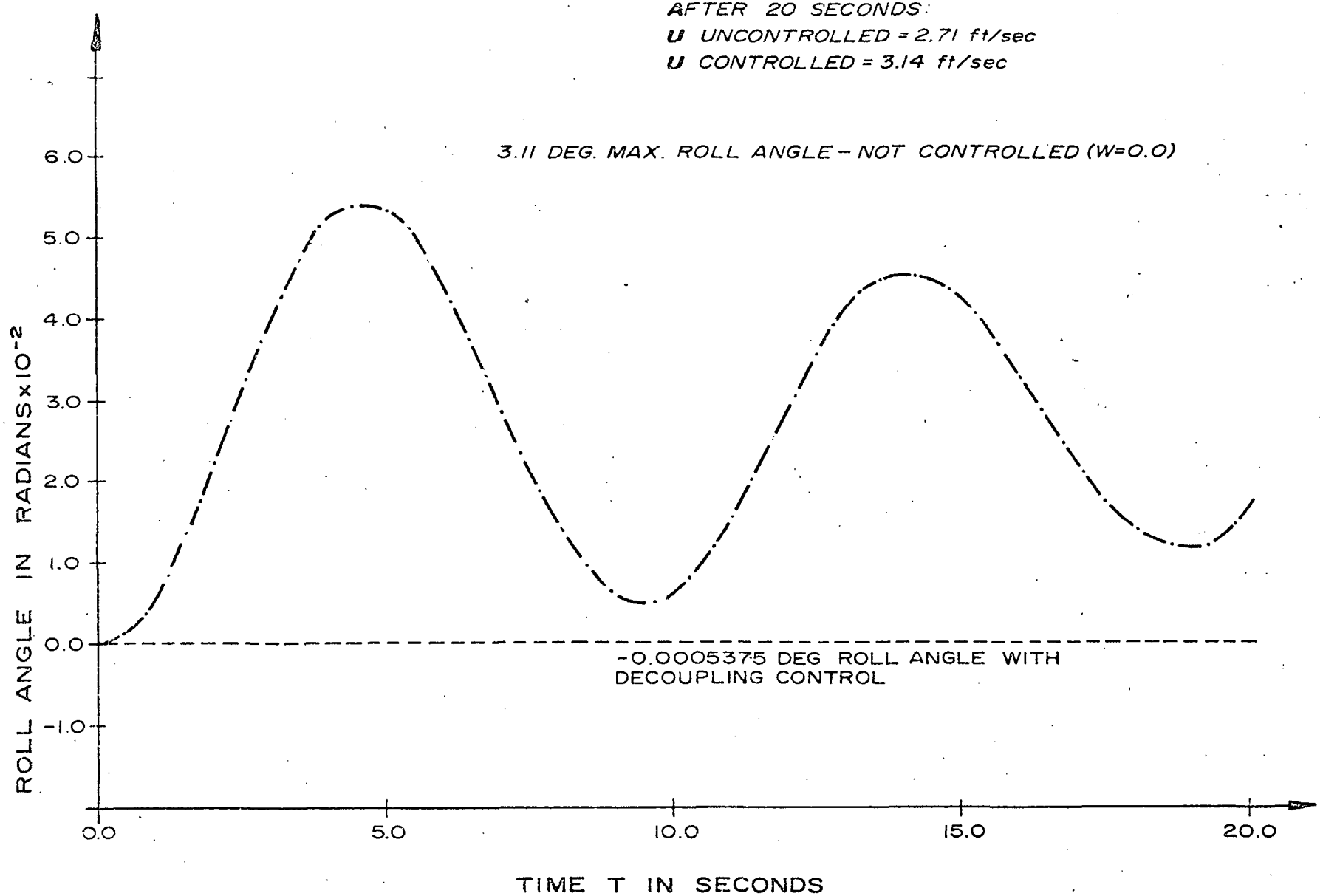

ESTABLISHING SUFFICIENT CONDITIONS FOR THE DECOUPLING AND SYNTHESIS OF CERTAIN NON-LINEAR SYSTEMS

Introduction

The decoupling of linear systems by state-variable feedback has been considered by several authors. (1)-(3) The work reported herein extends the definitions of Falb-Wolovich (1) and Freund (2) in an appropriate manner to decouple a larger class of non-linear systems. The paper supplies sufficient conditions for decoupling, a synthesis procedure, and some illustrative examples.

Definitions

The class of systems to be considered is described by the pair of vector equations

$$\dot{x} = A(x)x + B(x,u)u$$

$$y = C(x)x \qquad (1)$$

where u is the input vector of dimension m, y is the output vector of dimension m, and x is the state vector of dimension n.

The matrices A, B, and C are n×n, n×m, and m×n matrices. Furthermore, the individual terms of the A and C matrices may be differentiable functions of the state variable x, and components of the B matrix may be functions of x and u. Feedback will be of the form

$$u = F(x,u)x + G(x,u)w \qquad (2)$$

where F and G are m×n and m×m matrices with individual elements that may turn out to be functions of x and u. This results in a system of the form:

$$\dot{x} = (A(x) + B(x,u)\ F(x,u))x + B(x,u)\ G(x,u)w \qquad (3)$$

$$y = C(x)x$$

Figure 1 pictorially depicts the original system with feedback. The subscripts underneath the blocks represent the dimensions of the matrices. Note that both x and u are available for feedback or compensation.

The Separation of Variables

Notation: A capital letter followed by variables in parentheses represents a matrix whose elements are functions of the variables in parentheses. The meaning of the superscript (j) on K and L is developed below and is given explicitly by Equations (22) and (23). $K_i(x)$ means the ith row of $K(x)$.

Theorem I: If the relation

$$y_i^{(j)} = K_i^{(j)}(x)x \tag{4}$$

is satisfied, then

$$\frac{d}{dt} y_i^{(j)} \equiv y_i^{(j+1)} = K_i^{(j+1)}(x)x + L_i^{(j+1)}(x,u)u \tag{5}$$

Proof: Assume $y_i^{(j)} = K_i^{(j)}(x)x$ (6)

then

$$y_i^{(j+1)} = (\frac{d}{dt} K_i^{(j)}(x))x + K_i^{(j)}(x)\dot{x}$$

$$= (\frac{d}{dt} K_i^{(j)}(x))x + K_i^{(j)}(x)(A(x)x + B(x,u)u). \tag{7}$$

Examine the row vector $\frac{d}{dt} K_i^{(j)}(x)$:

$$(\frac{d}{dt} k_{i1}^{(j)}(x), \frac{d}{dt} k_{i2}^{(j)}(x), \ldots, \frac{d}{dt} k_{i_n}^{(j)}(x)) \tag{8}$$

Now examine an individual element of this row vector, say $\frac{d}{dt} k_{i\ell}^{(j)}(x)$

$$\frac{d}{dt} k_{i\ell}(x) = \frac{\partial k_{i\ell}^{(j)}}{\partial x_1}\dot{x}_1 + \frac{\partial k_{i\ell}^{(j)}}{\partial x_2}\dot{x}_2 + \ldots + \frac{\partial k_{i\ell}^{(j)}}{\partial x_n}\dot{x}_n \tag{9}$$

where it is understood that $k_{i\ell}^{(j)} \equiv k_{i\ell}^{(j)}(x)$.

From Equation (1), $\dot{x}_i = A_i(x)x + B_i(x,u)u.$ (10)

Substituting Equation (10) into (9)

$$\frac{d}{dt} k_{i\ell}(x) = \frac{\partial k_{i\ell}^{(j)}}{\partial x_1} (A_1(x)x + B_1(x,u)u + \frac{\partial k_{i\ell}^{(j)}}{\partial x_2} (A_2(x)x$$

$$+ B_2(x,u)u + \ldots + \frac{\partial k_{i\ell}^{(j)}}{\partial x_n} (A(x)x + B_n(x,u)u$$

$$= \left[\sum_{\gamma=1}^{n} \frac{\partial k_{i\ell}^{(j)}}{\partial x_\gamma} A_\gamma(x)\right] x + \left[\sum_{\gamma=1}^{n} \frac{\partial k_{i\ell}}{\partial x_\gamma} B_\gamma(x,u)\right] u \quad (11)$$

define: $$\alpha_{i\ell}^{(j)}(x) = \sum_{\gamma=1}^{n} \frac{\partial k_{i\ell}}{\partial x_\gamma} A_\gamma(x) \quad (12)$$

$$\beta_{i\ell}^{(j)}(x,u) = \sum_{\gamma=1}^{n} \frac{\partial k_{i\ell}}{\partial x_\gamma} B_\gamma(x,u) \quad (13)$$

Note: $\alpha_{i\ell}^{(j)}(x)$ and $\beta_{i\ell}^{(j)}(x,u)$ are n and m - dimensional row vectors respectively.

Then $$\frac{d}{dt} k_{i\ell}^{(j)}(x) = \alpha_{i\ell}^{(j)}(x)x + \beta_{i\ell}^{(j)}(x,u)u \quad (14)$$

and $$\frac{d}{dt} K_i^{(j)}(x) = (\alpha_{i1}^{(j)}(x)x + \beta_{i1}^{(j)}(x,u)u,\ \alpha_{i2}^{(j)}(x)x + \alpha_{i2}^{(j)}(x,u)u,$$

$$\ldots,\ \alpha_{in}^{(j)}(x)x + \beta_{in}^{(j)}(x,u)u) \quad (15)$$

giving $$\frac{d}{dt} K_i^{(j)}(x)x = (\alpha_{i1}^{(j)}(x)x,\ \alpha_{i2}^{(j)}(x)x,\ \ldots,\ \alpha_{in}^{(j)}(x)x)x \quad (16)$$

$$+ (\beta_{i1}^{(j)}(x,u)u,\ \beta_{i2}^{(j)}(x,u)u,\ \ldots,\ \beta_{in}^{(j)}(x,u)u)x$$

Examine the second term and rearrange to separate out the u vector

$$(\beta_{i1}^{(j)}(x,u)u,\ \beta_{i2}^{(j)}(x,u)u,\ \ldots,\ \beta_{in}^{(j)}(x,u)u)x$$

$$= x_1\beta_{i1}^{(j)}(x,u)u + x_2\beta_{i2}^{(j)}(x,u)u + \ldots + x_n\beta_{in}^{(j)}(x,u)u$$

$$= (x_1\beta_{i_1}^{(j)}(x,u) + x_2\beta_{i_2}^{(j)}(x,u) + \ldots + x_n\beta_{in}^{(j)}(x,u)u \qquad (17)$$

Define:

$$R_i^{(j)}(x) = (\alpha_{i1}^{(j)}(x)x,\ \alpha_{i2}^{(j)}(x)x,\ \ldots,\ \alpha_{in}^{(j)}(x)x) \qquad (18)$$

$$S_i^{(j)}(x,u) = x_1\beta_{i1}^{(j)}(x,u) + x_2\beta_{i2}^{(j)}(x,u) + \ldots + x_n\beta_{in}^{(j)}(x,u) \qquad (19)$$

Then: $$\frac{d}{dt}K_i^{(j)}(x)x = R_i^{(j)}(x)x + S_i^{(j)}(x,u)u \qquad (20)$$

thus, $$y_i^{(j+1)} = R_i^{(j)}(x)x + S_i^{(j)}(x,u)u + K_i^{(j)}(x)(A(x)x + B(x,u)u)$$

grouping common terms in x and u gives:

$$(R_i^{(j)}(x) + K_i^{(j)}(x)A(x))x + (S_i^{(j)}(x,u) + K_i^{(j)}(x)B(x,u))u \qquad (21)$$

define: $$K_i^{(j+1)}(x) = R_i^{(j)}(x) + K_i^{(j)}(x)A(x) \qquad (22)$$

$$L_i^{(j+1)}(x,u) = S_i^{(j)}(x,u) + K_i^{(j)}(x)B(x,u) \qquad (23)$$

then $$y_i^{(j+1)} = K_i^{(j+1)}(x)x + L_i^{(j+1)}(x,u)u \qquad (24)$$

The theorem is proved.

Corollary: The output Y_i may be differentiated until $L_i^{(j)}(x,u) \neq 0$

Proof: from eq. (1) $y_i = C_i(x)x$

define: $$K_i^{(0)}(x) = C_i(x) \qquad (25)$$

$$y_i = K_i^{(0)}(x)x \qquad (26)$$

The condition for the separation of variables is met, and the theorem is proven by induction:

$$\frac{d}{dt} y_i^{(0)} = y_i^{(1)} = K_i^{(1)}(x)x + L_i^{(1)}(x,u)u \tag{27}$$

if $L_i^{(1)}(x,u)u = 0$, the process may be repeated. It is entirely possible that $L_i^{(j)}(x,u) = 0$ for all j. The point is that $L_i^{(j)}(x,u) \neq 0$ may not necessarily be differentiable and, thus, differentiating y_i beyond that point may not be possible. This corollary motivates the definitions in the following section.

Definitions

$$\rho_i \equiv \min \{j : L_i^{(j)}(x,u) \neq 0,\ j = 0, 1, \ldots\}$$

$$\equiv 0 \text{ if } L_i^{(j)}(x,u) = 0 \text{ for all } j \tag{28}$$

$$L_i^{(0)}(x,u) \equiv 0 \tag{29}$$

$$D_i(x,u) \equiv L_i^{(\rho_i)}(x,u),\ i = 1,2, \ldots, m \tag{30}$$

$$y_i^* \equiv y_i^{(\rho_i)} \quad ,\ i = 1,2, \ldots, m \tag{31}$$

$$K_i^*(x) \equiv K_i^{(\rho_i)}(x) \quad ,\ i = 1,2, \ldots, m \tag{32}$$

The system is decoupled if, with appropriate feedback,

$$y = Q(s)w \tag{33}$$

such that $Q(s)$ is diagonal and nonsingular.

Decoupling Theorem

Define the space H as the set of points of x and u for which the matrix D(x,u) is nonsingular. Then the system:

$$\dot{x} = A(x)x + B(x,u)u$$

$$y = C(x)x$$

can be decoupled on H by the proper selection of feedback matrices F(x,u) and G(x,u).

Proof: By substituting Equations (30), (31) and (32) into (24):

$$y_i^{(\rho_i)} = K_i^{(\rho_i)}(x)x + L_i^{(\rho_i)}(x,u)u$$

or $$y^* = K^*(x)x + D(x,u)u \tag{34}$$

recall $$u = F(x,u)x + G(x,u)w$$

thus: $$y^* = (K^*(x) + D(x,u)F(x,u))x + D(x,u)G(x,u)w \tag{35}$$

Since D(x,u) is nonsingular on H, $D^{-1}(x,u)$ exists on H. A pair of matrices that decouples the system on H is:

$$G^*(x,u) = D^{-1}(x,u) \tag{36}$$

$$F^*(x,u) = -D^{-1}(x,u)K^*(x) \tag{37}$$

A more general class of decoupling matrices will be developed in the next section.

By substituting $G(x,u) = G^*(x,u)$ and $F(x,u) = F^*(x,u)$

$$y^* = w \tag{38}$$

or $$y_i^{\rho_i} = s^{\rho_i} y_i = w_i \quad i = 1, \ldots, m \tag{39}$$

$$y_i = \frac{1}{s^{\rho_i}} w_i \quad i = 1, \ldots, m \tag{40}$$

$$Q_i(s) = \frac{1}{s^{\rho_i}} \quad i = 1, \ldots, m \tag{41}$$

and the requirements of the definition for decoupling are met. Note that for constant coefficient matrices these results are identical to those of Falb and Wolovich.

The Synthesis Procedure

A synthesis procedure similar to that in the Falb and Wolovich paper will now be presented.

From the separation theorem, derivatives of the y_i^{th} output are available as functions of x up to the ρ_i-1 derivative. This motivates the following choice for the F matrix.

$$F(x,u) = D^{-1}(x,u)\left(\sum_{j=0}^{\delta} M^{(j)}P^{(j)}(x) - K^*(x)\right) \tag{42}$$

where: $\delta \equiv \max \rho_i - 1,\ i = 1, 2, \ldots, m$ (43)

$$P_i^{(j)}(x) = K_i^{(j)}(x),\ j < \rho_i$$
$$= 0 \qquad ,\ j \geq \rho_i \tag{44}$$

Assume $G(x,u) = D^{-1}(x,u)\Lambda$ (45)

such that Λ is a diagonal nonsingular m×m matrix.

The M^j are suitably chosen diagonal matrices. This results in the following form for the output.

$$\begin{aligned} y^* &= \{K^*(x) + D(x,u)[D^{-1}(x,u)(\sum_{j=0}^{\delta} M^{(j)}P^{(j)}(x) - K^*(x))]\}x \\ &\quad + D(x,u)\,D^{-1}(x,u)\Lambda w \\ &= [K^*(x) + \sum_{j=0}^{\delta} M^{(j)}P^{(j)}(x) - K^*(x)]x + \Lambda w \\ &= \sum_{j=0}^{\delta} M^{(j)}P^{(j)}(x)x + \Lambda w \end{aligned} \tag{46}$$

The $M^{(j)}$ are m × m diagonal matrices, and $P^{(j)}(x)$ are m × n matrices.

For instance: $M^{\circ}P^{\circ}(x)x = M^{\circ}C(x)x = M^{\circ}y$

Or, in general, from Theorem I and Equation (44),

$$M_i^{(j)}P^{(j)}(x)x = m_i^{(j)}y_i^{(j)} \qquad j < \rho_i \tag{47}$$

This results in

$$y_i^{(\rho_i)} = m_i^{(0)} y_i + m_i^{(1)} y_i^{(1)} + \ldots + m_i^{(\rho_i-1)} y_i^{(\rho_i-1)} + \lambda_i w \quad (48)$$

Figure two illustrates the additional compensation.

Numerical Examples

Example 1: Consider the system

$$A(x) = \begin{pmatrix} 1 & 1 & 0 \\ 0 & 2 & 0 \\ 0 & x_2 & 1 \end{pmatrix} \qquad B(x,u) = \begin{pmatrix} u_1 & 1 \\ -1 & 1 \\ 0 & 0 \end{pmatrix}$$

$$C(x) = \begin{pmatrix} 1 & 0 & 0 \\ 0 & 0 & 1 \end{pmatrix} \tag{49}$$

The output is differentiated to generate $K^*(x)$ and $D(x,u)$ (from $L_i^{(\bar{\rho}_i)}(x,u)$

$$y_1 = C_1 x = (1,\ 0,\ 0)x \tag{50}$$

$$y_1^{(1)} = \dot{C}_1 x + C_1 \dot{x} = C_1(A(x)x + B(x,u)u)$$

$$= (1,\ 1,\ 0)x + (u_1,\ 1)u \tag{51}$$

$$y_2 = C_2 x = (0,\ 0,\ 1)x \tag{52}$$

$$y_2^{(1)} = \dot{C}_2 x + C_2 \dot{x} = C_2(A(x)x + B(x,u)u$$

$$= (0,\ x_2,\ 1)x \tag{53}$$

$$y_2^{(2)} = (0,\ \dot{x}_2,\ 0)x + (0,\ x_2,\ 1)\dot{x}$$

$$= (0,\ 2x_2 - u_1 + u_2,\ 0)x + (0,\ x_2,\ 1)\ (A(x)x + B(x,u)u)$$

$$= (0,\ 5x_2,\ 1)x + (-2x_2, 2x_2)u \tag{54}$$

The parts of Equations (51) and (54) give:

$$K^*(x) = \begin{pmatrix} 1 & 1 & 0 \\ 0 & 5x_2 & 1 \end{pmatrix} \qquad D(x,u) = \begin{pmatrix} u_1 & 1 \\ -2x_2 & 2x_2 \end{pmatrix} \tag{55}$$

$$D^{-1}(x,u) = \frac{1}{2x_2(1+u_1)} \begin{pmatrix} 2x_2 & -1 \\ 2x_2 & u_1 \end{pmatrix} \tag{56}$$

D^{-1} is nonsingular for $x_2 \neq 0$, $u_1 \neq -1$

From Equation (37),

$$F^*(x,u) = \frac{1}{2x_2(1+u_1)} \begin{pmatrix} -2x_2 & 3x_2 & 1 \\ -2x_2 & -2x_2-5x_2u_1 & -u_1 \end{pmatrix} \tag{57}$$

Let $F(x,u) = F^*(x,u)$, $G(x,u) = D^{-1}(x,u)$, which results in

$$A(x) + B(x,u)F(x,u) = \begin{pmatrix} 0 & 0 & 0 \\ 0 & -\frac{1}{2} & -\frac{1}{2x_2} \\ 0 & x_2 & 1 \end{pmatrix} \tag{58}$$

$$B(x,u)\,G(x,u) = \begin{pmatrix} 1 & 0 \\ 0 & \frac{1}{2x_2} \\ 0 & 0 \end{pmatrix} \tag{59}$$

which gives the closed loop form of the system, Equation (3) as:

$$\dot{x}_1 = w_1 \tag{60}$$

$$\dot{x}_2 = -\frac{1}{2}x_2 - \frac{x_3}{2x_2} + \frac{1}{2x_2}w_2 \tag{61}$$

$$\dot{x}_3 = x_2^2 + x_3 \tag{62}$$

$$\begin{aligned} \ddot{x}_3 &= 2x_2\dot{x}_2 + \dot{x}_3 \\ &= 2x_2\left(-\frac{1}{2}x_2 - \frac{x_3}{2x_2} + \frac{w_2}{2x_2}\right) + x_2^2 + x_3 \\ &= w_2 \end{aligned} \tag{63}$$

Recall $y = Cx$ from Equation (49)

$$\dot{y}_1 = \dot{x}_1 = w_1$$

$$\ddot{y}_2 = \ddot{x}_3 = w_2$$

which is the decoupled system.

Note that the feedback matrices are not defined for $x_2(1+u_1) = 0$.

Example 2:

Consider the roll-surge equations for a submarine.

$$\dot{u} = C_1 u^2 + C_2 n^2 + C_3 un$$

$$\dot{\phi} = P$$

$$\dot{P} = K_1\phi + K_2 Pu + K_3 P|P| + K_4 W + K_5 n^2 + K_6 un + K_7 u^2 \qquad (64)$$

where

u = velocity in x direction (surge)

ϕ = roll angle about x-axis

P = angular velocity about x-axis

n = propellor speed

W = weight of mercury in trim tanks.

It is desired to decouple the roll and surge. In state variable form:

$$\begin{pmatrix} \dot{u} \\ \dot{\phi} \\ \dot{P} \end{pmatrix} = \begin{pmatrix} C_1 u & 0 & 0 \\ 0 & 0 & 1 \\ K_2 P + K_7 u & K_1 & K_3|P| \end{pmatrix} \begin{pmatrix} u \\ \phi \\ P \end{pmatrix}$$

$$+ \begin{pmatrix} C_2 n + C_3 u & 0 \\ 0 & 0 \\ K_5 n + K_6 u & K_4 \end{pmatrix} \begin{pmatrix} n \\ W \end{pmatrix} \quad ; \quad x \equiv \begin{pmatrix} u \\ \phi \\ P \end{pmatrix} \quad ; \quad v = \begin{pmatrix} n \\ w \end{pmatrix} \quad ; \quad w = \begin{pmatrix} u_c \\ \phi_c \end{pmatrix}$$

The outputs of interest are surge velocity and roll angle.

$$Y = \begin{pmatrix} 1 & 0 & 0 \\ 0 & 1 & 0 \end{pmatrix} \begin{pmatrix} u \\ \phi \\ P \end{pmatrix} \qquad (65)$$

$$Y_1 = (1, 0, 0)x \qquad (66)$$

$$\dot{Y}_1 = (C_1 u, 0, 0)x + (C_2 n + C_3 u, 0)v \qquad (67)$$

$$Y_2 = (0, 1, 0)x \qquad (68)$$

$$\dot{Y}_2 = (0, 0, 1)x \qquad (69)$$

$$y_2^{(2)} = (K_2P + K_7u,\ K_1,\ K_3|P|)x + (K_5n + K_6u,\ K_4)v \tag{70}$$

$$K^* = \begin{pmatrix} C_1u & 0 & 0 \\ K_2P+K_7u & K_1 & K_3|P| \end{pmatrix} \tag{71}$$

$$D = \begin{pmatrix} C_2n+C_3u & 0 \\ K_5n+K_6u & K_4 \end{pmatrix} \tag{72}$$

$$D^{-1} = \frac{1}{K_4(C_2n+C_3u)} \begin{pmatrix} K_4 & 0 \\ -K_5n-K_6u & C_2n+C_3u \end{pmatrix} \tag{73}$$

$$F^* = -D^{-1}K^* = \frac{1}{K_4(C_2n+C_3u)} \begin{pmatrix} -K_4C_1u & 0 & 0 \\ C_1u(K_5n+K_6u) - (K_2P + K_7u)(C_2n + C_3u) & -K_1(C_2n + C_3u) & -K_3|P|(C_2n + C_3u) \end{pmatrix} \tag{74}$$

Note that the system can be decoupled only if $K_4(C_2n + C_3u) \neq 0$. This choice of feedback will produce the following decoupled equations.

$$\begin{pmatrix} \dot{u} \\ \dot{\phi} \\ \dot{P} \end{pmatrix} = \begin{pmatrix} 0 & 0 & 0 \\ 0 & 0 & 1 \\ 0 & 0 & 0 \end{pmatrix} \begin{pmatrix} u \\ \phi \\ P \end{pmatrix} + \begin{pmatrix} 1 & 0 \\ 0 & 0 \\ 0 & 1 \end{pmatrix} \begin{pmatrix} u_c \\ \phi_c \end{pmatrix}$$

$$\dot{y} = \begin{pmatrix} 1 & 0 & 0 \\ 0 & 1 & 0 \end{pmatrix} \begin{pmatrix} u \\ \phi \\ P \end{pmatrix} \tag{75}$$

where u_c and ϕ_c are the new inputs.

Actually, $\dot{u}_1 = u_c$

$$\dot{\phi} = P$$

$$\dot{P} = \phi_c \quad \text{or} \quad \ddot{\phi} = \phi_c \tag{76}$$

The synthesis procedure could be used to specify 1 pole for the surge equation and 2 poles for the roll equation.

Suppose the desired form is:

$$\dot{u} = u_c - u$$

$$\ddot{\phi} = \phi_c - 2\xi\omega_n\dot{\phi} - \omega_n^2\phi \tag{77}$$

recall $$y_1 = (1 \quad 0 \quad 0)x \tag{78}$$

$$y_2 = (0 \quad 1 \quad 0)x \tag{79}$$

$$\dot{y}_2 = (0 \quad 0 \quad 1)x \tag{80}$$

then from the synthesis procedure:

$$M^{(1)} = \begin{pmatrix} -1 & 0 \\ 0 & -\omega_n^2 \end{pmatrix} \qquad M^{(2)} = \begin{pmatrix} 0 & 0 \\ 0 & -2\xi\omega_n \end{pmatrix}$$

$$P^{(1)} = \begin{pmatrix} 1 & 0 & 0 \\ 0 & 1 & 0 \end{pmatrix} \qquad P^{(2)} = \begin{pmatrix} 0 & 0 & 0 \\ 0 & 0 & 1 \end{pmatrix}$$

$$M^{(1)}P^{(1)} = \begin{pmatrix} -1 & 0 & 0 \\ 0 & -\omega_n^2 & 0 \end{pmatrix} \qquad M^{(2)}P^{(2)} = \begin{pmatrix} 0 & 0 & 0 \\ 0 & 0 & -2\xi\omega_n \end{pmatrix} \tag{81}$$

then

$$F = D^{-1}\left(\sum_{j=0}^{\delta} M^{(j)}P^{(j)} - K^*\right)$$

$$= D^{-1}\begin{pmatrix} -1-C_1u & 0 & 0 \\ -K_2P-K_7u & -\omega_n^2-K_1 & -2\xi\omega_n-K_3|P| \end{pmatrix} \tag{82}$$

This choice for F will produce the following output.

$$\dot{x} = \begin{pmatrix} -1 & 0 & 0 \\ 0 & 0 & 1 \\ 0 & -\omega_n^2 & -2\xi\omega_n \end{pmatrix}x + \begin{pmatrix} 1 & 0 \\ 0 & 0 \\ 0 & 1 \end{pmatrix}v$$

$$y = \begin{pmatrix} 1 & 0 & 0 \\ 0 & 1 & 0 \end{pmatrix}x \tag{83}$$

Because the control scheme is not applicable when $K_4(C_2n+C_3u) = 0$, this solution may not be the best one to use. An intuitive approach decouples this system without this constraint as shown below.

Let's return to the original equations.

$$\dot{u} = C_1u^2 + C_2n^2 + C_3un$$

$$\dot{\phi} = P$$

$$\dot{P} = K_1\phi + K_2Pu + K_3P|P| + K_4W + K_5n^2 + K_6un + K_7u^2$$

Suppose, as might realistically be the case, it is desired to keep the roll angle zero for any change in surge velocity. If the roll angle is to remain zero, then $\phi = P = \dot{P} = 0$, or:

$$0 = K_4W + K_5n^2 + K_6un + K_7u^2 \tag{84}$$

specify: $$W = \frac{-1}{K_4}(K_5n^2 + K_6un + K_7u^2) \tag{85}$$

then $$\dot{P} = K_1\phi + K_2Pu + K_3P|P| = 0 \tag{86}$$

Since $\dot{u}$ is a function of u and n, the system will act decoupled as long as the roll angle is zero, even if $K_4(C_2n + C_3u) = 0$.

The first example describes all of the calculations necessary to obtain a decoupled system. The second "practical" example illustrates the synthesis method and gives an alternate solution which works where the first solution fails.

Conclusions and Remarks

The results include the time varying case, as can be shown by the addition of another state variable,

$$\dot{x}_{n+1} = 1$$

and the replacement of the variable, t, by x_{n+1} in the state equations.

One of the more important points to keep in mind is that the system can be decoupled with this technique only if the D matrix remains non-singular. This divides the state space into distinct regions which can be decoupled. It will not necessarily be possible to cross from one region to the other by use of the decoupling controller.

This paper supplies only sufficient conditions for decoupling. It is hoped that this paper will stimulate further research in the areas of decoupling and non-linear control.

References

1. P. L. Falb and W. A. Wolovich, "Decoupling in the Design and Synthesis of Multivariable Control Systems," I.E.E.E. Trans. Automatic Control, Vol. AC-12, Dec. 1967, pp. 651-659.

2. E. Freund, "Design of Time-Variable Multivariable Systems by Decoupling and by the Inverse," I.E.E.E. Trans. Automatic Control, Vol. AC-16, Apr. 1971, pp. 183-185.

3. E. G. Gilbert, "The Decoupling of Multivariable Systems by State Feedback," SIAM J. Control, Vol. 7, No. 1, Feb. 1969, pp. 50-63.

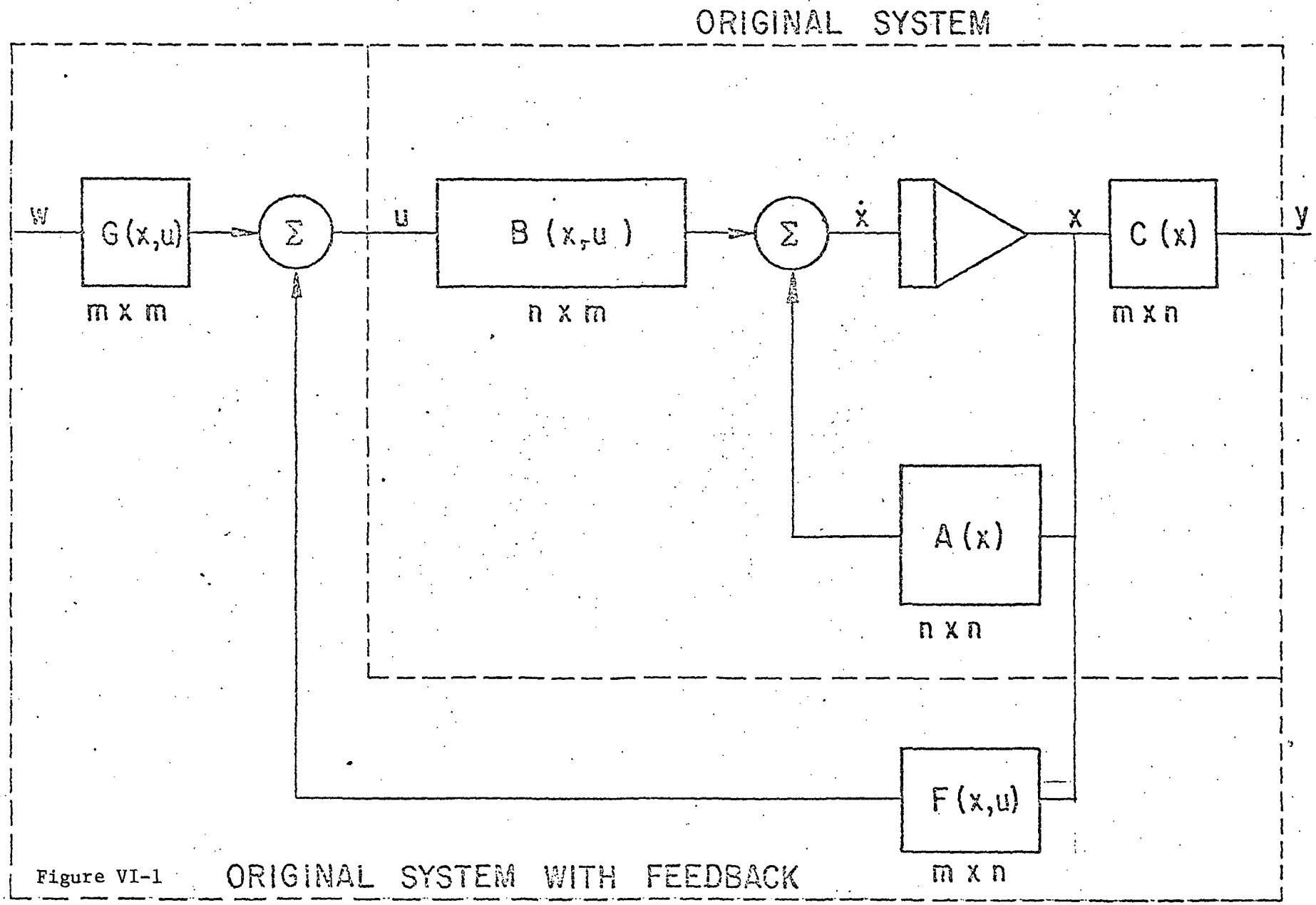

Figure VI-1 ORIGINAL SYSTEM WITH FEEDBACK

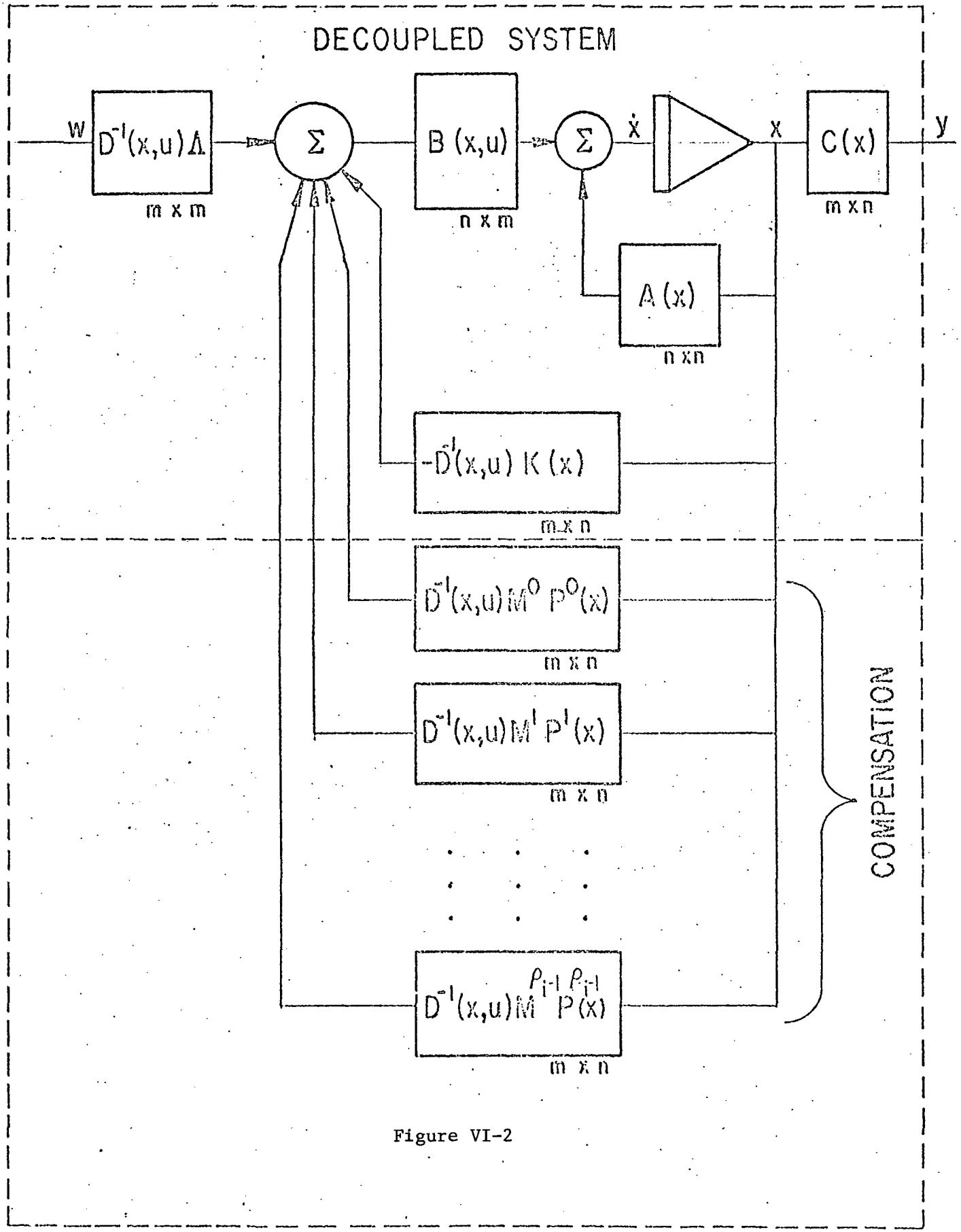
DECOUPLED SYSTEM
W
$D^{-1}(x,u)\Delta$
m x m
Σ
B (x,u)
n x m
Σ
ẋ
x
C(x)
y
m x n
A (x)
n x n
$-D^{-1}(x,u)\ K\ (x)$
m x n
$D^{-1}(x,u)M^{0}\ P^{0}(x)$
m x n
$D^{-1}(x,u)M^{1}\ P^{1}(x)$
m x n
$D^{-1}(x,u)M^{\rho_{i-1}}\ P^{\rho_{i-1}}(x)$
m x n
COMPENSATION

Figure VI-2

Appendix VII

A NOVEL APPROACH TO SUBMERSIBLE VEHICLE PROPULSION, STEERING AND CONTROL

M. S. Thesis

Mechanical Engineering Department

University of New Hampshire

by

John J. Wozniak

June 1971

The proposed wake steering device (see Figures 1-2) consists of a propeller surrounded by an accelerating type of flow nozzle. The length to diameter ratio of the nozzle is greater than that usually found in an operational Kort nozzle. The nozzle has the effect of increasing the velocity through the propeller and creating a low ambient pressure in this region. By opening a small port in the nozzle wall, the exterior fluid is induced into the main propeller wake by this low pressure. A circumferential variation in the internal pressure is developed which results in a net radial force.

All yaw and pitch forces may be produced by opening one or a combination of ports. Pure axial thrust is produced when all ports are closed.

An important feature to be noted is the relatively small size of the control port area to that of the nozzle interior surface area. It should be noted that opening a port alters a major portion of the flow throughout the nozzle. This has the effect of amplifying the control signal. Thus by indirectly altering the direction of the propeller wake (as opposed to rudders and gimbaled motors) a vast reduction in actuator

steering power requirements are anticipated. Additional advantages are as follows:

a) In the forward motion operation, the shroud acts as a Kort nozzle, increasing the efficiency of the propulsor system.

b) The shroud provides direct underwater hazard protection.

c) One unit is capable of providing both main and maneuvering propulsion, effecting an overall weight reduction.

The present concept of wake steering device was developed from a basic desire to reduce the compexity of maneuvering a submersible vehicle. Early unsuccessful attempts to employ propeller driven fluidic-like components were undertaken. These failed because of instabilities of the attachment downstream from a propeller.

It is the purpose of this thesis to explore the operational behavior of the wake steering device. The investigation carried out and presented in subsequent chapters is both experimental and theoretical in nature. The intent of this analysis is to present a preliminary investigation of the steering shroud concept. Thus throughout this study many simplifying assumptions are made in order to obtain quantitative results.

A scale model of the wake steering shroud and propeller was constructed and tested at zero shroud powered velocity. A force and moment coordinate system was established as shown in Figure VII-3. The experimental results are shown in Table VII-I. Forces and moments were derived from pressure measurements inside the shroud using a computer program to derive the resultant forces and moments. A theoretical analysis of the flow inside the shroud provided theoretical radial force values which were composed to be experimental results as shown in Figure VII-4.

From these results it can be seen that the shroud and propeller produce appreciable steering forces. Also it is seen that these forces and their direction depend on propeller speed and for a two bladed propeller are not strongly dependent on propeller pitch to diameter ratio at the test propeller speed of 290 rad/sec.

TABLE I

RESULTANT FORCES AND MOMENTS

PROPELLER P/D	PORT CONDITION	RADIAL FORCE F_r	DIRECTION DEGREES β	AXIAL FORCE F_a	X-MOMENT M_x	Y-MOMENT M_y	SPEED RAD/SEC.
1.4	All closed	0.0	-	.30	0.0	0.0	290
1.4	0^o Open	.25	36.	.29	.68	.90	290
1.4	270^o Open	.26	301.	.31	-1.75	.60	290
1.4	180^o Open	.28	281.	.32	- .87	-1.1	290
1.4	90^o Open	.27	130.	.31	..96	- .94	290
1.6	All closed	0.0	-	.33	0.0	0.0	290
1.6	0^o Open	.26	39.	.33	.72	.87	290
1.6	270^o Open	.27	309	.32	- .92	.82	290
1.6	180^o Open	.28	223	.31	- .93	-1.0	290
1.6	90^o Open	.26	132	.32	.97	-1.0	290
1.8	All closed	0.0	-	.34	0.0	0.0	290
1.8	0^o Open	.26	45	.32	.87	.89	290
1.8	270^o Open	.28	310	.33	-1.00	.90	290
1.8	180^o Opem	.27	224	.32	-1.0	- .85	290
1.8	90^o Open	.28	135	.31	.95	-1.0	290

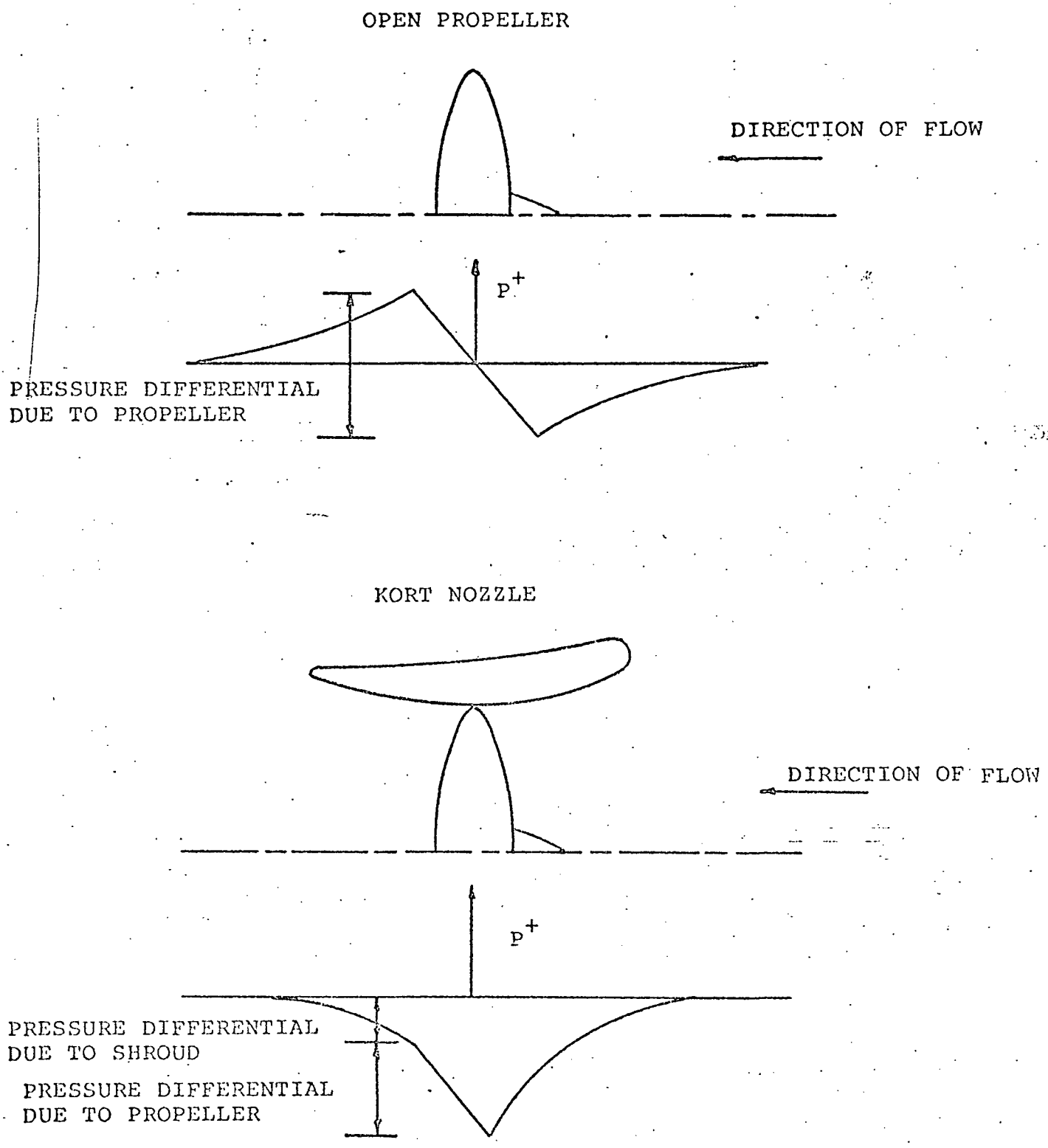

Figure VII,1 PRESSURE DISTRIBUTION FOR OPEN AND SHROUDED PROPELLER

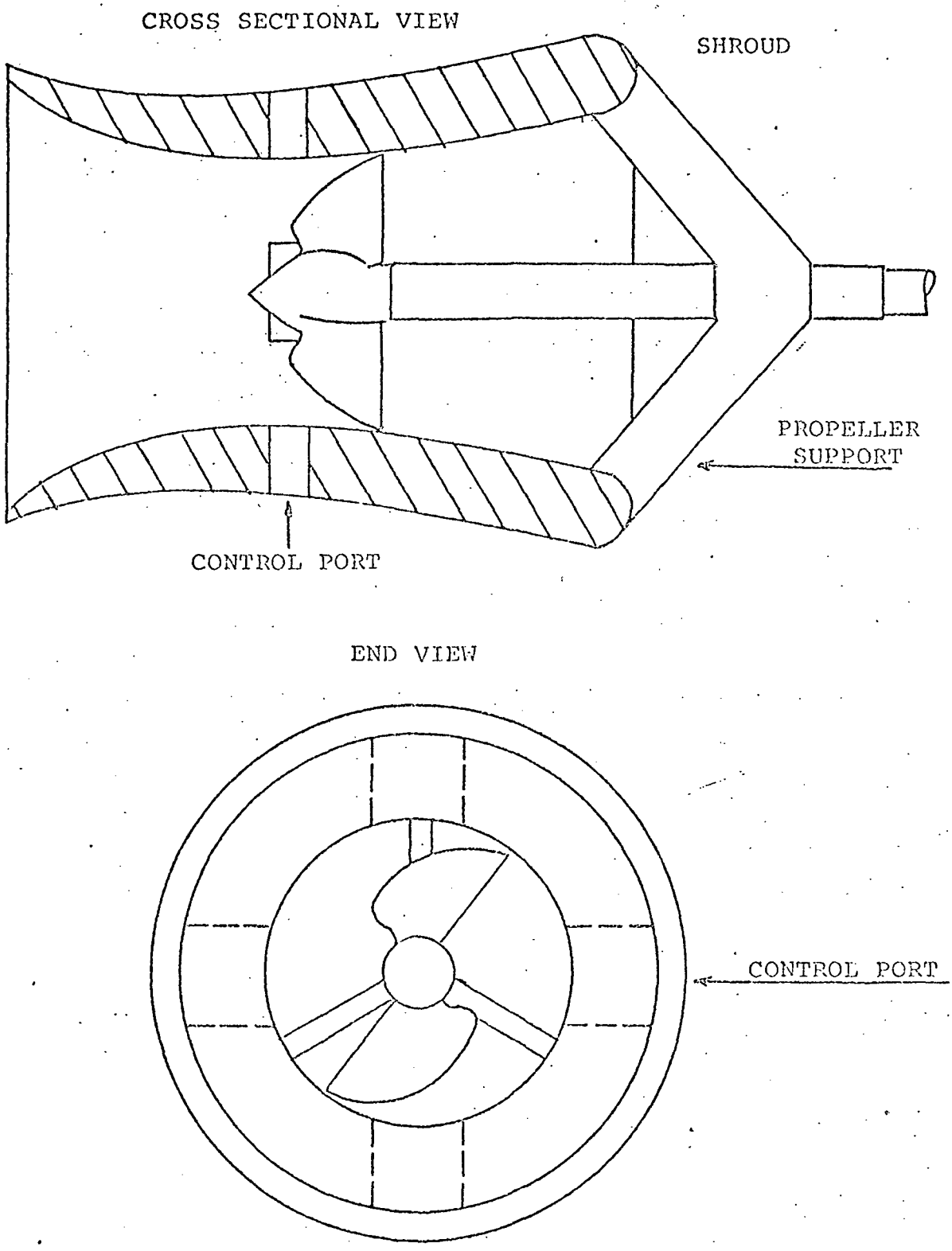

Figure VII,2 BASIC STEERING SHROUD CONFIGURATION

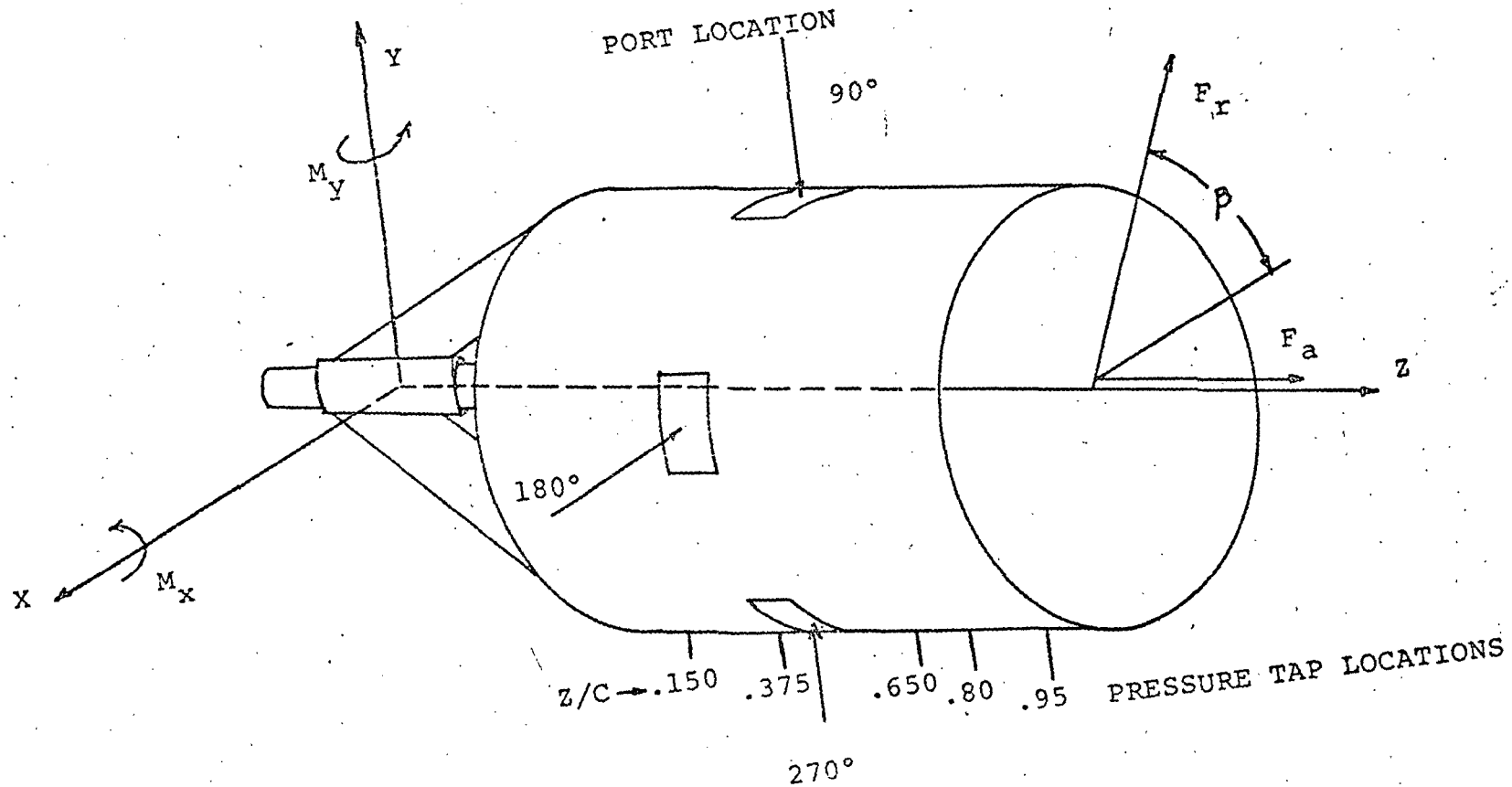

Figure VII,3 SHROUD NOMENCLATURE

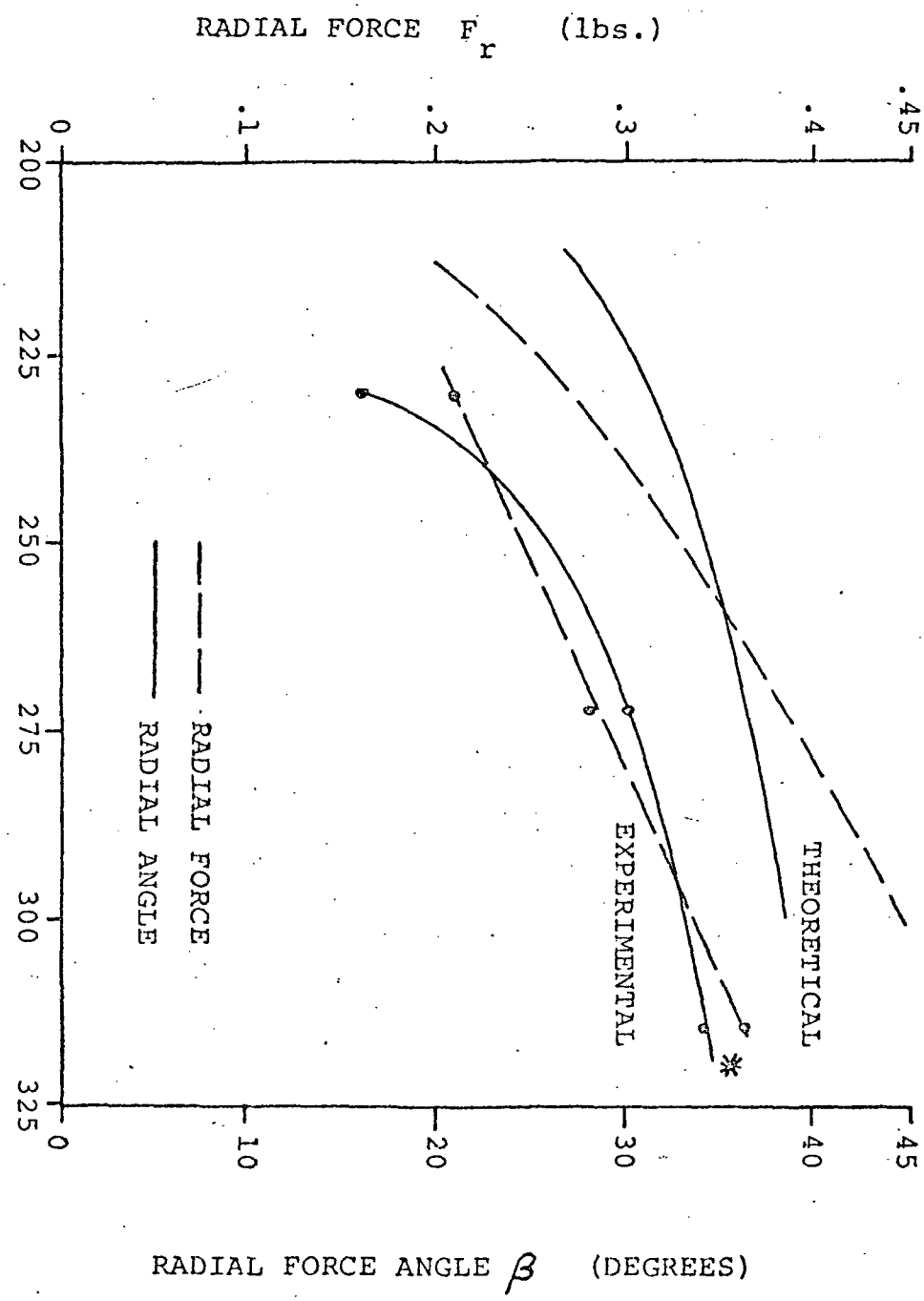

Figure VII.4 THEORETICAL AND EXPERIMENTAL SHROUD RADIAL FORCE AS A FUNCTION OF MOTOR SPEED

Appendix VIII

ELECTRO HYDRAULIC FLUIDIC CONVERTER

A fluid jet at Reynolds numbers of about 0 to 2,000 exiting into a region of fluid at rest near a curved wall has a laminar section which extends downstream for several nozzle diameters, then becomes turbulent. The jet separates from the curved wall near the supply nozzle. The resulting free jet has a mass flow which increases as the jet moves downstream since additional fluid is entrained on both sides of the jet. As the Reynolds number of the jet is increased, the laminar region becomes shorter and fluid entrainment is increased. When the supply jet Reynolds number reaches some critical value, the jet has acquired a degree of turbulence and jet spreading such that the jet boundary is sufficiently large to restrict the incoming fluid that is moving back along the wall to supply the entrainment flow. This reduces the pressure and deflects the jet further. The process is cumulative and the jet quickly attaches to the wall. The phenomena is statistical in nature and a prediction of the exact critical Reynolds number is difficult analytically. Fortunately, the attachment is repetitive and many investigators have used this behavior to design fluidic elements.[1,2,3,4,5]

Because the flow phenomena is very complicated, simplifying assumptions as outlined below must be made in order to perform a mathematical analysis of jet behavior (refer to Fig. VIII,1). The jet issues from a supply channel of width a. One wall of this channel is tangent to a convex circular wall of radius R. Flow is entrained in the regions on both sides of the jet. The flow entrained between the jet and the wall is supplied by a counter flow far from the wall where the pressure is P_e

through a restriction of height h parallel to the y-axis located 60° down the wall as shown (this choice arbitrary). The x-axis is the axis of the jet. The pressure along the curved wall is assumed uniform. The outer limit of the jet will be defined as a line where the velocity in the x direction is 1/10 of the centerline velocity $\bar{u} = .1u_0$. Assuming a fully developed laminar profile, it is possible to write for a unit depth:

$$\text{mass flow w per unit depth} = 2\rho\left[\frac{3}{4}\frac{Jx}{\rho\sigma}\right]^{\frac{1}{2}}$$

J = supply jet momentum per unit depth

σ = spreading constant

ρ = mass density

x = axial distance

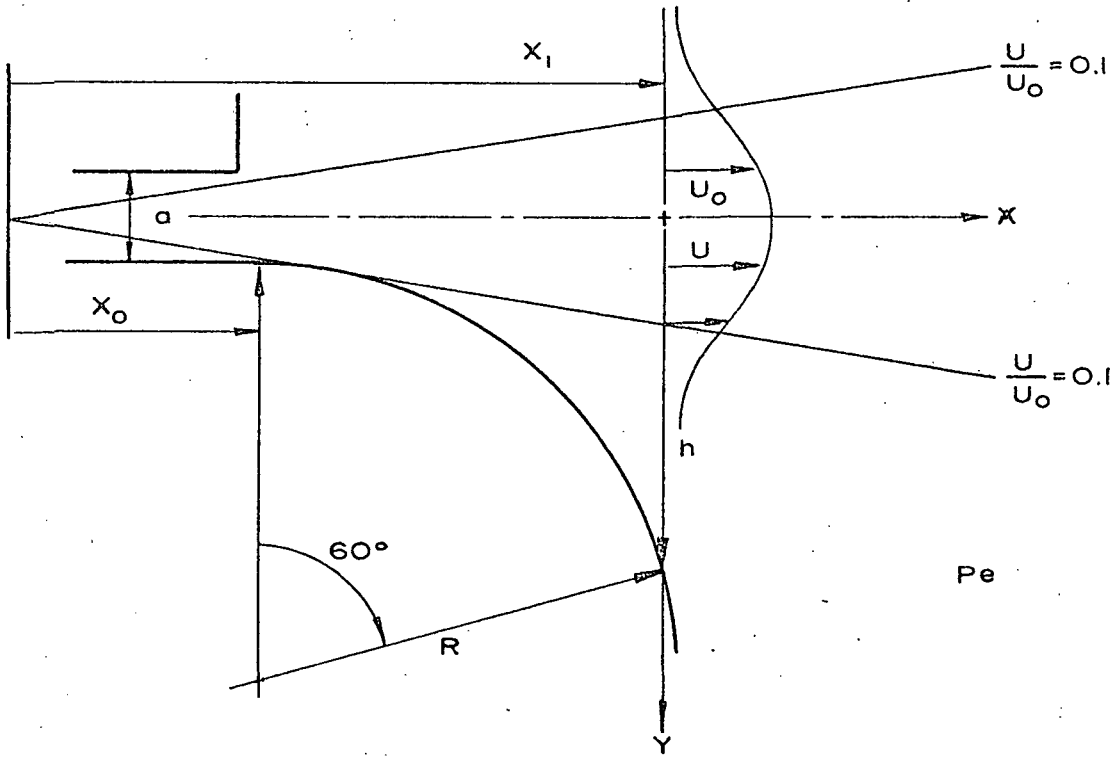

Figure VIII-1

Jet-Curved Wall Geometry

However, at the supply channel exit $w = (\rho Ja)^{\frac{1}{2}}$. Hence, if the jet is assumed symmetrical about its centerline, then for the bottom half of the jet adjacent to the curved wall the mass flow which must be supplied by entrainment is one-half the difference between the supply mass flow and the flow through an arbitrary location jet a distance x_1 from the apparent jet origin.

$$We = \left[\frac{3}{4}\frac{J(x_1-x_0)}{\rho\sigma}\right]^{\frac{1}{2}} - \tfrac{1}{2}(\rho Ja)^{\frac{1}{2}}$$

but $x_1 - x_0 = R \sin 60^o$

also since $\frac{\bar{u}}{u_0} = 1 - \tan h^2 \left(\frac{\sigma Y}{x}\right)$

at the jet exit for $y \simeq \frac{a}{2}$, $\frac{\bar{u}}{u_0} = .1$, $\frac{\sigma Y}{x} = 1.825$

$$\text{thus } x_0 = \frac{\sigma a}{3.65} \quad \text{so} \quad y = \frac{1.825}{\sigma}\left[R \sin 60^o + \frac{\sigma a}{3.65}\right]$$

$$\text{also } h = R(1 - \cos 60^o) + \frac{a}{2} - y$$

Thus, the flow through the restriction between the jet and the wall is approximately

$$w_e = \rho h \sqrt{\frac{2(Pe-Pw)}{\rho}}$$

eliminating h and w_e yields

$$\frac{Pe-Pw}{J} = \tfrac{1}{2}\left[\frac{\frac{3}{4}\left(\frac{R \sin 60^o}{\sigma}\right)^{\frac{1}{2}} - \tfrac{1}{2}a^{\frac{1}{2}}}{R(1-\cos 60^o) + \frac{a}{2} - \frac{1.825}{\sigma}\left(R \sin 60^o + \frac{\sigma a}{3.65}\right)}\right]^2$$

This result indicates that for a spreading constant σ determined experimentally, and a channel wall radius R, the pressure far downstream minus the wall pressure divided by the supply jet momentum is fixed. This relationship only holds as long as the jet is not attached to the curved

wall. When the jet attaches to a curve wall, it remains attached to the wall for some distance and then separates at some point downstream. Theoretical studies of the problem of separation are incomplete at this time. For the flow along the wall during attachment, we can write:

$K\bar{u}^{-2} = \frac{1}{\rho}\frac{\partial \bar{p}}{\partial y}$ integrating this relation from $y = \frac{a}{2}$ to ∞ yields

$\frac{Pe - Pw}{J} = \frac{1}{R}$ which holds as long as the jet is attached to the wall. This indicates that for short radius elements, the pressure difference must be high to bend the jet and maintain attachment.

Jets have stability characteristics different from those of flows adjacent to solid walls. A jet issuing from the nozzle has three flow regions, a potential core and a laminar region that later develops into a turbulent region. The length of this laminar region depends not only on the supply jet Reynolds number, but on the past history of the jet. Predictions of definite points of transition are difficult. Experimental work on the stability of a two-dimensional jet was done by Sato and Sakao[6,7]. At low Reynolds numbers their mean velocity distributions agree well with the laminar jet solutions by Schlichting[8]. They consider that when residual disturbances in and around the jet were made extremely small, the transition of a jet from a laminar to a turbulent regime is the natural transition. Even in this case, the transition is influenced by small, uncontrollable disturbances. The intensity of the disturbances which cause transaction seemed to be different from one run to another. The intensity of the fluctuations in the velocity at different downstream positions (x) are similar for small distances downstream from the supply nozzle and the y locations of peak fluctuations of velocity approximately coincide with the position of a maximum gradient in the mean velocity distribution as

expected. As the jet moves downstream, the peaks in fluctuation move closer and the differences in the fluctuations across the jet become smaller and smaller. Finally, maximum fluctuations occur at about 12 nozzle widths downstream and decrease gradually at larger x. Thus, the turbulent fluctuations of jet velocity and the jet width and profile are related. As turbulent fluctuations increase, the jet spreads faster.

By artificially applying sinusoidal disturbances to the velocity of the jet, it may be possible to alter the spreading of the jet and thereby change the x location or its transition point from laminar to turbulent flow[9, 10]. When this occurs, it will, of course, increase the turbulent eddies in the region of the curve wall and cause the jet to attach to the curve wall at a lower Reynolds number than it would without the induced disturbances.

Experimental Element

A fluidic device was constructed to investigate the phenomena described above. It is shown in Figure VIII-2. A supply chamber was supplied with fluid under pressure p. This fluid was expanded as a jet through a supply nozzle whose length could be varied. At the exit of this supply nozzle, a curved wall was formed tangent to the bottom edge of the supply nozzle with pressure taps located at angles θ = 20, 45 and 60°. The region of the interaction chamber at pressure p_e was vented to tank, downstream a receiver was located to collect the supply jet when it was in the unattached position. The pressure received by the receiver p_0 is measured in a chamber at the end of the receiver. The element was designed so that the length and width of the supply nozzle, the radius of the curved wall and the location of the receiver could be changed at will.

Figure VIII-2.
Experimental Element

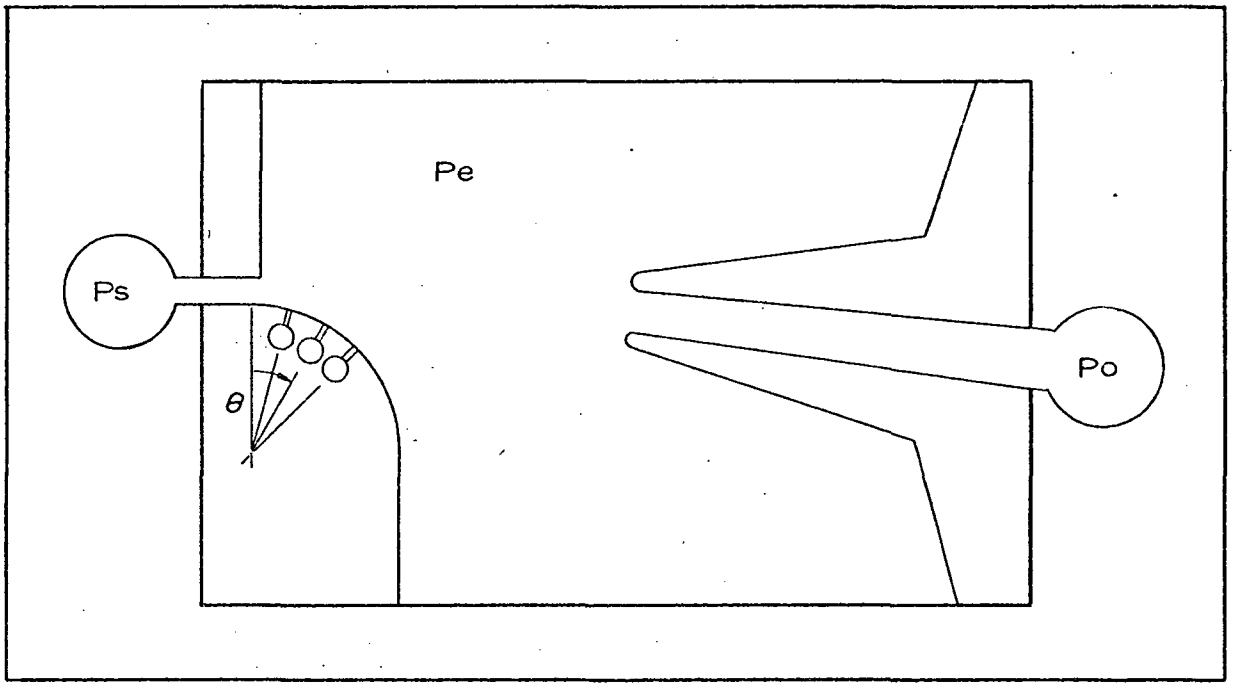

Output pressure, the pressure in the interaction chamber and supply pressure were all measured by means of Pace variable reluctance pressure transducers.

The first goal of this experimental work was to find the effect of supply jet Reynolds number on the jet behavior. Jet behavior was determined by measuring output pressure with the output blocked. This pressure was used as an indication of the location or condition of the jet. Referring to Figure VIII-3, as the supply jet Reynolds number is increased from zero, the output pressure increases continuously until some critical Reynolds number is reached Rey_{c1}. At this Reynolds number, the jet attaches to the curve wall. The output pressure suddenly decreases, since the receiver is now collecting fluid from the outer edge of the velocity profile. As the supply jet Reynolds number is increased, this output pressure gradually increases as before. This is due to the increase in supply jet momentum with Reynolds number and the receiver is simply collecting higher kinetic energy fluid in the outer edges of the velocity profile. As the supply jet Reynolds number is decreased, the output pressure decreases until another critical Reynolds number is reached Rey_{c2} where the output pressure suddenly jumps to a larger value and retraces the original curve. Referring to Figure VIII-3, it is possible to divide this characteristic up into three regions. In region A, the jet is not attached to the curve wall. In region B, the jet is attached to the curve wall when the Reynolds number is decreasing, but not attached when it is increasing. Hence, in region B the output pressure p_0 depends on the past history. In region C the jet is attached to the curve wall at all times. Measurements were made at several wall radii, supply nozzle widths and receiver locations. It was found that as the ratio of

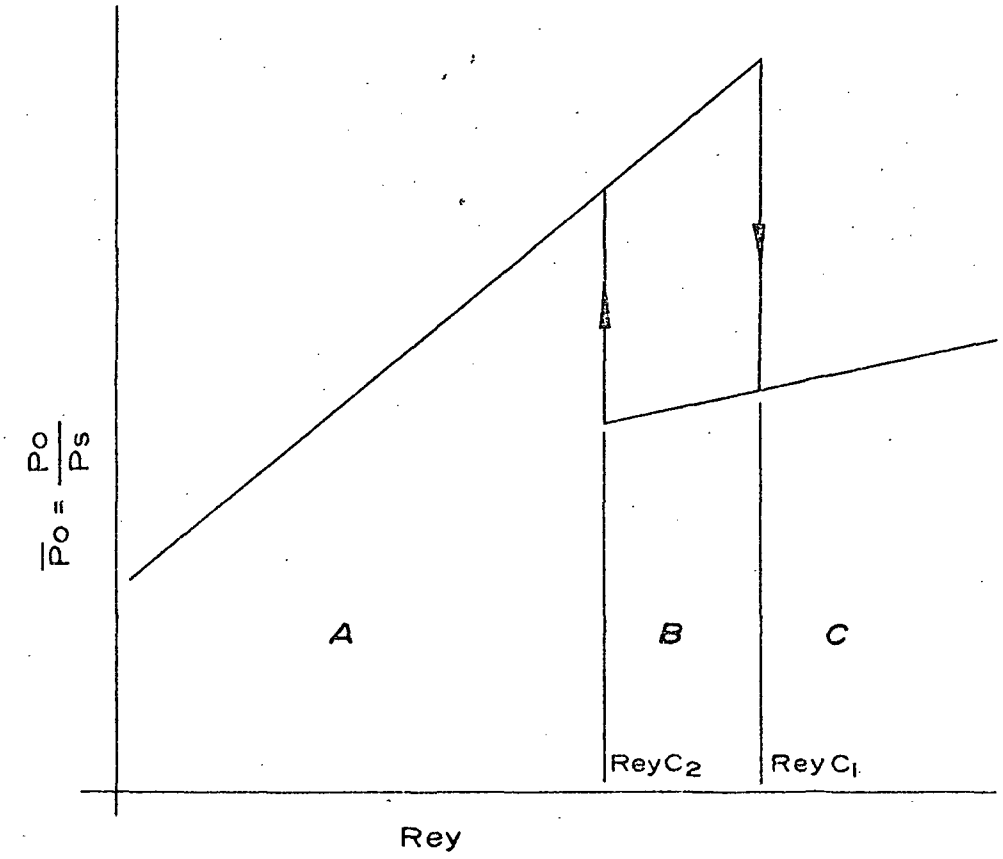

Figure VIII-3. Normalized Output Pressure versus Supply Jet Reynolds Number

supply nozzle width a to wall radius R is increased, the critical Reynolds numbers increased and the difference between them decreased. That is, as a/R increases, region B becomes narrower and located at higher Reynolds numbers. As the receiver was moved closer to the supply nozzle, the cirtical Reynolds numbers decreased and the difference between them increased. Thus, as the receiver is moved closer to the supply nozzle, region B became wider and located at a lower Reynolds number. The optimum location of the receiver seemed to be about 32 to 36 nozzle widths downstream from the supplying nozzle, Beyond 36 nozzle widths, changes in receiver location seem to have very little effect. Below 36 nozzle widths a decrease in the critical Reynolds numbers was observed and a decrease in the change in output pressure at the critical Reynolds number occurred.

Region B is particularly interesting since two stable states are possible depending upon the past history of the jet. If the supply jet Reynolds number is located in this region, it is possible for the jet to be either attached or unattached. Thus, the output pressure is bistable in this region. Velocity fluctuations were not measured in the region of the supply jet, but it was felt that as the receiver nozzle is moved closer to the supply jet, disturbances are introduced into the jet by the presence of the receiver which causes the onset of turbulence adjacent to the curve wall to occur at earlier Reynolds numbers. This causes greater jet spreading as well and reduces the differences in the jet velocity profile in the region of the receiver, reducing the difference in the output pressure at Rey_{c1} and Rey_{c2}. For this reason, it was felt that the receiver should be located far downstream.

Pressure measurements were at the taps along the curve wall before and after attachment. Before the critical Reynolds number Rey_{c1} is reached, the pressure along the curve wall p_w is uniform, justifying the assumptions in the earlier analysis. In addition, the parameter $\frac{P_e - P_w}{J}$ also remained constant before attachment. $\frac{P_e - P_w}{J}$ was measured versus Reynolds number for various receiver locations and supply nozzle widths with a fixed wall radius. It was found that for a given receiver location and supply nozzle width, $\frac{P_e - P_w}{J}$ before attachment could be used to calculate the jet spreading parameter σ. As the receivers are moved closer to the supply jet exit, the spreading constant σ decreases indicating that the entrainment is increased as the receiver is moved closer to the supply jet. The entrainment strongly influences attachment and the pressure P_0 received by the receiver. It is interesting to note that the largest difference between the number $\frac{P_e - P_w}{J}$ before and after attachment occurs when there is a minimum amount of hysteresis, or the two critical Reynolds numbers are close together. After attachment, this number seems to be nearly constant and approximately equal to $\frac{1}{R}$. The significance of this has not yet been established.

Changing the temperature of the working fluid effects jet behavior in addition to supply pressure, since supply jet Reynolds number is affected by the kinematic viscosity of the fluid. For oil, kinematic viscosity decreases with temperature. Consequently, the supply jet Reynolds number will change with temperature for a fixed supply jet pressure. This indicates a temperature sensitivity of the phenomena which can be important in its application.

In order to exercise control over the attachment or separation of the jet to the curve wall, a piezoelectric crystal was mounted at the exit of the supply jet nozzle on the curved wall. An AC electrical signal of variable amplitude and frequency was applied to the crystal. The purpose of the crystal was to introduce an artificial disturbance to produce turbulent fluctuations of the supply jet velocity. As was shown earlier, these variations are closely related to the onset of the turbulent region of the jet. The piezoelectric crystal has a fast response and is capable of responding to very high frequencies. The natural frequency of the crystal chosen was considerably higher than the frequencies used in these tests. The internal impedance of the crystal was very high. Consequently, one would expect a very low power signal would be necessary to exercise control. The amplitude of the applied voltage varied from zero to 170 volts peak to peak. The crystal was driven by Hewlett Packard Audio Oscillator and the output pressure was measured for a fixed output restriction and a fixed supply jet pressure. The frequency of the signal applied to the crystal was varied from 0 to approximately 20 kilohertz. During the experimental tests, as the voltage on the crystal was increased, the jet became more responsive to crystal frequencies, indicating that as the voltage was increased, the amount of disturbance applied to the crystal and the resulting turbulence in the velocity profile became larger. Figure VIII-4 shows the supply jet at a Reynolds number of 2,000, which places it in region A of the curve shown in Figure VIII-3. In this region, the supply jet is not attached to the curved wall. As the frequency of the applied signal was increased, the output pressure decreased sharply and then returned to a constant level when the signal was increased further, as shown in Figure VIII-4. The test indicated that when a signal

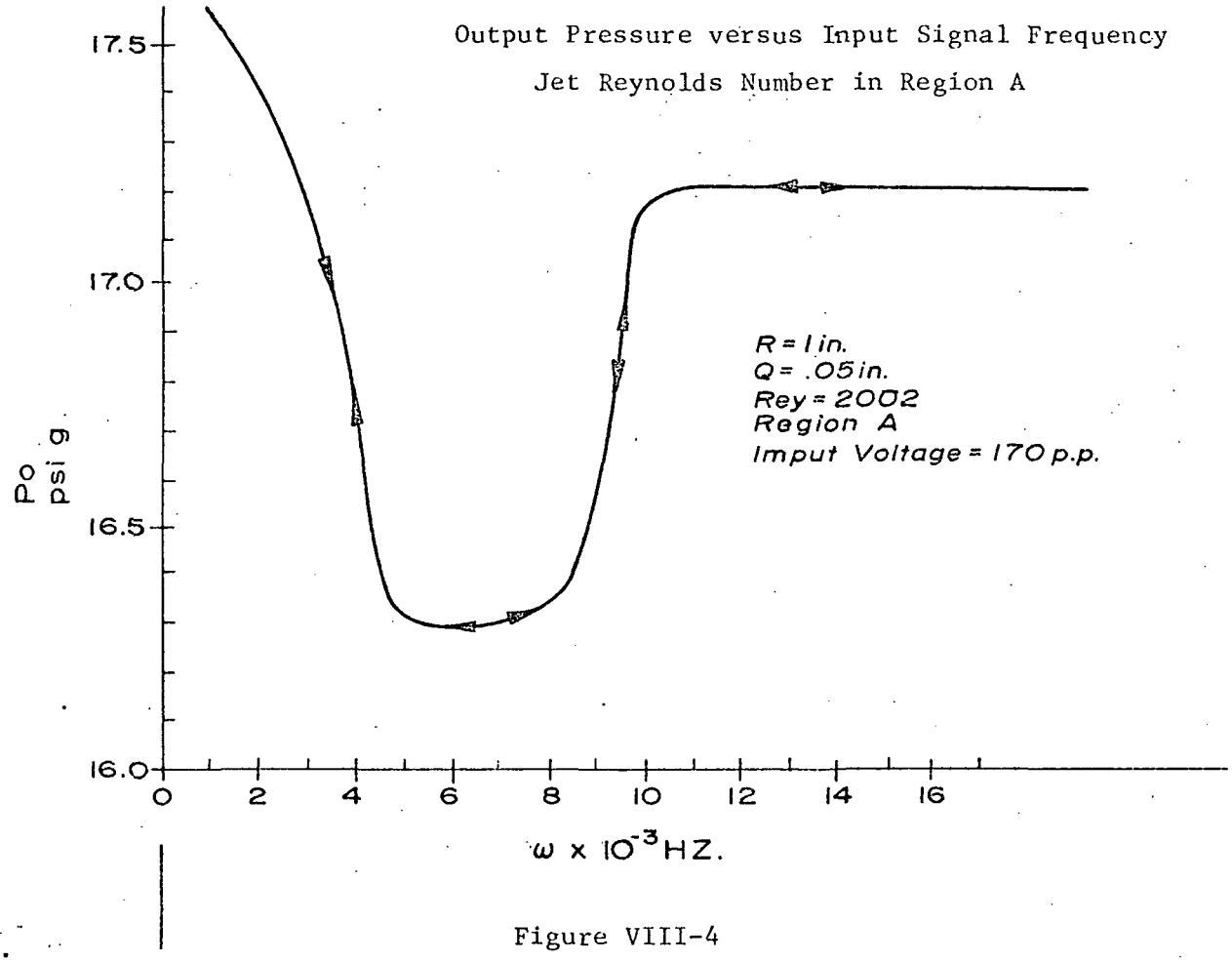

Figure VIII-4

of a frequency between 5 and 8 kilohertz was introduced, the jet attached to the curved wall. When the signal was removed, the jet did not remain attached to the curved wall.

If the jet is in region B where it may be attached or unattached at a given supply jet Reynolds number, then the output pressure versus frequency curve exhibits hysteresis. As the signal frequency is increased, the jet suddenly attaches to the curve wall and the output pressure decreases at approximately 4 kilohertz. As the frequency is increased further, the output pressure decreases and then increases in a non-linear manner about a minimum which occurs about 8 kilohertz. This appears to be the natural frequency of the jet where it is most sensitive to disturbance and exhibits the largest turbulence. In this region, it appears that the output pressure could be frequency modulated by the control signal. As the frequency is decreased, the jet remains attached to the curved wall and the output pressure even at zero frequency is below the original output pressure level, Figure VIII-5. This indicates that the element has memory properties and could exhibit bistable behavior. It would be necessary, however, to provide some means of moving the jet from the curved wall, perhaps by either decreasing the supply jet Reynolds number or by injecting a control signal into the curved wall to cause it to separate again.

A step change in crystal frequency caused a transient in the supply jet behavior. The supply jet Reynolds number was placed so that the jet was in region A, and not attached to the curved wall. The signal frequency into the crystal was changed suddenly from 8.8 kilohertz to 20 kilohertz. As can be seen from the data shown in Figures 4 and 5, this

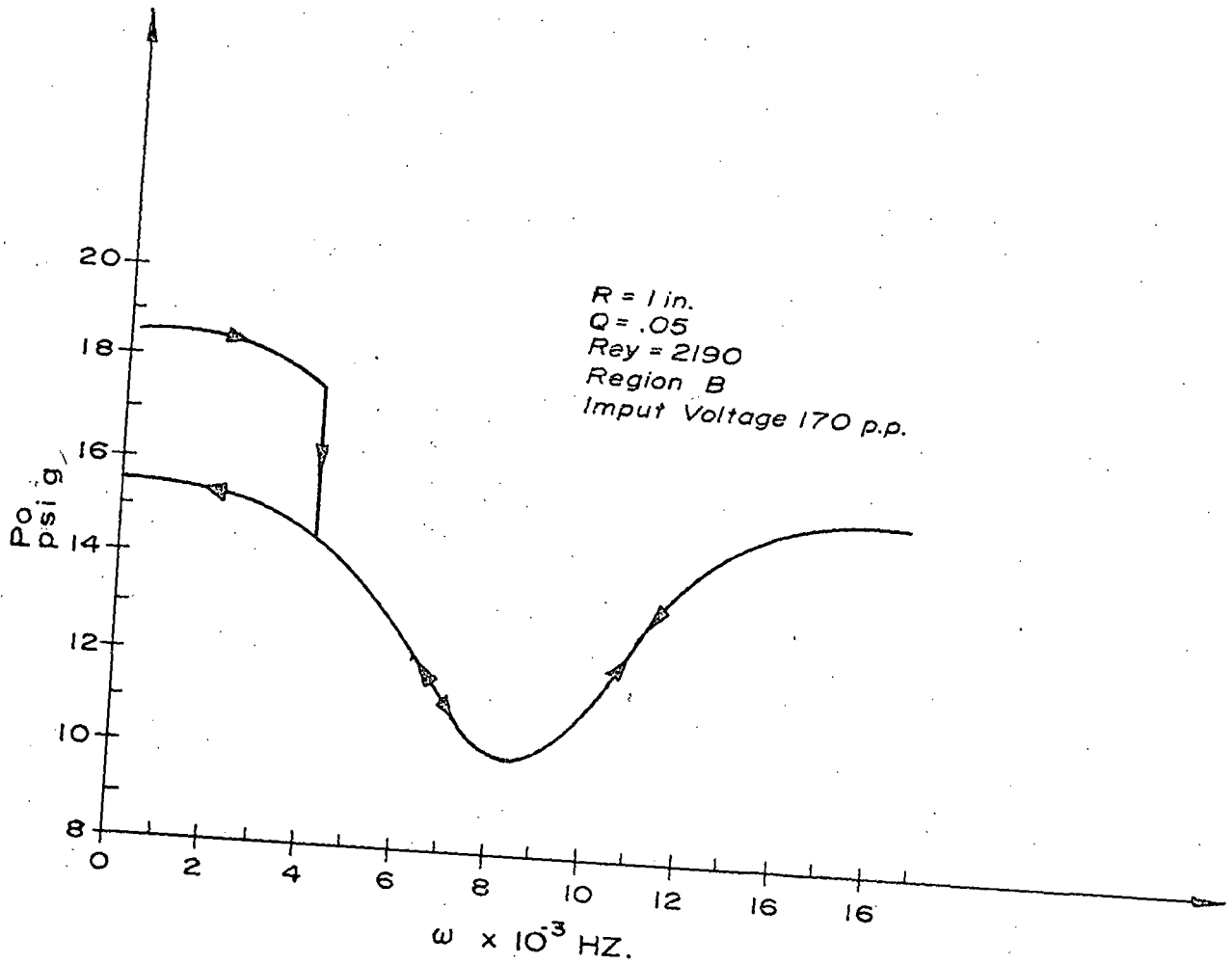

Figure VIII-5

Output Pressure versus Input Signal Frequency Jet Reynolds Number in Region B

signal frequency change causes the jet to change from a region where it is being excited by a frequency to which it is particularly sensitive to one where it is insensitive. The resulting dynamic response is shown in Figure VIII-6. This data indicates a rather slow response. The rise and fall time of the jet is of the order of 200 milliseconds. It is believed that this very slow response time is the result of a very low crystal efficiency. The particular crystal chosen did not expand in the radial direction, but rather expanded in the axial direction so that the bulk of the disturbance was not applied to the fluid. Future tests will make use of a crystal which expands and contracts in the direction such as to produce the most efficient injection of disturbances into the jet. It is believed that this will cause much faster system response. The results of this work are preliminary and indicate that it is possible to control the attachment and separation of a hydraulic jet to a curved wall by means of an electrically excited piezoelectric crystal. On the other hand, the results so far indicate that this response may not be very fast and that it has some sensitivity to temperature. Further work should be conducted to determine methods of using the phenomena without suffering disadvantages due to the temperature sensitivity and slow speed of the response.

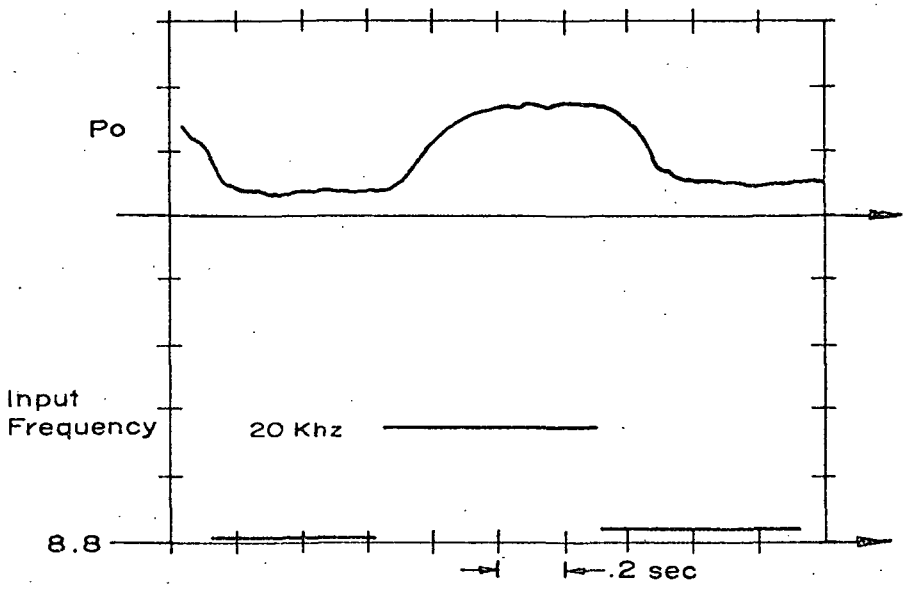

Figure VIII-6

Output Pressure versus Time for Step
Change in Input Signal Frequency

LIST OF REFERENCES

(1) McGlaughlin, D. W., Taft, C. K., "Fluidic Electrofluid Converter", ASME Transactions, p. 334-340, June 1967.

(2) Sarpkaya, T., "Deflection of Plane Jets by Convex Walls", H.D.L. Report, 1968.

(3) Kadosch, M., "Laminar Versus Turbulent Separation Jet From a Curved Wall", Advances in Fluidics, 1967.

(4) Rockwell, J., "Effect of Applied Acoustic Fields on Attached Jet Flows."

(5) Newman, B., "The Deflection of Plane Jets by Adjacent Boundaries - Coanda Effect"; "Boundary Layer and Flow Control", Lachman 1961, Pergamon Press, pp. 233-262.

(6) Sato, Hiroshi, "The Stability and Transition of a Two Dimension Jet", Journal of Fluid Mechanics, Vol. 7, 1960, p. 53.

(7) Sato and Sakao, "An Experimental Investigation of the Instability of a Two Dimensional Jet at Low Reynolds Number"", Journal of Fluid Mechanics, Vol. 720, 1964, pp. 337.

(8) Schlichting, Herman, Boundary Layer Theory, McGraw-Hill.

(9) Rockwell, D., "The Macroscopic Nature of Jet Flows Subjected to Small Amplitude Periodic Disturbances", Proceedings of Chemical Engineering Progress Symp. in Sonochemical Engineering, December 1970.

(10) Chang, D., Casarella, M., and Kelnofer, W., "Effect of Sound on the Incompressible Jet Flow Over a Curved Wall", Journal of the Acoustical Society of America, 42 No. 4, 908 (1967).

Appendix IX

ELECTRICAL NETWORK ANALYSIS OF SOCIO-ECONOMIC SYSTEMS UTILIZING GRAPH THEORY

M. S. Thesis

Electrical Engineering Department

University of New Hampshire

by

Darrel D. Lynch

February 1970

There has not been a great deal of work done in the general area of electrical modeling of socio-economic systems. A good example of what has been done is Koenig's model of a university's flow of finances (1).

Koenig's paper demonstrates the application of the methodology of system modeling developed for physical systems in establishing a discrete state model of a nonprofit organization supported by the surrounding community.

One of the larger models which has been done is the outdoor recreational system model of the state of Michigan by Ellis (2). Ellis' problem was very similar to the one which we have chosen to do. He has modeled the outdoor recreational facilities of the state of Michigan utilizing a linear graph method with nodes representing recreational areas and links representing connecting highways. One unique feature of Ellis' system is the fact that he has actually utilized two separate complete models to represent his total model. One model is used to represent the recreational areas themselves while another model is used to represent the localities from which the users of these facilities originate. Dr. Ellis also uses a computer solution for his models which includes the use of computer mapping.

Two examples of work done in the field of transportation utilizing the Integrated Civil Engineering System (ICES) are:

a. Traffic Volume Data Analysis (TRAVOL) (3)

ICES TRAVOL is a subsystem for processing, storing, and applying traffic volume data for the purposes of transportation planning and research in an urban, regional, or statewide context.

b. Transportation Network Analysis (TRANSET) (4)

ICES TRANSET I is a processor of transportation network information. It is designed to provide computerized techniques which will aid the engineer in solving transportation engineering problems.

For this research project it is proposed to develop one particular model of the New Hampshire highway system and then to thoroughly investigate this model to determine if it will or will not provide useful information. There are many models which could be proposed and tested and therefore I feel it to be important to concentrate on only one model at a time. By doing this, models may be systematically eliminated until a satisfactory one is found.

The model proposed consists of a graph with nodes representing population centers and links representing connecting highways. This model will represent a D.C. resistive network.

The limitations of the proposed model are as follows:

a. Simplicity. Since there is very little precedent to fall back on, the first model should be as simple as possible.

b. D.C. Resistive Network. This goes along with the simplicity desired (as outlined previously). Later refinements may include the addition of inductance, capacitance, transients, etc.

c. Number of Nodes. The maximum number of nodes allowed in the ECAP computer program (5) is 50. If ECAP is to be used for analysis, as I propose, the number of nodes is then limited to this figure.

Additional links and nodes may be added as necessary to refine the model. This provides a valuable research tool as the model can be changed to simulate such things as the construction of new highways, etc., and then analyzed to determine the effects these would have on the actual highway system.

The type of model proposed lends itself easily to analysis by the IBM ECAP computer program. By using ECAP the model can be accurately and fully investigated with a minimum of time, effort, and money.

The results of the analysis of this model indicate that the model is unsatisfactory in its present form. The model merits some further investigation, but unless the problem areas outlined below can be resolved, a new, and probably significantly different model, will need to be devised.

A principal problem area is a conflict between net current flow and total traffic flow. The ECAP analysis solves for the net current flow in a branch, i.e. the difference between positive and negative currents flowing between nodes. The traffic count data, in contrast, represents the total traffic in a branch, i.e. the sum of "positive" and "negative" traffic flows between nodes.

Analysis of the traffic flow vs. current ratio (as presented in Chapter III) clearly shows three categories, or groups, of roads (among the branches analyzed). A listing of the highway segments in these groups is included as Appendix V to this report.

For example, the traffic count vs. current ratio for an adjusted

average day in February, 1966* (with the potentials of the out-of-state nodes set equal to zero and using R=L for all roads), separates into the three following distinct groups:

1. 80 - 200
2. 1100 - 3100
3. 65,000 - 68,000

These ratios represent Actual Traffic/Computed Current.

It can be shown that anohter way of expressing this ratio, with T'_{ij} represents actual traffic count, is $\frac{kLT'_{ij}}{Q_i - Q_j}$.

This is quite a significant development and should be thoroughly investigated. On a first analysis it would seem that these categories would represent "grades" of roads corresponding to "resistance", or difficulty in traveling on these roads.

A comparison of these figures with known road conditions seems to bear out this assumption. The group with the largest ratios represents low-current branches, which in turn represent high-resistance (and/or low-voltage) branches due to Ohm's Law.

(*Traffic count data for the month of February, 1966, was used in this analysis since it represents the low traffic count of the year and thus the out-of-state nodes can be logically set equal to zero. This was tested and proved true. Ratios in Chapter III when out-of-state nodes were not zero were not significantly different from those when they were zero. This is due to the fact that in this model each node is "tied" to a definite potential; and varying any nodal potential, including the out-of-state nodes, only affects current flow in the branches directly connected to that node.

The year 1966 was used because this is one of the years for which population data is available.)

An analysis of these ratio groups shows that the roads represented by low current branches are actually difficult-to-travel roads, while those represented by low ratios (high current) are for the most part multi-land easily traveled roads (refer to list in Appendix V).

The exception to the above is that the branches which have a zero-population highway intersection for one node (e.g., Branch 32 and Branch 13) fall in a resistance category much higher than they should be. The only reasonable explanation for this lies solely in the differences in nodal potentials across the affected braches. As pointed out earlier, the ratio

$$\frac{T'_{ij}}{T_{ij}} = \frac{T'_{ij}{}^{kL_{ij}}}{Q_i - Q_j} = \frac{T'_{ij}{}^{kL_{ij}}}{\Delta Q}$$

Where $\Delta Q = Q_i - Q_j = vQ$

The range of Δv for each group is as follows:

1. 200 - 775
2. 30 - 105
3. 0.7 - 1.6

These Δv's easily account for the separation of the various groups. The zero-potential node affects these Δv's by making either Q_i or Q_j equal to zero.

Utilization of a resistance multiplier of 1, 2, or 3 to indicate general ease of travel over each road and highway (see Chapter III) did not provide any conclusive results. The three categories of highways remained intact, but the ratios became more widely scattered. This was to be expected, since the value for "k" in the ratio $\frac{T'_{ij}{}^{kL_{ij}}}{Q_i - Q_j}$ was being

assigned a value of 1, 2, or 3 instead of being kept at 1 as it had been previously. Since the higher resistance roads were assigned the values of 2 and 3, and since the ratios for these roads were already the largest ratios, these ratios naturally became larger and diverged. This indicates that this method of resistance adjustment is not valid. A more appropriate method to try would be the use of resistance scaling factors which would merge all three ratio groups into one group. These factors would probably be divisors and could be selected to force the ratios to converge to any desired quantity.

However, I feel that additional effort toward adjusting the resistances values would be of little use at this time. This model has serious deficiencies which should be resolved first.

In addition to the conflict between net current flow and total traffic flow discussed earlier, another major problem has resulted from the decision to "tie down" the potential at each node to the value of the population potential at that node. Although this procedure eliminates the problem of determining the meaning of polarities in the various current flows, it presents the very serious problem of "fixing" the current flow in each branch completely independent of variations in other branches. For example, changing the out-of-state node potentials from zero to a very large value has virtually no effect on the current flow in any branch except the ones containing the out-of-state nodes. This is due to Ohm's Law in that the current solved for in each branch is $I = \frac{E}{R} = \frac{Q_i - Q_j}{kL_{ij}}$. As just explained, Q_i and Q_j (as well as k and L_{ij}) are fixed quantities for each branch and therefore almost complete isolation exists between branches.

I feel that this model has been reasonably thoroughly investigated and, while satisfactory results were not obtained, much knowledge and insight into the problem were gained. This investigation can easily form a sound basis for development of a "second-generation" model.

BIBLIOGRAPHY

Appendix IX

1. Koenig, "Mathematical Models of Socio-Economic Systems: An Example," IEEE Transactions on Systems Science and Cybernetics, November, 1965.

2. Ellis, J. B., "Outdoor Recreation Planning In Michigan by a Systems Analysis Approach," Technical Report No.1, State Resource Planning Program, Michigan Department of Commerce, May, 1966.

3. Johnson, W. F., "ICES TRAVOL I, Traffic Volume Data Analysis, General Description and Engineering Users' Manual," MIT Research Report R68-62, June, 1968.

4. Ruiter, E. R., "ICES TRANSET I, Transportation Network Analysis, Engineering Users' Manual," MIT Research Report R68-10, March, 1968.

5. Jensen & Lieberman, "IBM Electronic Circuit Analysis Program," Prentice Hall, New Jersey, 1968.

Appendix X

COMPUTERIZED NETWORK SIMULATION OF THE HIGHWAY SYSTEM OF THE STATE OF NEW HAMPSHIRE

M.S. Thesis

Electrical Engineering Department

University of New Hampshire

by

Anthony S. Magliveras

August 1971

This model has resulted from the continuation of Major Lynch's work and it is discussed throughout the remaining chapters of this report. It is different from the first generation model in both structure and approach.

The second generation model resulted from a variety of seasonal and data considerations and was picked to represent the average week-day system from a number of possible systems.

Its nodes are basically the same as those of the first generation model, with a few exceptions. The links represent all physically existing connection paths beyween two nodes, in contrast with the first generation model where only one link, representing the most travelled route, exists between two nodes. The voltage at the nodes is again represented by the "Population Potential" index, but it is left floating instead of being tied down to a common node through an infinitesimal resistance. The resistance of the links has been postulated to fit more the resistance discussed in the outline of Michigan's Recreational Model rather than that of a wire in a D.C. network.

In an effort to better understand the existing traffic patterns of the links in the model and possibly classify them into groups, various studies were done on existing traffic count data. Of these the most

important study is the "Fourier Analysis" carried on hourly daily traffic counts.

In order to calculate the flows in the links, a program has been written to fit the travelling behavior of people and the nature of the existing traffic count data. This program represents the backbone of the system and is entirely different from ECAP.

The model has finally been calibrated so that calculated flows fit the actual 1969 traffic count data. Thus in a manner similar to that described in Michigan's Recreational Model, a "Base Model" has been created describing the average week-day traffic conditions in the State and can be suitably used, by varying the appropriate parameters, for prediction of future traffic changes and trends in the State. This prediction is done in a manner analogous to that used in Connecticut's "Planning for the Future" study.

A. Results

The two seasonal variations of the model that were run using the two programs described in the previous chapter were those of February and August 1970.

At first the population potentials for the two models were obtained. Since the month of February is the month of lowest traffic in the state, the populations of the out-of-state nodes were set at zero resulting in zero population potentials for these nodes. This is justified from the

fact that during the weekend days in February the influence of the out-of-state node populations on the in-state traffic is minimal. In addition the population potentials for all in-state cities whose populations exceeded 20,000 people, with the exception of Keene, were adjusted to 30% of their value. This is justifiable assuming that on no week-day in February, nor at any other time does the portion of the population of anyone of these nodes interacting with the rest of the state exceed 30% of its maximum value. These nodes are Concord, Manchester, Nashua, Salem, Portsmouth, and Dover-Somersworth. Keene was excluded because its population is a border-line case and it is also economically and physically isolated from the rest of the state.

In the August model the population potentials were at first obtained taking into account the populations of the out-of-state nodes. The population of the Boston node was set to include the population of the entire Suffolk county and the population of the Lowell-Lawrence node was set to include the populations of both cities. Then, as for February and for the same reason, the population potentials of the six in-state nodes were adjusted to 30% of their value and the population potentials of the three Massachusetts nodes were adjusted to 15% of their value. In both cases of August and February the two percentages were arbitrarily chosen.

The population potentials, shown in Table X,1, as calculated and adjusted for each of the two seasonal models were loaded in the computer program for the calculation of the uncalibrated traffic flow and the resistance calibration constants K_1. The population potentials for August exceed those for February because of the inclusion of the out-of-state nodes.

The four different link categories indicate the existence of four in all resistance ranges for the highways and roads in the state. Category 1 with links having $K_1 = 1$ contains all roads and highways which are unclassifiable at the present time, as far as resistance is concerned, due to the lack of traffic count data. Category 2 with links having relatively small K_1, $1 \leq K_1 \leq 30$, contains all roads of small per unit of length resistance. Categories 3 and 4 with links of relatively medium and high values of K_1 , $30 \leq K_1 \leq 100$ and $K_1 > 100$ respectively, contain roads of medium and high per unit of length resistance.

The three classifiable links categories divide the state into two sections. Category 2 contains all links representing roads and highways that are located either in the northern or the south-western part of the state. Categories 3 and 4 contain links which represent roads and highways that are mainly located in the center-southern or south-eastern part of the state. This division of the state in two sections coincides with the regions in the state where the traffic is low to medium or medium to high respectively. These two sections are superimposed and indicated on the traffic map published by the Planning Division of the State Highway Department shown in Section E of the supplement.

The separation of the state into these two sections by the three classifiable link categories is correctly predicted by the model. The category 2 links have smaller per unit of length resistances, as indicated by the K_1 constants, than the category 3 or 4 links but their lengths are larger resulting in larger overall resistances which when coupled with the correspondingly smaller population potentials give rise to smaller traffic flows in agreement with the traffic count map shown in Section E of the supplement.

The average width for all one-lane highways was set at 18 ft. and for all two-lane highways at 24 ft. This was done because the widths of the roads and highways in the state vary tremendously in a non-prescribed way from place to place. The average speed of travel was similarly set at 45 miles/hr and 60 miles/hr for one-lane and two-lane highways, respectively. The traffic count for links without any actual data was set at zero and the K_1 calibration constants for all links were orginally set at one.

The values for the K_1 calibration constants obtained for both models fell into four distinct intervals, and based on these intervals the links were separated into four distinct categories. These categories are shown in Table 2, which in addition to K_1 contains the corresponding value of the uncalibrated traffic flow and where blanks are inserted whenever a link is not part of that category for the particular month of either February or August. The four categories are as follows.

a) Category 1: It contains all links for which the K_1 calibration constant was set to one due the absence of actual traffic counts.

b) Category 2: It includes all links for which the K_1 calibration constant fell in the interval (1,30) i.e. $1 \leq K_1 \leq 30$

c) Category 3: It includes all links with K_1 in the interval (30,100) i.e. $30 \leq K_1 \leq 100$.

d) Category 4: It includes all links with K_1 in the interval $(100, \infty)$ i.e. $100 < K_1$.

In order to establish the connection between the link categories of Table X2 and the traffic count station categorization tables resulting from the Fourier Analysis of the traffic data, a comparison was made between the three classifiable link categories and the traffic count station categorization tables.

The results of this comparison are shown in Table X3. Table X3 contains each link category separately and gives the link identification numbers the associated traffic count station or stations and their location. For each month of February and August the groups to which these stations belong in the Fourier Analysis both with respect to the magnitude of Co and the number of Harmonics are also given. In Table X3 a blank indicates that the corresponding link does not belong to the category in question for either February or August, and No Anal. indicates that there has been no Fourier Analysis done on the data of the associated with the link traffic count station.

The comparison between the link categories and the traffic count station categorization tables indicate once more that the links of category 2 are associated with low or medium traffic count areas and regions in the state since groups 1 and 2 in the Fourier Analysis correspond to low and medium traffic counts respectively.

Similarly, most links in categories 3 and 4 are associated with medium or high traffic count areas and regions because groups 2 and 3 in the Fourier Series Analysis correspond to medium and high traffic counts.

The actual computer outputs for the population potentials the uncalibrated traffic flow and the K_1 calibration constants for both models are included in Section E of the supplement.

B. Conclusions and Suggestions

From Table X2 we see that most links remain in the same category for

both models of February and August. In addition we observe that the order of magnitude of the K_1 calibration constants for many links remains approximately the same suggesting that a further investigation into the actual form of the resistance may result in a single all-seasons model for the entire highway system of the State.

One of the main problems associated with the present models is that of assigning a link the proper traffic count. As it stands now with a limited number of nodes a particular traffic count has been assigned to more than one link because part of the link is common to more than one path. This problem can be solved by increasing the number of nodes in the model which in turn will increase the number of links. The present situation has also made it necessary to average the traffic count on a link when more than one count are present. The increase in nodes and links will also eliminate this problem.

For example, the links 110 140 101 000 101 and 110 130 101 000 101 from Peterborough to Nashua and from Peterborough to Manchester respectively have the part from Peterborough to Milford Common. The first of the two links is associated with two counts, one at Temple and the other outside of Nashua while the second is associated with only one count, that at Temple. For the first link it is necessary to average the two counts to obtain a more meaningful count for the traffic moving from Peterborough to Nashua, a procedure which can be eliminated by inserting a node at Milford. This would result in three links instead of two for the system Peterborough-Nashua, Peterborough-Manchester. One of the three links would be Peterborough-Milford with only one count, and the other two Milford-Nashua again with one count and Milford-Manchester which would be countless.

The increase in the number of nodes is also recommended since many

towns with equal or larger population potentials in comparison to present nodes in the system have been eliminated assuming that most traffic will move from one Growth Center to the other. This assumption is erroneous because it neglects feeding and bleeding into and from the arteries of the system along the paths connecting the Growth Centers. An example of this would be the town of Newport whose population potential is 4597×10^3 and is definitely comparable to the towns or cities of Hanover, Lebanon and Claremont whose population potentials are 4599×10^3, 5741×10^3 and 7335×10^3 respectively. The influence of Newport on routes 10, 11 and interstate 89 is rather obvious by looking at a map of the state.

The present models as they stand can be theoretically used for prediction purposed. This can be done by first calibrating a base model and then making any necessary alterations to it. The populations of all in-state and out-of-state cities and towns are projected to the year of prediction and the population potentials, for that year, to be loaded in the model are obtained. The Data Deck is altered to agree with any changes or alterations and the K_1 calibration constants from the base model are inserted as described in the previous chapter, along with the existing or uncalibrated traffic counts and flows. The model is run and in the output, columns forty-one to fifty-nine indicate the predicted traffic flow while columns sixty to sixty-seven give its ratio to the traffic count or flow of the base year.

The uncalibrated traffic flows obtained for the links without any actual traffic count can be manipulated to arrive at a reasonable traffic flow for the link. This can be done by assigning each such link to one of categories 2, 3, or 4 based on regional considerations and giving it a K_1 calibration constant equal to the average of all the K_1 constants in the

category. For example, the links 010 020 026 000 026 and 010 020 033 000 110 both from Colebrook to Berlin could be assigned to category 2 with K_1 calibration constant equal to the average of all the K_1 constants in the category, or equal to the average of the K_1 constants associated with the links in the immediate area of the two links. Once this is done, the uncalibrated traffic flow can be divided by the average K_1 constant and an approximate traffic flow for the link can be obtained. If then this traffic flow is used, rather than the uncalibrated traffic flow, along with the average K_1 constant for any prediction runs the results to be obtained for the predicted traffic flow will also be more reasonable.

Table X,1: Population Potentials

Node	February $\times 10^3$	August $\times 10^3$	Remarks
Colebrook	318	408	
Berlin	3489	4485	
Gorham	1487	1670	
Lancaster	930	1156	
Littleton	1371	1940	
Haverhill	762	1033	
Plymouth	2477	3000	
Conway	1113	1673	
Laconia	14026	16540	
Franklin	7403	8769	
Lebanon & Hanover	10340	12269	
Claremont	7335	9322	
Keene	13026	18714	
Peterborough	3548	5066	
Jaffrey	3897	4153	
Concord	11694	14336	30% of Real Value
Manchester	50209	65571	30% of Real Value
Nashua	25688	49670	30% of Real Value
Salem	11098	30527	30% of Real Value
Portsmouth	12758	15995	30% of Real Value
Rochester	22099	28235	
Dover & Somersworth	21031	24298	30% of Real Value
St. Johnsbury		1847	
Brattleboro		7876	

Table X,1: Population Potentials (continued)

Node	February $\times 10^3$	August $\times 10^3$	Remarks
Worcester		22540	15% of Real Value
Lowell & Lawrence		59005	15% of Real Value
Boston		63818	15% of Real Value
Sanford		12462	
Portland		16736	

Table X,2: Uncalibrated Traffic Flow and K_1 Calibration Constant

Category 1: K_1 - 1

Link Identification					February		August	
Origin	Destination		Path		Traffic x 10^3	K_1	Traffic x 10^3	K_1
010	020	026	000	016	11	1	14	1
010	020	003	000	110	10	1	13	1
020	021	016	000	016	109	1	134	1
030	031	003	000	116	17	1	23	1
030	180	002	000	002	5	1	17	1
031	180	018	000	002	11	1	30	1
032	180	005	000	005	3	1	14	1
032	080	005	000	005	53	1	63	1
040	050	093	003	200	9	1	12	1
040	060	003	025	003	87	1	103	1
050	240	302	000	302	2	1	47	1
060	070	003	000	011	252	1	298	1
080	090	089	005	012	93	1	114	1
080	090	089	091	012	166	1	203	1
090	190	012	000	005	21	1	49	1
090	190	012	000	091	37	1	88	1
100	200	012	000	012	30	1	97	1
110	111	202	000	202	141	1	202	1
110	120	202	000	089	51	1	66	1
111	200	202	000	202	6	1	62	1
140	210	EVE	000	495	318	1	1347	1
160	220	001	000	001	32	1	204	1
160	210	095	000	495	82	1	487	1
160	240	095	000	095	65	1	168	1
170	230	202	000	202	199	1	367	1
171	230	009	004	109	129	1	225	1

Table X,2: Uncalibrated Traffic Flow and K_1 Calibration Constant

Category 2: $1 < K_1 < 30$

Link Identification					February		August	
Origin	Destination	Path			Traffic x 10^3	K_1	Traffic x 10^3	K_1
010	030	003	000	003	5	2	6	2
021	030	002	000	002	14	9	17	4
021	050	016	000	016	11	8	14	4
031	032	302	000	010	11	7	15	5
031	050	302	000	302	6	15	9	3
031	040	093	003	093	13	4	16	2
032	040	025	000	025	13	8	16	4
040	060	093	000	003	132	26	156	16
040	070	093	000	011	86	17	103	10
040	120	093	000	093	82	10	100	7
050	170	016	000	016	57	28	74	14
060	120	003	000	093	250	21	300	18
060	120	011	028	202	---	---	89	19
070	080	011	004	010	---	---	65	20
070	090	011	000	103	49	27	60	19
070	120	011	000	093	229	18	273	17
080	120	089	000	089	101	14	122	14
090	100	012	005	012	56	17	78	19
100	110	101	000	101	121	26	173	23
100	120	009	000	202	---	---	93	28
100	190	009	000	009	---	---	185	28
120	160	004	004	004	---	---	108	26
150	210	093	000	495	232	13	---	---
160	220	095	000	095	63	5	395	11

Table X,2: Uncalibrated Traffic Flow and K_1 Calibration Constant

Category 3: $30<K_1<100$

Link Identification					February		August	
Origin	Destination	Path			Traffic x 10^3	K_1	Traffic x 10^3	K_1
032	080	010	000	010	54	74	65	38
060	120	106	000	202	164	69	197	43
060	120	011	028	202	74	32	---	---
060	170	011	000	011	---	---	176	43
070	080	011	004	010	55	30	---	---
070	080	011	000	089	94	51	112	35
070	120	003	000	004	162	81	196	65
090	100	012	091	012	100	31	139	34
090	120	103	011	089	89	45	111	39
100	120	009	000	202	70	46	---	---
100	190	009	000	009	90	30	---	---
110	130	010	000	101	284	99	373	87
110	140	101	000	101	149	76	279	97
120	130	003	000	003	499	88	645	59
120	130	093	000	093	---	---	1362	70
120	160	004	004	004	87	38	---	---
120	170	202	004	202	148	50	186	34
120	070	202	004	009	132	48	155	30
130	150	093	000	093	726	57	1139	59
130	160	101	000	101	224	44	290	33
130	170	101	000	125	231	71	299	46
150	210	093	000	495	---	---	1878	51
160	171	SPA	000	SPA	---	---	1221	82
160	171	016	000	016	575	58	686	47

Table X,2: Uncalibrated Traffic Flow and K_1 Calibration Constant

Category 4: K_1 100

Link Identification					February		August	
Origin	Destination		Path		Traffic x 10^3	K_1	Traffic x 10^3	K_1
060	170	011	000	011	142	116	---	---
120	130	093	000	093	1055	104	---	---
130	140	003	000	003	895	180	1359	186
130	140	EVE	000	EVE	1592	188	2417	170
160	171	SPA	000	SPA	1023	112	---	---
170	171	SPA	000	SPA	1470	474	1790	292
170	171	016	000	016	827	207	1007	209

Table X, 3
Category 1

Not Applicable

Table X,3: Comparison of Link Category 2 with Fourier Analysis Results

Category 2: $1<K_1<30$

Link #	Link Identification	Associated Traffic Count Station #	Location	Fourier Analysis			
				Magnitude Co		# Harmonics	
				February	August	February	August
27	010 030 003 000 003	34701	Northumberland	1	2	2B	1A
28	021 030 002 000 002	23501	Jefferson	1	2	1A	1A
29	021 050 016 000 016	23101	Jackson	1	2	2B	1A
30	031 032 302 000 010	24901	Landaff	1	2	2B	1A
31	031 050 302 000 302	02901	Bartlett	1	2	2B	1A
32	031 040 093 003 093	25901,06702	Lincoln, Campton	1,	3,	1A,	1A
33	032 040 025 000 025	39521	Rumney	1	2	3C	1A
34	040 060 093 000 003	01990	Ashland	No Anal.	No Anal.	No Anal.	No Anal.
35	040 070 093 000 011	01990,29590	Ashland, Meredith	No Anal.	No Anal.	No Anal.	No Anal.
36	040 120 093 000 093	01990,20590 09990	Ashland, Meredith Concord Bypass	No Anal.	No Anal.	No Anal.	No Anal.
37	050 170 016 000 016	35721,30701	Ossipee, Milton	1,1	3,2	1A,3C	1A,1A
38	060 120 003 000 093	09991,09990	Concord No NH 3B, Concord Bypass	No Anal.	No Anal.	No Anal.	No Anal.
39	060 120 011 028 202	08901	Chichester	---	2	---	3C
40	070 080 011 004 010	01501	Andover	---	2	---	1A
41	070 090 011 000 103	01501	Andover	1	2	3C	1A
42	070 120 011 000 093	09991,09990	Concord No NH 3B, Concord Bypass	No Anal.	No Anal.	No Anal.	No Anal.
43	080 120 089 000 089	22790,	Hopkinton	No Anal.	No Anal.	No Anal.	No Anal.
44	090 100 012 005 012	09101,47901 28702	Claremont, Westmoreland	2,	2,	3C,	1A
45	100 110 101 000 101	28702	Marlborough	3	3	3C	2B
46	100 120 009 000 202	21701	Hillsborough	---	2	---	1A
47	100 190 009 000 009	08721	Chesterfield	---	No Anal.	---	No Anal.
48	120 160 004 004 004	34901	Northwood	---	No Anal.	---	No Anal.
49	150 210 093 000 495	39990	Salem NH-Mass State Line	No Anal.	---	No Anal.	---
50	160 220 095 000 095	19799	NH Tpk. Total	No Anal.	No Anal.	No Anal.	No Anal.

Table X,3: Comparison of Link Category 3 with Fourier Analysis Results

Category 3: $30<K_1<100$

Link #	Link Identification	Associated Traffic Count Station #	Location	Fourier Analysis			
				Magnitude Co		# Harmonics	
				February	August	February	August
51	032 080 010 000 010	27721	Lyme	No Anal.	No Anal.	No Anal.	No Anal.
52	060 120 106 000 202	03901	Belmont	1	2	3C	2B
53	060 120 011 028 202	08901	Chichester	2	---	3C	---
54	060 170 011 000 011	01101	Alton	---	2	---	1A
55	070 080 011 004 010	01501	Andover	1	---	3C	---
56	070 080 011 000 089	01501	Andover	1	2	3C	1A
57	070 120 003 000 004	04901	Boscawen	No Anal.	No Anal.	No Anal.	No Anal.
58	090 100 012 091 012	09101,47901	Claremont, Westmoreland	2	2	3C	1A
59	090 120 103 011 089	32101,01501	Newbury, Andover	1,1	2,2	3C	1A,1A
60	100 120 009 000 202	21701	Hillsborough	1	---	1A	---
61	100 190 009 000 009	08721	Chesterfield	No Anal.	---	No Anal.	---
62	110 130 101 000 101	44501	Temple	2	2	2B	1A
63	110 140 101 000 101	44501,30301	Temple, Milford	2,3	2,3	2B,3C	1A,3C
64	120 130 003 000 003	22501	Hooksett	3	3	3C	2B
65	120 130 093 000 093	09901,22590	Concord, Bypass, F.E.EV. Tpk. Hooksett	---	3,	---	LA
66	120 160 004 004 004	34901	Northwood	No Anal.	---	No Anal.	---
67	120 170 202 004 202	08902,34901	Chichester, Northwood	2,	3,	3C,	2B,
68	120 171 202 004 009	08902,34901, 25501	Chichester, Northwood, Lee	2, ,2	3, ,2	3C, ,3C	2B, ,2B
69	130 150 093 000 093	26990,48902	Londonderry, Windham	No Anal.		No Anal.	
70	130 170 101 000 125	07101,43101	Candia, Stratham	3,3	,3	3C,3C	,3C
71	130 170 101 000 125	07101,25501	Candia, Lee	3,2	,2	3C,3C	,2B
72	150 210 093 000 495	39990	Salem NH-Mass State Line	---	No Anal.	---	No Anal.
73	160 171 SPA 000 SPA	33101,12590	Newington, SPA Dover	---	3,	---	2B
74	160 171 016 000 016	33101,12501	Newington, Dover	3,3	3,3	3C,3C	2B,2B

Table X,3: Comparison of Link Category 4 with Fourier Analysis Results

Category 4: K_1>100

Link #	Link Identification	Associated Traffic Count Station #	Location	Fourier Analysis			
				Magnitude Co		# Harmonics	
				February	August	February	August
75	060 170 011 000 011	01101	Alton	1	---	2B	---
76	120 130 093 000 093	09901,22590	Concord Bypass, F.E. EVE Tpk Hookset	3,	---	3C,	---
77	130 140 003 000 003	29701	Merrimack	3,	3	3C	3C
78	130 140 EVE 000 EVE	29790	F.E. EVE Tpk. Merrimack	No Anal.	No Anal.	No Anal.	No Anal.
79	160 171 SPA 000 SPA	33101,12590	Newington, SPA Dover	No Anal.	---	No Anal.	---
80	170 171 SPA 000 SPA	38990	SPA Rochester	No Anal.	No Anal.	No Anal.	No Anal.
81	170 171 016 000 016	41501	Somersworth Between NH 16A & 16B	2	2	3C	2B